NASA CR- 132349

BOEING



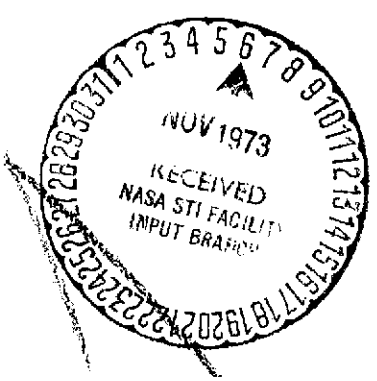

NASA CR- 132349

THE BOEING COMPANY
WICHITA DIVISION

CODE IDENT. NO. 81205

Pen corrections submitted Aug 16, 1973

NUMBER D3-8884 REV LTR A

INITIAL RELEASE DATE 13 June 1972

TITLE ANALYSIS AND TESTING OF STABILITY AUGMENTATION SYSTEMS - FINAL REPORT
B-52 Aeroelasticity Model

Revisions inserted (incorrect pages removed) this copy

FOR LIMITATIONS IMPOSED ON THE USE OF THE INFORMATION CONTAINED IN THIS DOCUMENT AND ON THE DISTRIBUTION OF THIS DOCUMENT, SEE LIMITATIONS SHEET.

MODEL _____ CONTRACT NAS1-10885

ISSUE NO. _____ ISSUED TO _____

PREPARED BY F. D. Sevart, S. M. Patel, W. J. Wattman

SUPERVISED BY G. E. Bergmann

APPROVED BY G. O. Thompson

APPROVED BY _____

1250

| REVISIONS | | | |
|---|---|---|---|
| LTR | DESCRIPTION | DATE | APPROVED |
| A | Replaced erroneous frequency response plot (Fig. 3.6) and revised linearized mathematical model derivation accordingly. Inserted omitted symbol in nomenclature on Page 69. | 8-10-73 | HE Hodges |

TABLE OF CONTENTS


| | | PAGE |
|---|---|---|
| | ABSTRACT | 3 |
| 1.0 | INTRODUCTION | 4 |
| 2.0 | SST WING MODEL FLUTTER SUPPRESSION SYSTEM ANALYSIS | 5 |
| 2.1 | Introduction | 5 |
| 2.2 | Equations of Motion | 5 |
| 2.3 | Flutter Suppression System Evaluation | 8 |
| 2.3.1 | Midspan Surfaces with Nominal Flutter Suppression System | 8 |
| 2.3.2 | Effects of Surface/Sensor Variations | 12 |
| 2.3.3 | SST Airplane Analysis | 22 |
| 2.4 | Remaining Work | 22 |
| 2.5 | Supporting Data | 22 |
| 3.0 | SST WING MODEL CONTROL SURFACE MECHANIZATION | 52 |
| 3.1 | Introduction | 52 |
| 3.2 | Control Surface Actuation System Design | 53 |
| 3.2.1 | Actuator Design | 53 |
| 3.2.2 | Electrohydraulic Servovalve Selection | 53 |
| 3.2.3 | Actuation System Installations | 55 |
| 3.3 | Baseline System | 59 |
| 3.3.1 | Baseline System Testing | 59 |
| 3.3.2 | Baseline System Analysis | 59 |
| 3.4 | Remaining Work | 68 |
| 3.5 | Nomenclature and Drawings | 68 |
| 3.5.1 | Nomenclature | 69 |
| 3.5.2 | Detail Drawings | 70 |
| 4.0 | B-52 AEROELASTIC MODEL RIDE CONTROL SYSTEM SYNTHESIS | 77 |
| 4.1 | Introduction | 77 |
| 4.2 | Design of Ride Control System | 77 |
| 4.2.1 | Phase I - Existing Control Surfaces | 79 |
| 4.2.2 | Phase II - Canard Surfaces | 88 |
| 4.2.3 | Phase III - Canard-Flaperon-Elevator Surfaces | 97 |
| 4.3 | Remaining Work | 120 |
| 5.0 | REFERENCES | 123 |

# ABSTRACT

This document is the final report of analyses and testing of stability augmentation systems accomplished under NASA-Langley Research Center Contract NAS1-10885 and is intended to be used as a working reference in future program activities. Section 2 describes the active flutter suppression analyses conducted on the NASA 1/17 scale supersonic transport wing model. Results predict a 16.7% increase in model flutter true airspeed for Dr. Nissim's flutter suppression concept with outboard control surfaces and sensor locations. Mechanization of the flutter suppression system on the wing model is discussed in Section 3. The analysis, design, fabrication and testing of a subminiature electro-hydraulic actuator, weighing approximately 2 ounces and producing 41 in-lb. of torque, are described. Section 4 presents the results of the ride control system synthesis for the NASA 1/30 scale B-52 aeroelastic model. A ride control system design using elevator, flaperon and horizontal canards is described which reduces fuselage RMS vertical accelerations due to random gusts more than 30%.

RETRIEVAL REFERENCE WORDS:

Aeroelastic Models
Flutter Suppression Systems
Ride Control Systems

## 1.0 INTRODUCTION

This document is the final report of analyses and testing of stability augmentation systems accomplished from 25 May 1971 to 24 May 1972 under NASA-Langley Research Center Contract NAS1-10885 and is intended to be used as a working reference in future program activities.

Section 2 describes the flutter suppression system analysis conducted on the NASA 1/17 scale supersonic transport wing model, and Section 3 discusses the work that was accomplished on the mechanization of the flutter suppression system. The ride control system synthesis for the NASA B-52 aeroelastic model is discussed in Section 4.

Each section is written to be independent of the other sections. The sections discuss not only the work accomplished, but also contain a general discussion of the work remaining to complete the three work items.

## 2.0 SST WING MODEL FLUTTER SUPPRESSION SYSTEM ANALYSIS

Evaluation of a flutter suppression system developed by Dr. Eliahu Nissim on the NASA one-seventeenth scale supersonic transport (SST) wing model is described in this section. This work was accomplished to demonstrate active flutter mode control on the model in the Langley transonic dynamics tunnel.

### 2.1 Introduction

An analytical study was conducted to determine performance of the flutter suppression system on the SST wing model. A similar evaluation was conducted in 1970 with the flutter system on the 969-300 SST airplane configuration. Results of the airplane analysis are contained in Boeing document D3-8390-1 (Reference 1). This report is also contained in Section 2 of D3-8390-4 (Reference 2).

Results of the airplane analysis showed a 28 percent increase in flutter speed at Mach 0.9 over the unaugmented airplane using midspan leading and trailing edge control surfaces. Based on these results, the midspan control surface location was chosen for the mechanization of the flutter suppression system on the model for the wind tunnel demonstration. The primary objective of the current analysis was to determine if the flutter speed could be increased sufficiently for wind tunnel demonstration of the flutter suppression system. The results show that a 12.3 percent increase in flutter speed at Mach 0.9 can be attained with these surfaces, with the feedback sensors located at the inboard edge of the wing strip. Although the flutter speed improvement is less than attained on the SST airplane, the midspan control surfaces will be used for the wind tunnel tests.

The model analyses were conducted using equations of motion generated from generalized mass and stiffness data supplied by NASA. The Mach 0.9 equations were written to include the inboard and outboard, as well as the midspan, control surface locations to permit assessment of the system performance for all surface locations. The analyses described in Section 2.3 were conducted using the Mach 0.9 equations, with the assumption that ideal actuators were driving the control surfaces. To complete the analysis, effects of non-ideal actuators must be determined and the system evaluated at Mach 0.6 and 1.2.

### 2.2 Equations of Motion

Equations of motion were developed for the wing model for Mach 0.6, 0.9, and 1.2 using generalized mass and stiffness data supplied by NASA. The equations were written with wind tunnel velocity and fluid mass density as explicit functions to permit variations in dynamic pressure by varying either the velocity or mass density, or both. A 95 percent freon, 5 percent air environment was assumed for the wind tunnel fluid.

The equations included six elastic degrees-of-freedom plus the two control surface displacements. The Mach 0.9 equations were subsequently revised

to include the inboard and outboard leading and trailing edge control surfaces, with the actuator mass assumed at the inboard edge of each surface. Three separate structural mass matrices were required to properly account for the actuator mass.

In the equation generation, structural damping was assumed to be zero. Doublet-lattice unsteady lifting surface theory was used for the two subsonic conditions, and mach box theory for the Mach 1.2 condition, to obtain aerodynamic loading. The resulting complex matrices of unsteady aerodynamic coefficients were transformed through a curve fitting procedure to rational functions of the Laplace transform operator, S, with fourth order denominators. The equations were then rearranged to the form

$$\left(S^2[M + \rho C_1] + S[D + \rho V C_2] + [K + \rho V^2 C_3] + \rho V^2 \sum_{K=1}^{4} [D_K][S/(S + V d_{KJ})]\right)\left\{q_J(S)\right\} = \left\{0\right\}$$

where:

$\left\{q_J(S)\right\}$ = Elastic and control surface displacement degrees-of freedom

$S$ = Laplace transform operator

$\rho$ = Fluid mass density (95% freon, 5% air)

$V$ = Velocity of fluid relative to the wing

$[M]$, $[K]$, $[D]$ = Structural mass, stiffness, and damping

$[C_1]$, $[C_2]$, $[C_3]$ = Aerodynamic parameters

$[d_{KJ}]$ = Lift growth parameters

$[D_K]$ = Aerodynamics parameters.

Numerical values of the matrix elements for the three test conditions are presented in Section 2.5. Locations of the control surfaces and doublet-lattice panels are shown in Figure 2.1. The sign convention used in the equations is:

X - Positive aft

Y - Positive outboard

Z - Positive up

Trailing edge surface displacement - Positive trailing edge down

Leading edge surface displacement - Positive leading edge up.

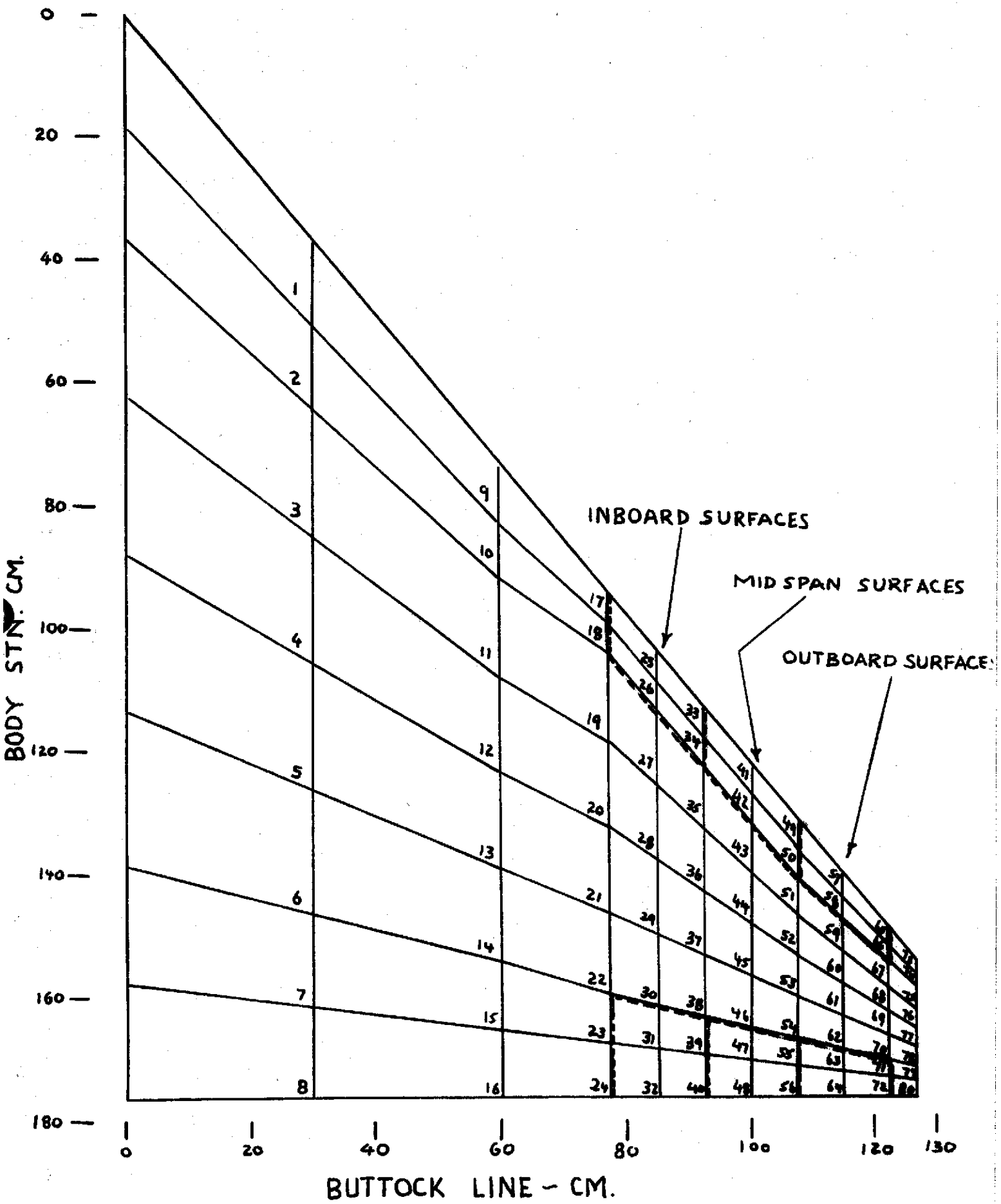


FIGURE 2.1 DOUBLET-LATTICE PANELS

The spanwise length of all control surfaces included in the equations is 5.88 inches (11.76 percent of the wing semispan) with 20 percent chord width on all but the inboard and midspan leading edge surfaces. These two surfaces have a constant 3.65 inch width so they could be installed in the model without cutting into the aluminum alloy plate that forms the model elastic structure.

## 2.3 Flutter Suppression System Evaluation

The flutter suppression system analysis initially assessed the flutter speed improvement attainable with the control law identical to that used on the airplane analysis. A block diagram of the system is shown in Figure 2.2. Feedback sensors were located at 30 percent and 70 percent of the wing chord at the center of the wing strip defined by the midspan leading and trailing edge control surfaces. The Mach 0.9 equations were expanded later to include the inboard and outboard control surface locations. This was done to permit an evaluation of system performance for the other control surfaces, including sensor location variations.

All model analyses were conducted with the sixth elastic mode omitted from the equations of motion. This was done because of the unrealistic influence of this mode on the flutter characteristics. With the sixth mode included, the dynamic pressure at which flutter occurred for the unaugmented wing was about half the dynamic pressure at flutter with the sixth mode omitted.

The flutter suppression system includes feedback variables whose amplitudes are proportional to displacements, but in phase with rates. These variables were generated for the stability analysis using phase root locus to introduce the 90° phase lead ($e^{j90^\circ}$) to displacements at all frequencies, without changing amplitude as a function of frequency.

Dynamic pressure was varied by changing the fluid mass density in all the analyses except where the SAS performance was evaluated as a function of mass density. For this analysis, wind tunnel velocity was varied to vary dynamic pressure.

### 2.3.1 Midspan Surfaces with Nominal Flutter Suppression System

The flutter suppression system evaluation began with the midspan control surfaces and the feedback sensors located at the center of the wing strip. The equations of motion used were for the Mach 0.9 condition without actuator mass included.

A dynamic pressure root locus for the open and closed loop cases is shown in Figure 2.3. With the flutter suppression system loop open, the wing first elastic mode crosses the imaginary axis at about 136 $lb/ft^2$ dynamic pressure. The dynamic pressure at flutter with the loop closed is about 159 $lb/ft^2$, an increase of 16.9 percent on dynamic pressure (8.1 percent in terms of wind tunnel fluid velocity). Figure 2.4 shows the open and closed loop damping ratios for the flutter mode as a function of dynamic pressure.

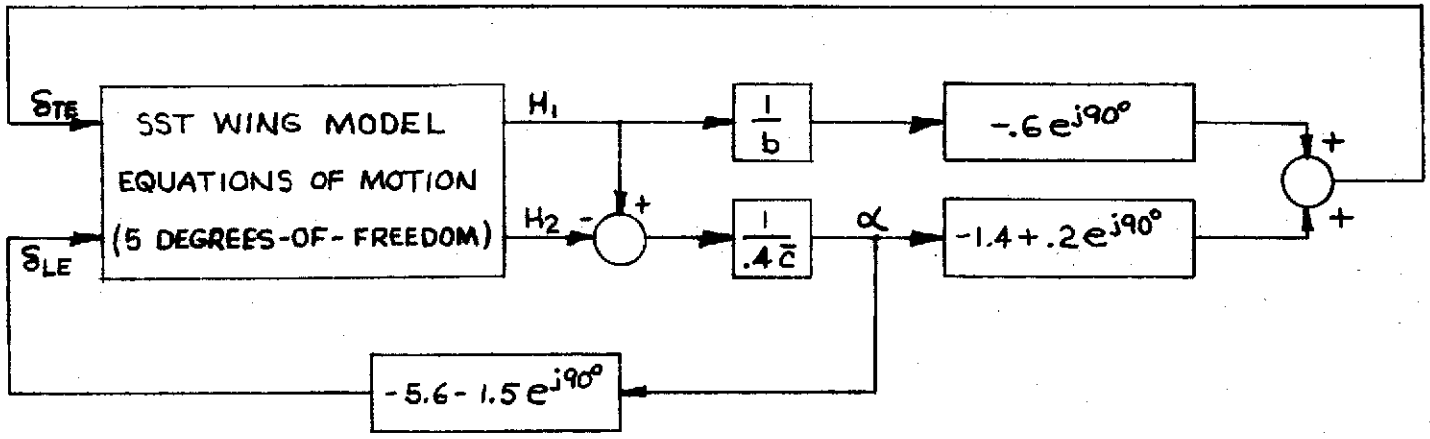


WHERE $H_1$ = VERTICAL DISPLACEMENT AT 30% WING CHORD (POSITIVE UP)

$H_2$ = VERTICAL DISPLACEMENT AT 70% WING CHORD (POSITIVE UP)

$\alpha = \frac{1}{.4\bar{c}}[H_1 - H_2]$ (POSITIVE LEADING EDGE UP)

$\delta_{TE}$ = TRAILING EDGE SURFACE DISPLACEMENT

$\delta_{LE}$ = LEADING EDGE SURFACE DISPLACEMENT

$\bar{c}$ = WING CHORD LENGTH AT SENSOR LOCATION

$b = \bar{c}/2$

FIGURE 2.2 FLUTTER SUPPRESSION SYSTEM BLOCK DIAGRAM

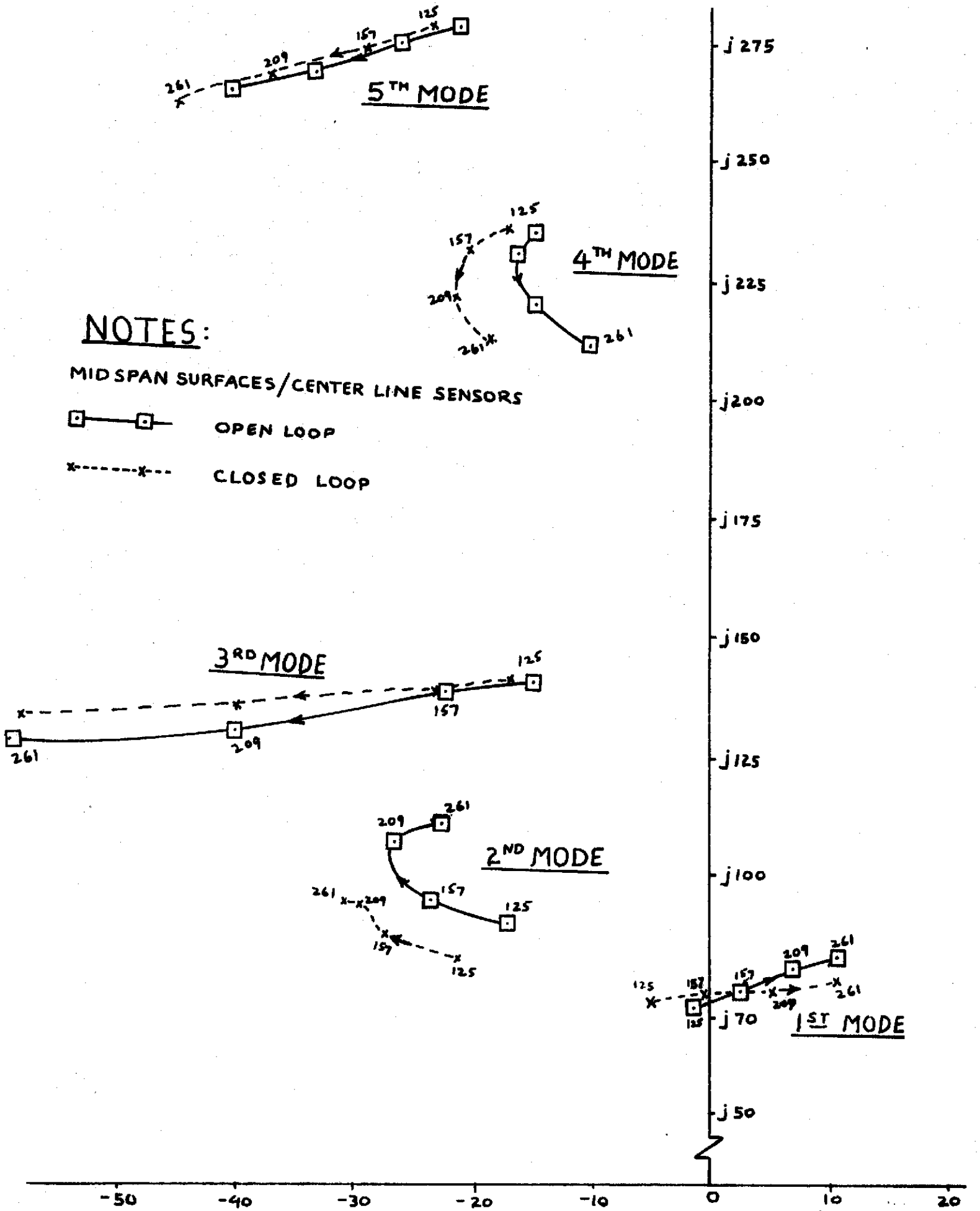


FIGURE 2.3 DYNAMIC PRESSURE ROOT LOCUS (MIDSPAN STRIP)

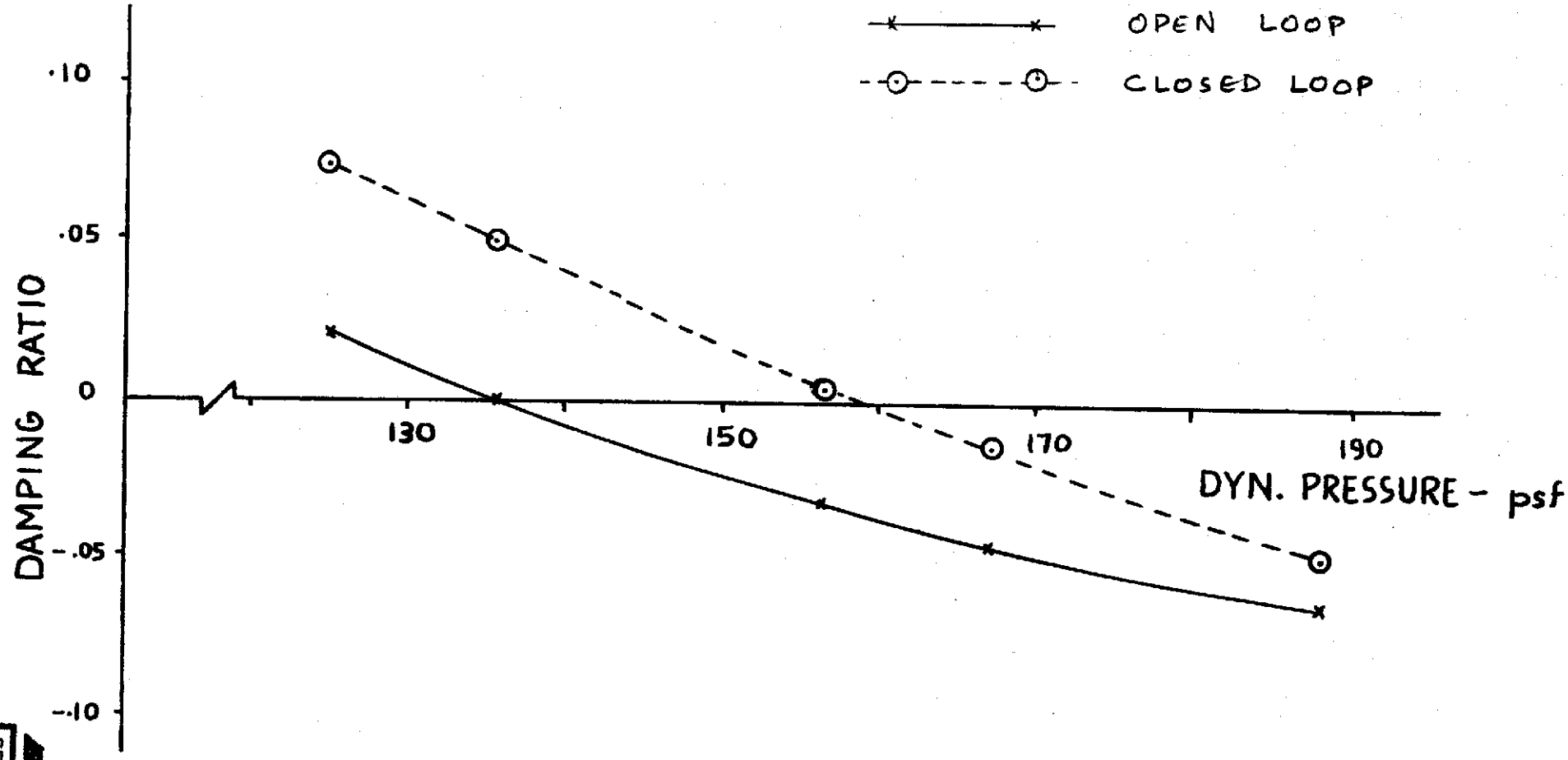


FIGURE 2.4 VARIATION OF FLUTTER MODE DAMPING RATIO WITH DYNAMIC PRESSURE (MID SPAN STRIP)

An analysis was conducted to evaluate system performance as a function of fluid mass density. Figure 2.5 shows the flutter mode damping ratio as a function of true airstream velocity for variations in mass density. Effectiveness of the flutter suppression system as a function of fluid mass density is illustrated in Figure 2.6. The flutter speed improvement decreases with increasing mass density.

### 2.3.2 Effects of Surface/Sensor Variations

Since the flutter speed improvement attained on the model was considerably lower than expected from the previous airplane analysis, the Mach 0.9 equations were modified to include the inboard and outboard control surfaces. The mass of each actuator was included to provide a more accurate representation of the model as it would be tested in the wind tunnel.

The revised equations were used to assess the flutter suppression system performance attainable with each set of leading and trailing edge control surfaces, with the feedback sensors located at the inboard edge, center, and outboard edge of each wing strip as shown in Figure 2.7. The control law gains used in this analysis were the same as used previously for the midspan surfaces, center sensors configuration.

Damping ratios of the flutter mode as a function of dynamic pressure for the three control surface configurations are shown in Figures 2.8, 2.9, and 2.10. Each plot shows the effect of sensor location within the wing strip. Dynamic pressure root loci for the flutter mode are presented in Figures 2.11, 2.12, and 2.13.

Table 2.1 summarizes the results of this analysis. The outboard control surfaces, with outboard edge sensor location, provides the most improvement in dynamic pressure at flutter, 36.1 percent (or 16.7 percent increase in flutter speed assuming fluid mass density held constant). The midspan surfaces, inboard edge sensors were the next most effective surface/sensor combination with 26.1 percent increase in dynamic pressure (12.3 percent increase in flutter speed).

TABLE 2.1
EFFECT OF SURFACE/SENSOR LOCATION
ON FLUTTER DYNAMIC PRESSURE

| SURFACE LOCATION | DYNAMIC PRESSURE ~ psf | | | |
|---|---|---|---|---|
| | | CLOSED LOOP | | |
| | OPEN LOOP | INBOARD EDGE SENSORS | CENTER LINE SENSORS | OUTBOARD EDGE SENSORS |
| INBOARD (BL 77.5 - 92.5) | 135 | 159.5 | 165. | 163. |
| MIDSPAN (BL 92.5 - 107.5) | 136 | 171.5 | 159.5 | 147. |
| OUTBOARD (BL 107.5 - 122.5) | 133 | 141.5 | 166. | 181. |

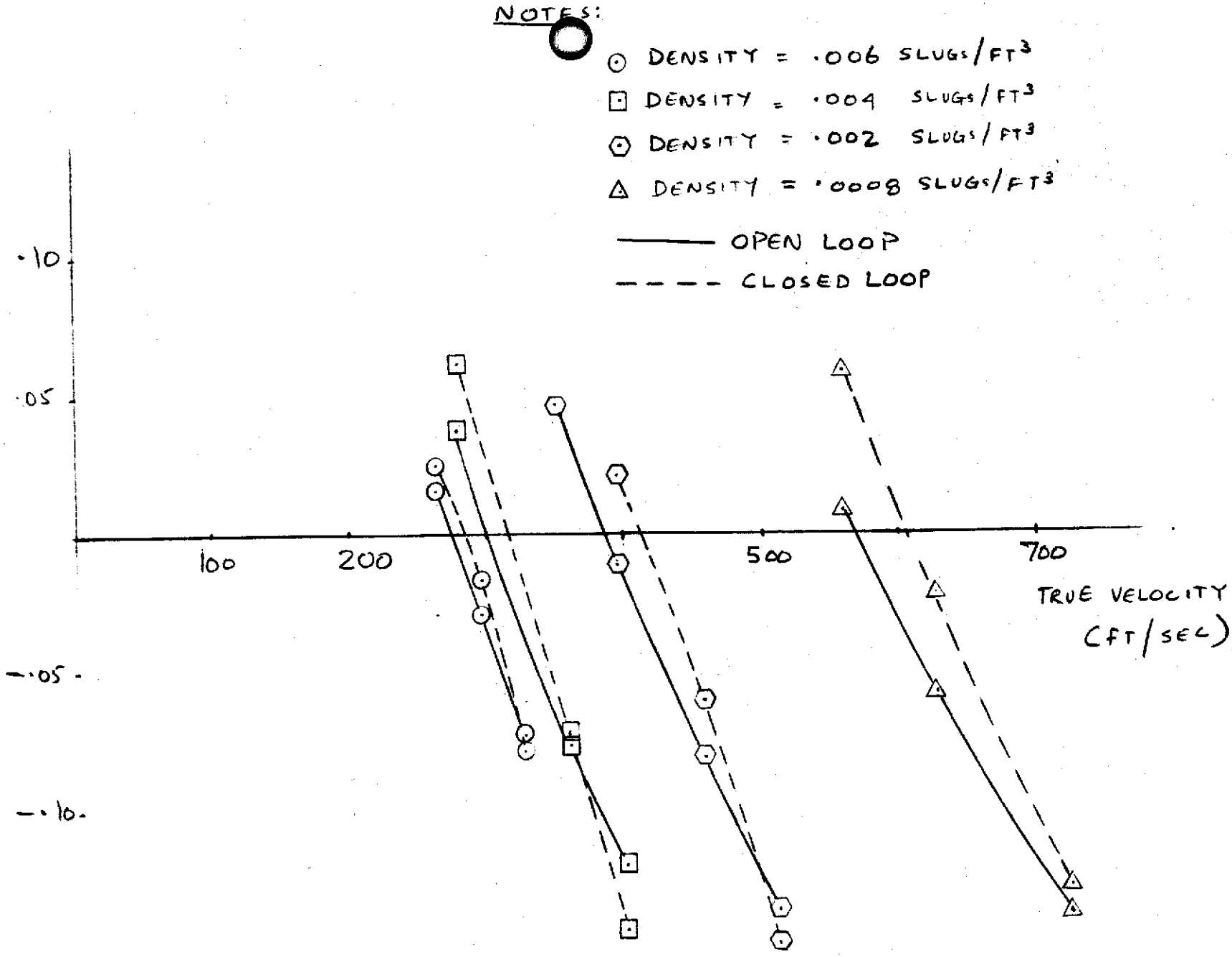


FIGURE 2.5 VARIATION OF FLUTTER MODE DAMPING RATIO WITH TRUE VELOCITY (MID SPAN STRIP)

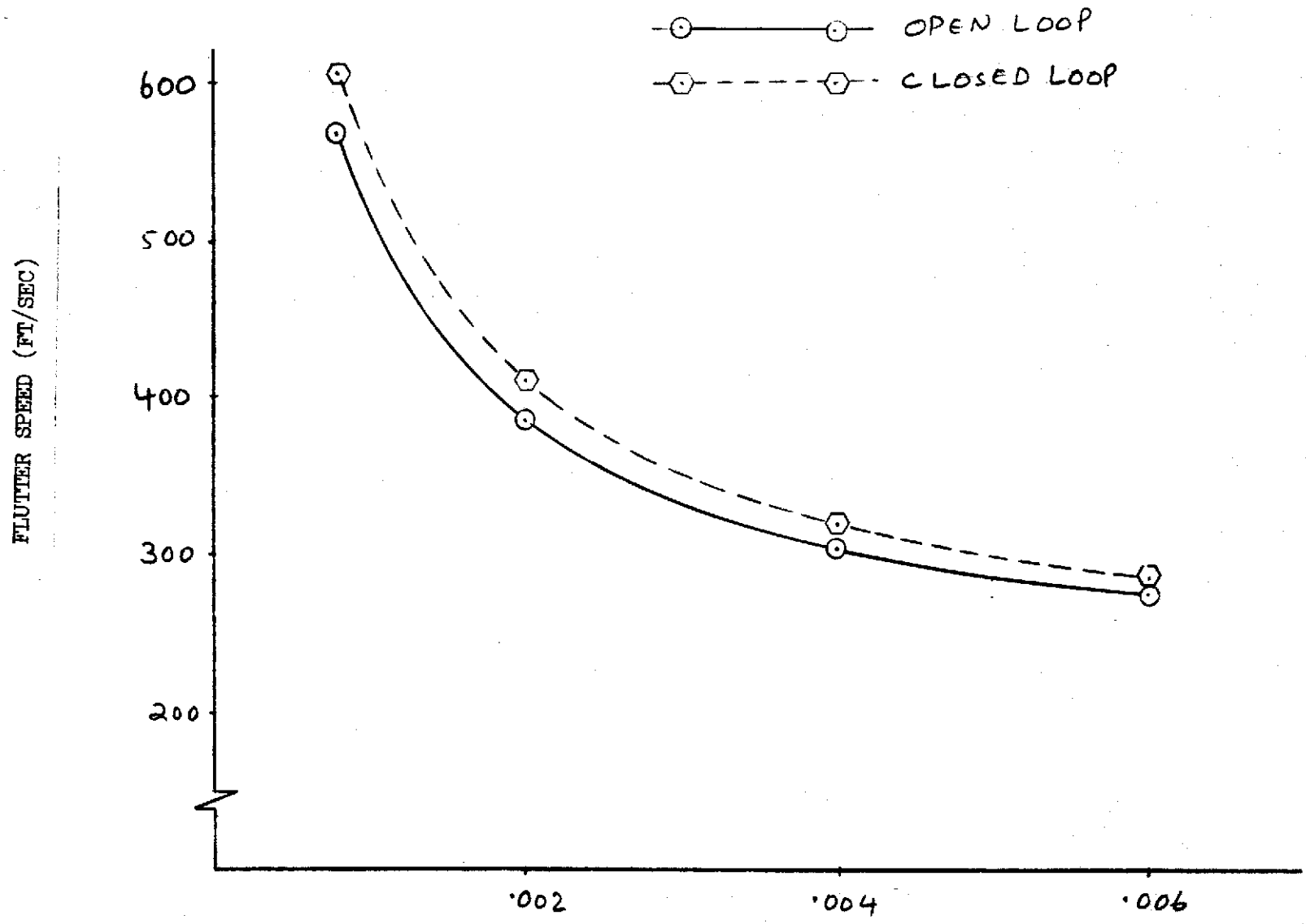


FIGURE 2.6 EFFECT OF MASS DENSITY ON FLUTTER SPEED

FLUTTER 2.7 LOCATIONS OF SURFACES AND SENSORS

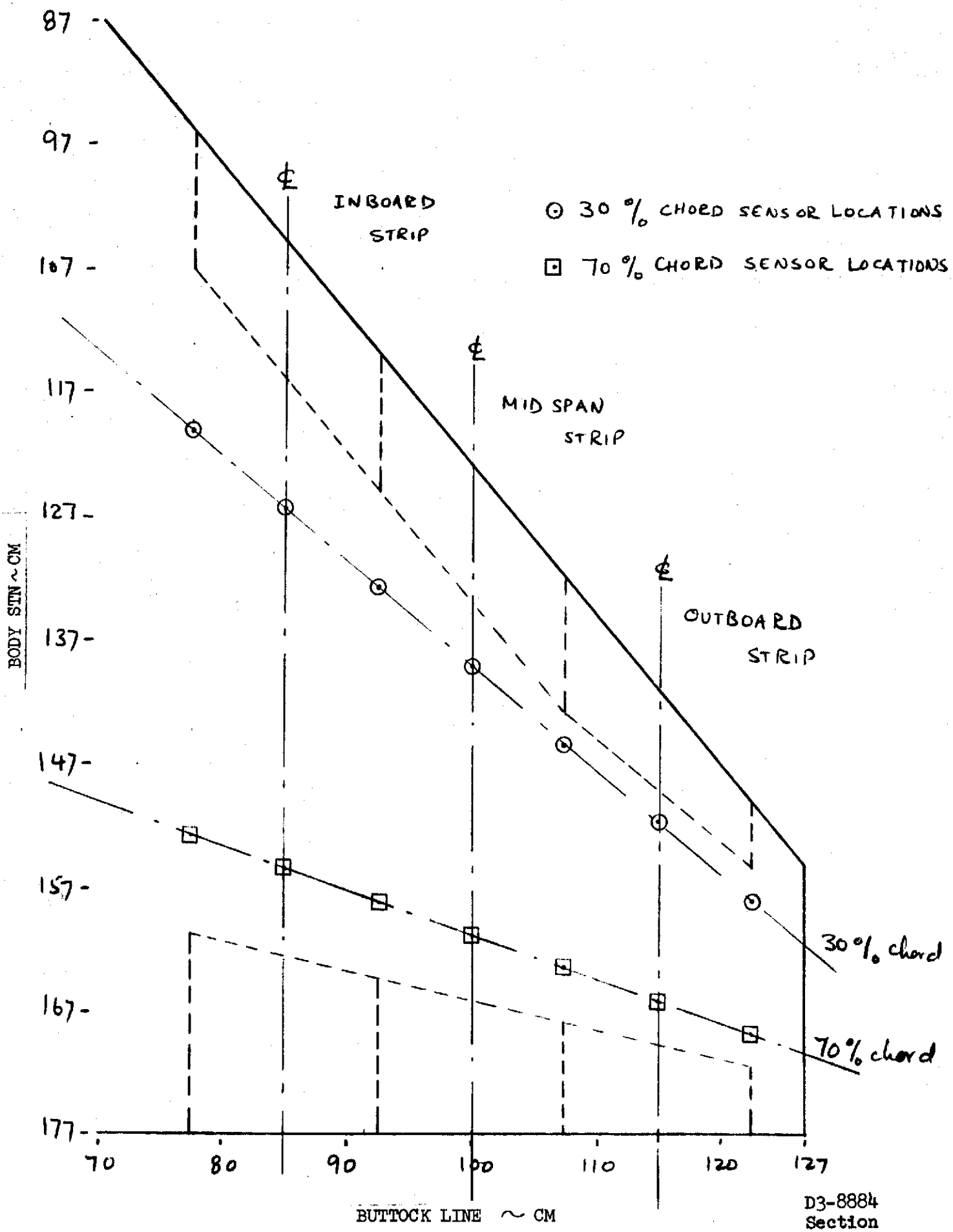

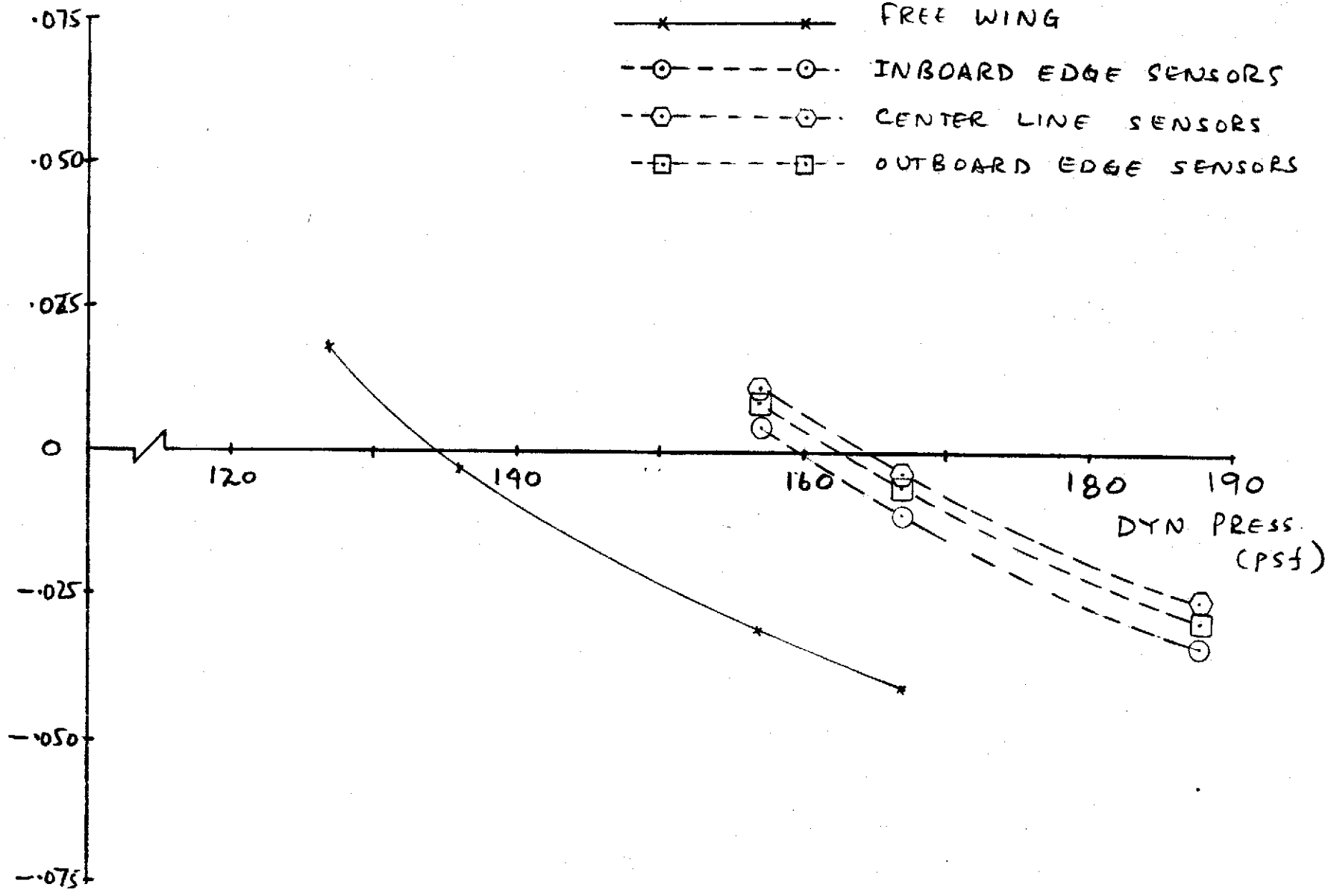


FIGURE 2.8 VARIATION OF FLUTTER MODE DAMPING RATIO WITH DYNAMIC PRESSURE (INBOARD SURFACES)

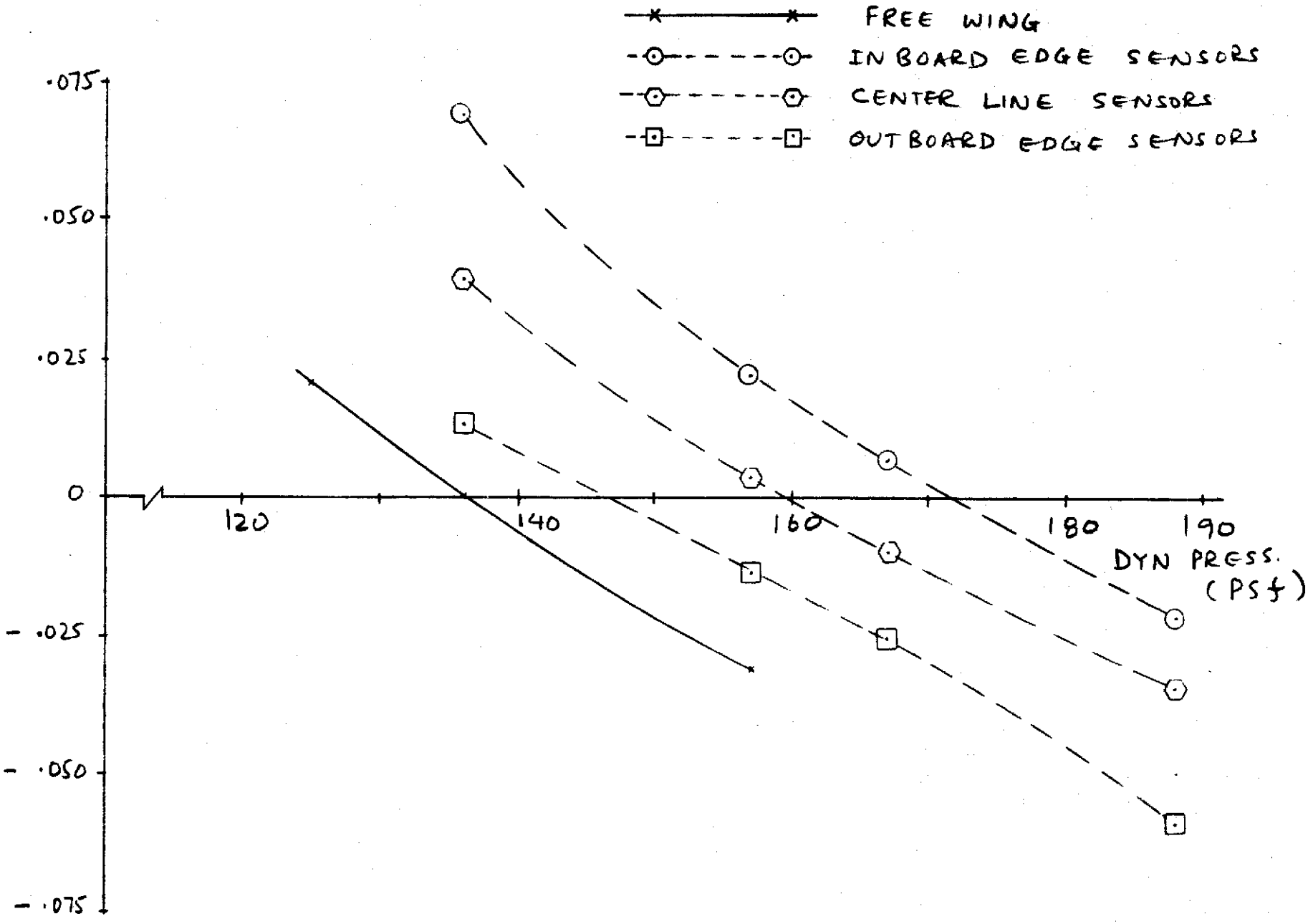


FIGURE 2.9 VARIATION OF FLUTTER MODE DAMPING RATIO WITH DYNAMIC PRESSURE (MID SPAN SURFACES)

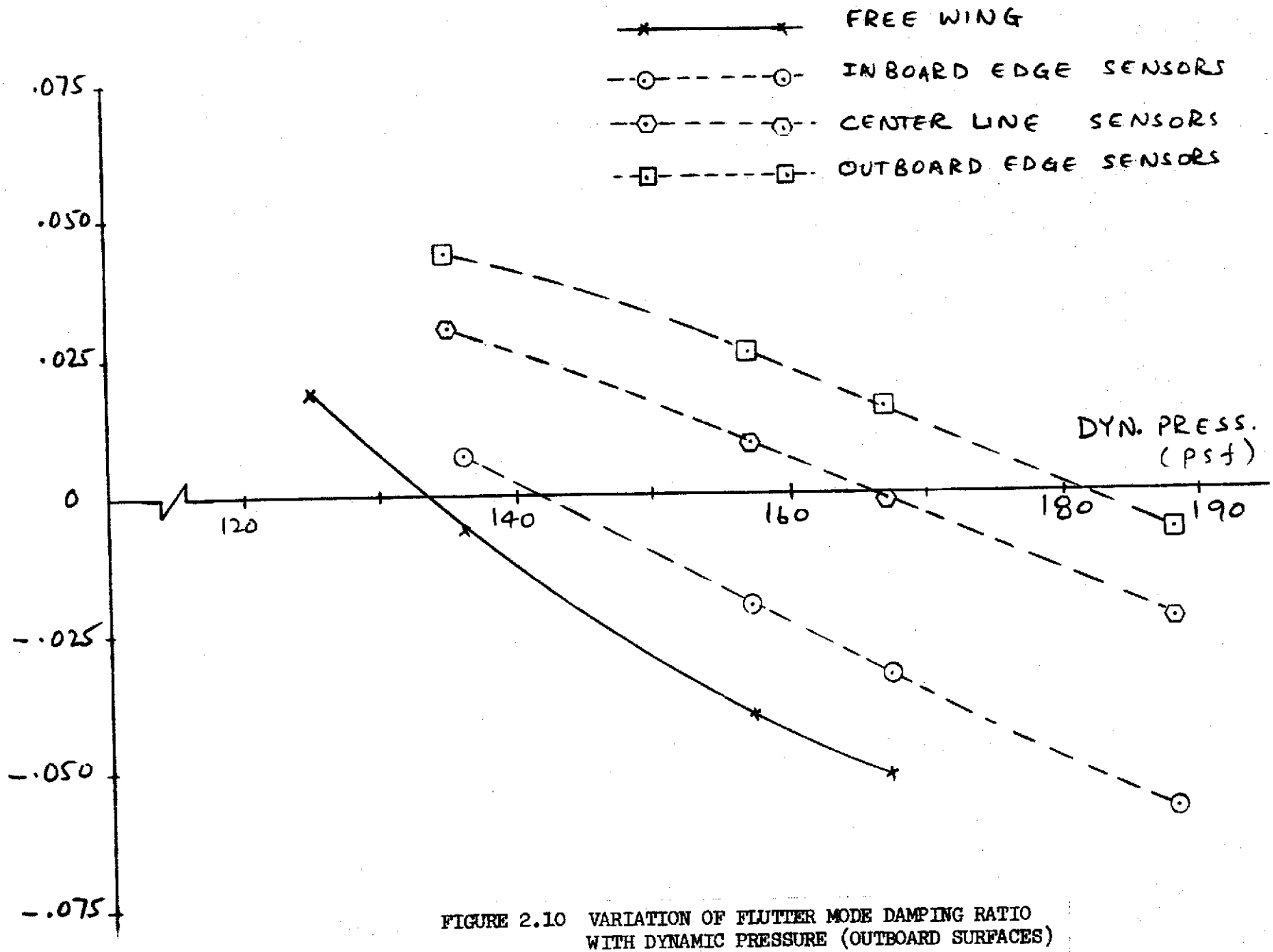


FIGURE 2.10 VARIATION OF FLUTTER MODE DAMPING RATIO WITH DYNAMIC PRESSURE (OUTBOARD SURFACES)

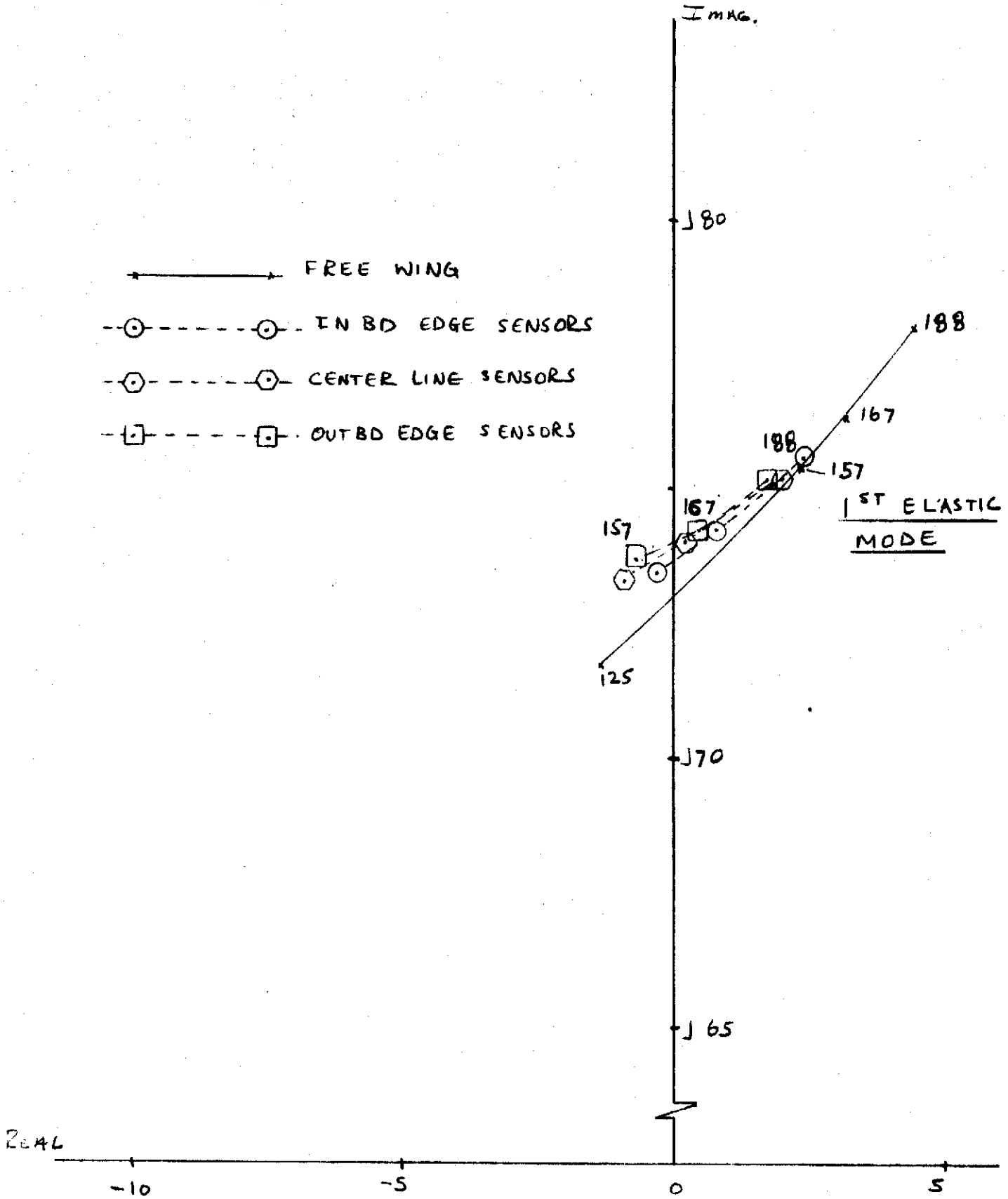


FIGURE 2.11 DYNAMIC PRESSURE ROOT LOCUS
(INBOARD SURFACES)

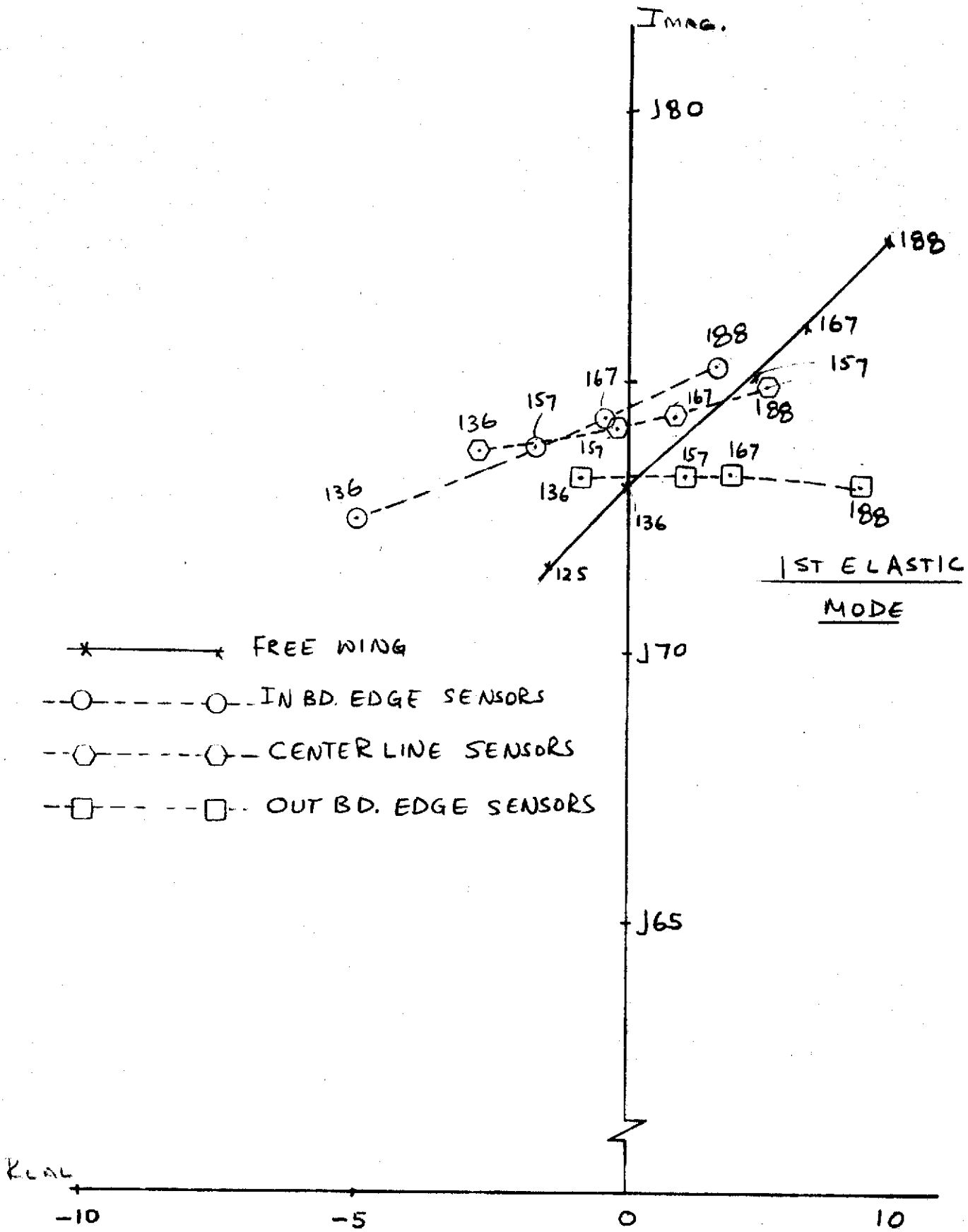


FIGURE 2.12 DYNAMIC PRESSURE ROOT LOCUS
(MID SPAN SURFACES)

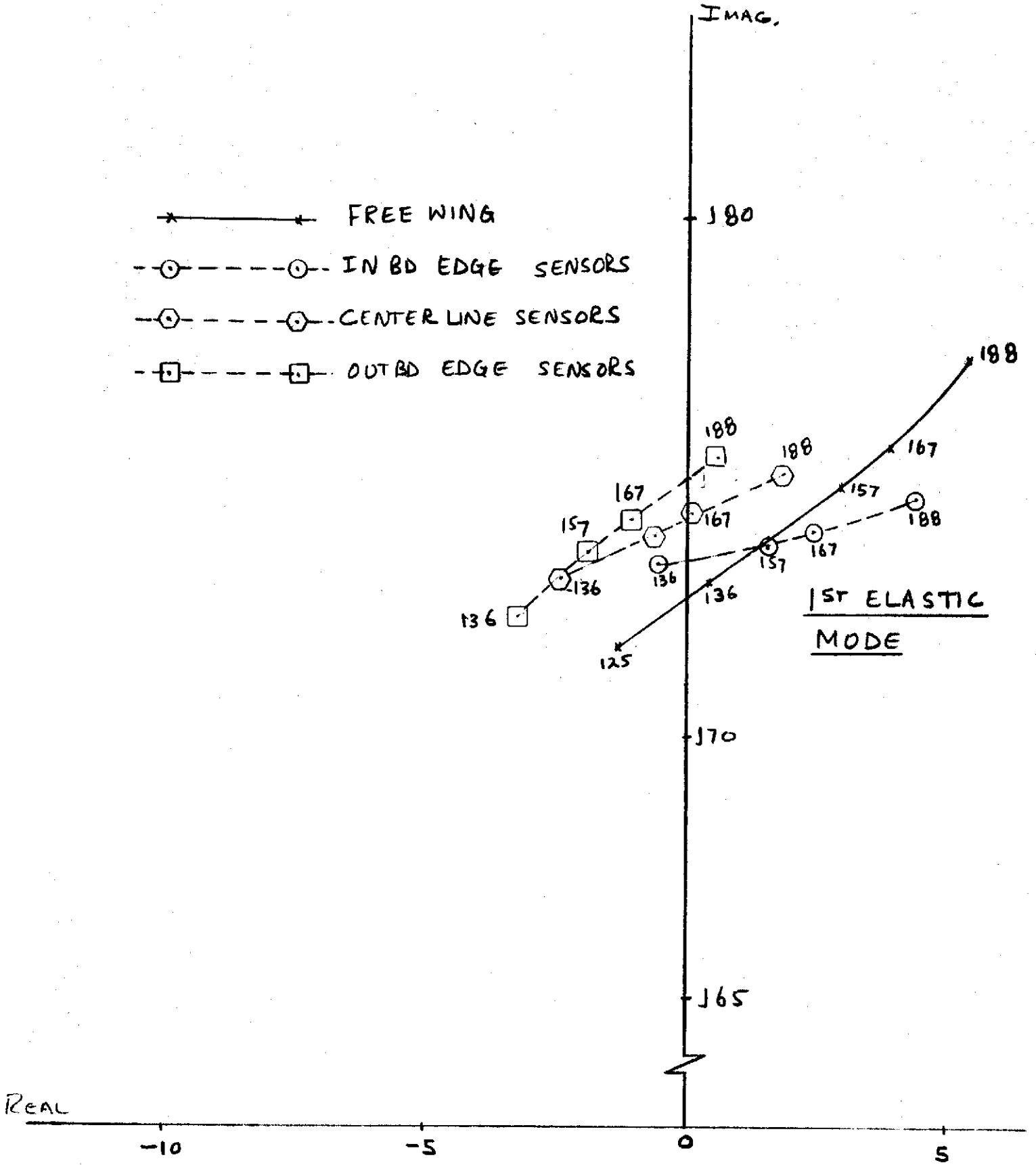


FIGURE 2.13 DYNAMIC PRESSURE ROOT LOCUS
(OUTBOARD SURFACES)

### 2.3.3 SST Airplane Analysis

A brief study was conducted to determine the effects of the flutter suppression system performance due to truncation of the mathematical model. The SST 969-300 configuration equations of motion were truncated to the first seven degrees-of-freedom from the 12 degrees-of-freedom used previously in the airplane analysis. The control surface and sensor locations, and the control law, were identical to that used previously.

The equations of motion were written with velocity and air density as explicit functions to permit varying forward velocity as a function of altitude at constant Mach number to determine flutter speed.

Figure 2.14 shows a dynamic pressure root locus for the two airplane flutter modes for the unaugmented full mathematical model and the seven degree-of-freedom equations. The mode damping ratios as a function of velocity (KCAS) are shown in Figure 2.15 with the flutter suppression system loop open and closed. Although the basic airplane flutter speed was higher for the truncated mathematical model, the improvement attained with the flutter suppression system was about the same.

## 2.4 Remaining Work

The flutter suppression system has been evaluated on the model Mach 0.9 equations of motion with the assumption of ideal actuators driving the control surfaces. The effects of the actual actuator dynamics on system performance must be determined. To minimize mechanization difficulties, the midspan control surfaces with inboard edge feedback sensors will be used during the wind tunnel tests.

The flutter suppression system will also be evaluated at Mach 0.6 and 1.2. The equations have been derived and once the Mach 0.9 analysis is completed, the Mach 0.6 and 1.2 evaluations should be straightforward.

When the control law to be mechanized on the model is finalized, subcritical responses must be generated for correlation of wind tunnel test data with theoretical results. These responses should be generated on the most accurate mathematical model possible, including the non-ideal frequency measuring circuit required by the control law mechanization as well as actual actuator dynamics and the effects of the actuators and hydraulic lines on the wing dynamic behavior. A discussion of the control surface mechanization on the model is presented in Section 3.

## 2.5 Supporting Data

Numerical values of the equation of motion coefficients are presented below. The Mach 0.9 equations contain three structural mass matrices corresponding to the inboard, midspan, and outboard control surface locations with actuator mass at the inboard edge of each surface. The equations for Mach 0.6 and 1.2 contain coefficients for the midspan control surfaces only.

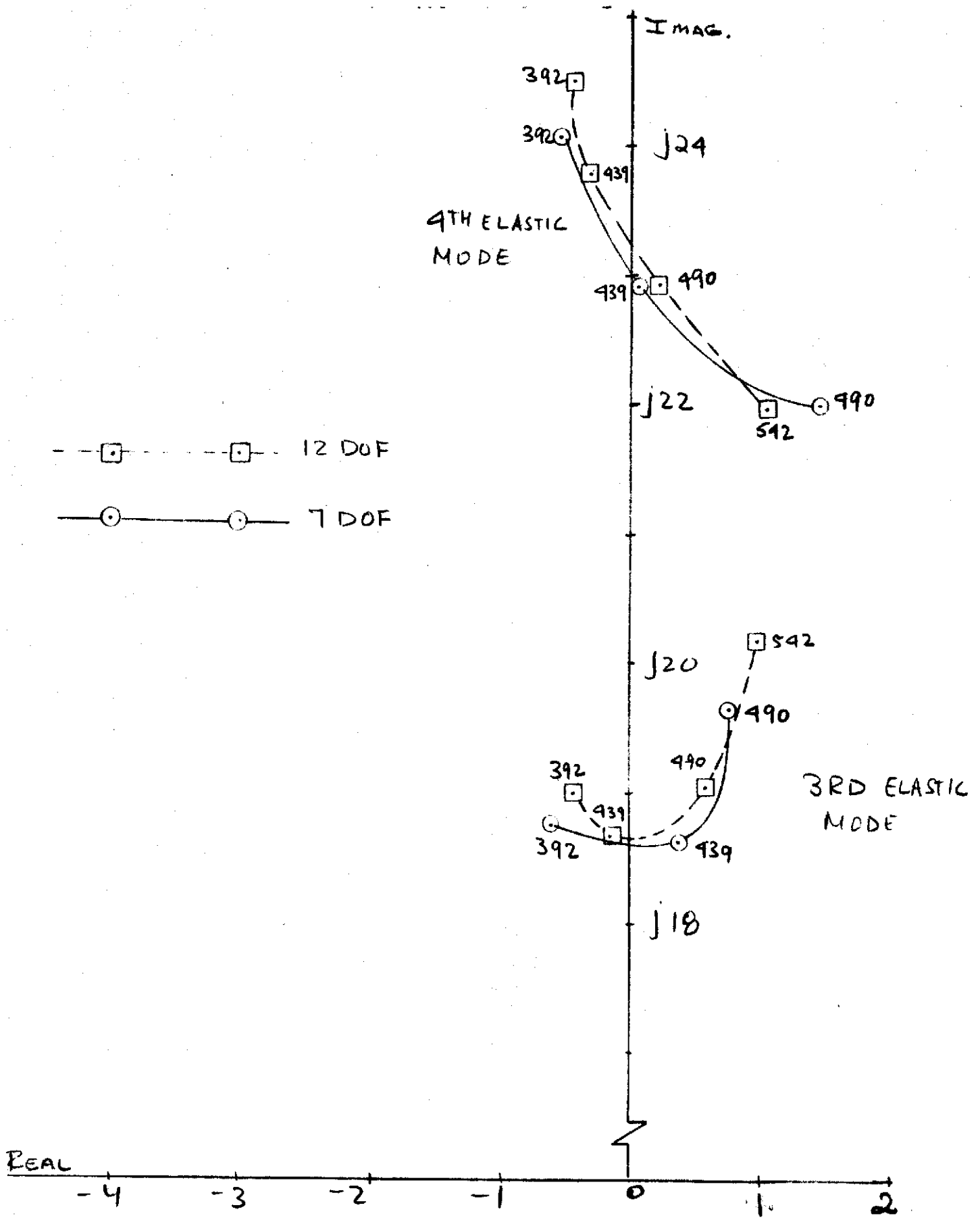


COMPARISON OF 7 AND 12 DOF AIRPLANE MODEL OPEN LOOP ROOT LOCUS
FIGURE 2.14

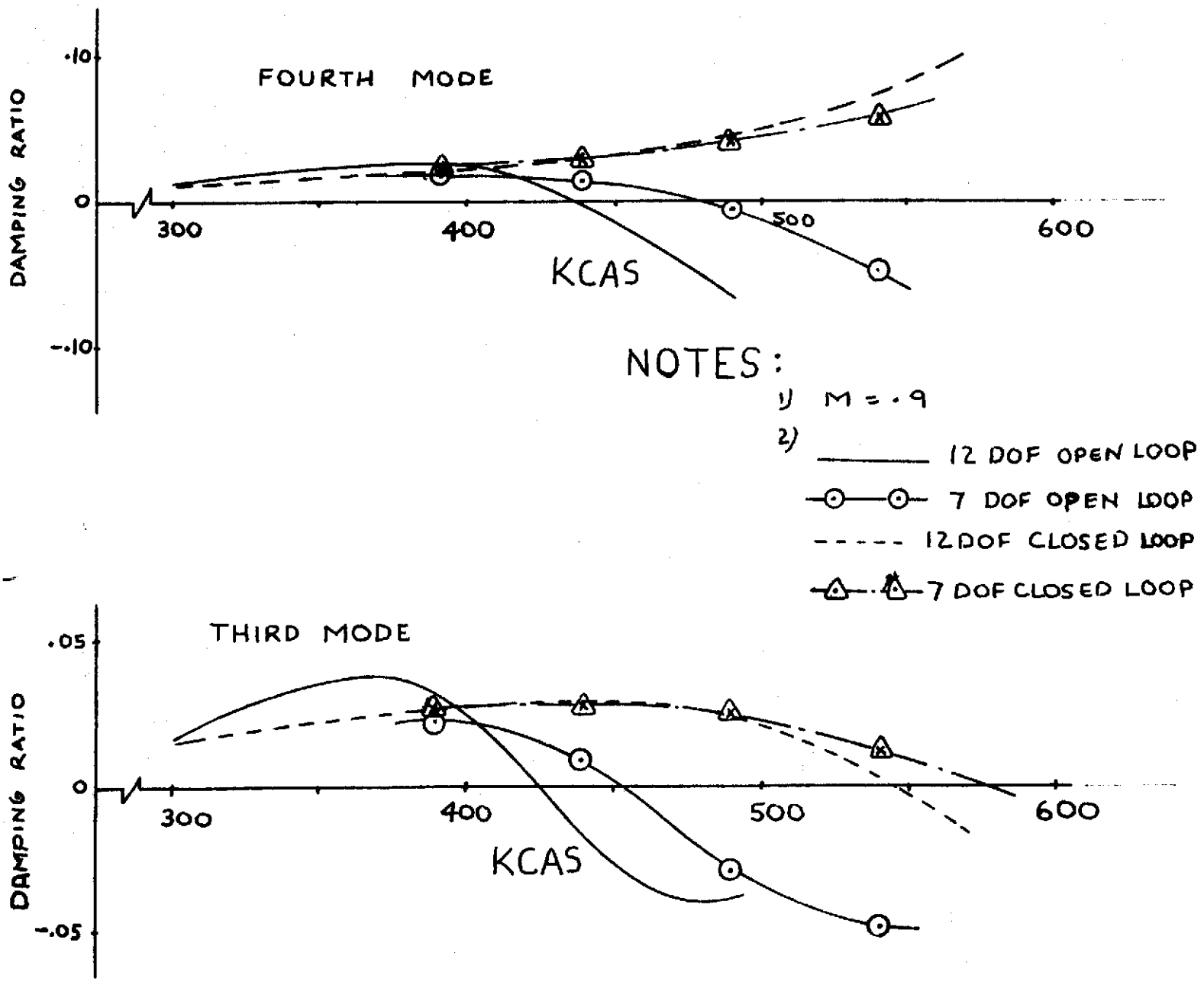


EFFECTS OF LEADING/TRAILING EDGE (MIDSPAN SURFACES)
FLUTTER SUPPRESSION SYSTEM ON SST 969-300 AIRPLANE
FLUTTER CHARACTERISTICS
FIGURE 2.15

The motion variable vector, $\{q_j\}$ , for the Mach 0.9 equations has dimension 12 x 1. The first six elements are the wing elastic modes; the seventh and eighth elements are inboard leading and trailing edge control surface displacements, respectively; the ninth and tenth elements are midspan leading and trailing edge control surface displacements, respectively; and the eleventh and twelfth elements are outboard leading and trailing edge control surface displacements, respectively. For the Mach 0.6 and 1.2 equations, this vector is 8 x 1 with the first six elements the elastic modes and the seventh and eighth elements are the midspan leading and trailing edge control surface displacements, respectively.

The structural mass, stiffness, and damping matrices are constant for the three wind tunnel conditions, except that the Mach 0.6 and 1.2 equations have aerodynamic coefficients for the midspan control surface location only. For these two test conditions, the first six and the ninth and tenth rows and columns of the mass, stiffness, and damping matrices are to be used.

MATRIX 'M' 12 x 12: INBOARD SURFACE MECHANIZATION

ROW 1
7.2683E 02 -6.1328E-02 -9.2844E 00 -2.0736E 00 -2.7918E 00 -1.3119E 01
3.4121E 01 -2.4087E 02 4.3332E 01 -1.9281E 02 4.1346E 01 -6.2867E 01
ROW 2
-6.1327E-02 2.7018E 02 -1.0920E 00 4.1373E-01 -6.3935E 00 8.8776E-01
1.1035E 01 -3.9796E 01 2.9538E 01 -1.0223E 02 3.6191E 01 -5.0941E 01
ROW 3
-9.2844E 00 -1.0920E 00 4.8665E 02 -9.3756E-01 4.2988E 01 5.0809E 00
-4.5802E 01 -1.8365E 01 -3.2175E 01 -6.4271E 01 4.9542E 00 -5.5438E 01
ROW 4
-2.0736E 00 4.1373E-01 -9.3756E-01 9.2830E 01 -1.3930E 01 4.1450E 00
-6.4176E 00 1.3715E 02 -3.1614E 01 8.9813E 01 -9.5785E 00 -2.6748E 01
ROW 5
-2.7918E 00 -6.3935E 00 4.2988E 01 -1.3930E 01 3.4208E 03 -2.6235E 01
-1.9838E 02 -9.0788E 02 -1.8632E 02 -6.0310E 02 -1.1190E 02 -1.0415E 02
ROW 6
-1.3119E 01 8.8776E-01 5.0809E 00 4.1450E 00 -2.6235E 01 1.8451E 02
9.7208E 01 7.3279E 02 2.0682E 02 6.8965E 02 1.8020E 02 2.0033E 02
ROW 7
3.4121E 01 1.1035E 01 -4.5802E 01 -6.4176E 00 -1.9838E 02 9.7208E 01
3.4758E 02 0.0000E-01 0.0000E-01 0.0000E-01 0.0000E-01 0.0000E-01
ROW 8
-2.4087E 02 -3.9796E 01 -1.8365E 01 1.3715E 02 -9.0788E 02 7.3279E 02
0.0000E-01 4.0587E 03 0.0000E-01 0.0000E-01 0.0000E-01 0.0000E-01
ROW 9
4.3332E 01 2.9538E 01 -3.2175E 01 -3.1614E 01 -1.8632E 02 2.0682E 02
0.0000E-01 0.0000E-01 2.8206E 02 0.0000E-01 0.0000E-01 0.0000E-01
ROW10
-1.9281E 02 -1.0223E 02 -6.4271E 01 8.9813E 01 -6.0310E 02 6.8965E 02
0.0000E-01 0.0000E-01 0.0000E-01 1.6917E 03 0.0000E-01 0.0000E-01
ROW11
4.1346E 01 3.6191E 01 4.9543E 00 -9.5785E 00 -1.1190E 02 1.8020E 02
0.0000E-01 0.0000E-01 0.0000E-01 0.0000E-01 1.5570E 02 0.0000E-01
ROW12
-6.2867E 01 -5.0941E 01 -5.5438E 01 -2.6748E 01 -1.0415E 02 2.0033E 02
0.0000E-01 0.0000E-01 0.0000E-01 0.0000E-01 0.0000E-01 2.5553E 02

MATRIX 'M' 12 x 12: MIDSPAN SURFACE MECHANIZATION

ROW 1
7.4782E 02 1.0651E 01 -1.4161E 01 -1.9078E 01 -3.9026E 00 2.9930E-01
3.4121E 01 -2.4087E 02 4.3332E 01 -1.9281E 02 4.1346E 01 -6.2867E 01
ROW 2
1.0651E 01 2.7348E 02 -4.9555E 00 -6.1521E 00 -3.6665E 00 2.0496E 00
1.1035E 01 -3.9796E 01 2.9538E 01 -1.0223E 02 3.6191E 01 -5.0941E 01
ROW 3
-1.4161E 01 -4.9555E 00 4.8703E 02 7.1738E 00 5.9995E 01 -4.7862E 01
-4.5802E 01 -1.8365E 01 -3.2175E 01 -6.4271E 01 4.9542E 00 -5.5438E 01
ROW 4
-1.9078E 01 -6.1521E 00 7.1738E 00 1.0278E 02 -4.7197E 00 5.5530E 00
-6.4176E 00 1.3715E 02 -3.1614E 01 8.9813E 01 -9.5785E 00 -2.6748E 01
ROW 5
-3.9026E 00 -3.6665E 00 5.9995E 01 -4.7197E 00 3.5769E 03 -3.1563E 02
-1.9838E 02 -9.0788E 02 -1.8632E 02 -6.0310E 02 -1.1190E 02 -1.0415E 02
ROW 6
2.9929E-01 2.0495E 00 -4.7862E 01 5.5530E 00 -3.1563E 02 4.2452E 02
9.7208E 01 7.3279E 02 2.0682E 02 6.8965E 02 1.8020E 02 2.0033E 02
ROW 7
3.4121E 01 1.1035E 01 -4.5802E 01 -6.4176E 00 -1.9838E 02 9.7208E 01
3.4758E 02 0.0000E-01 0.0000E-01 0.0000E-01 0.0000E-01 0.0000E-01
ROW 8
-2.4087E 02 -3.9796E 01 -1.8365E 01 1.3715E 02 -9.0788E 02 7.3279E 02
0.0000E-01 4.0587E 03 0.0000E-01 0.0000E-01 0.0000E-01 0.0000E-01
ROW 9
4.3332E 01 2.9538E 01 -3.2175E 01 -3.1614E 01 -1.8632E 02 2.0682E 02
0.0000E-01 0.0000E-01 2.8206E 02 0.0000E-01 0.0000E-01 0.0000E-01
ROW10
-1.9281E 02 -1.0223E 02 -6.4271E 01 8.9813E 01 -6.0310E 02 6.8965E 02
0.0000E-01 0.0000E-01 0.0000E-01 1.6917E 03 0.0000E-01 0.0000E-01
ROW11
4.1346E 01 3.6191E 01 4.9543E 00 -9.5785E 00 -1.1190E 02 1.8020E 02
0.0000E-01 0.0000E-01 0.0000E-01 0.0000E-01 1.5570E 02 0.0000E-01
ROW12
-6.2867E 01 -5.0941E 01 -5.5438E 01 -2.6748E 01 -1.0415E 02 2.0033E 02
0.0000E-01 0.0000E-01 0.0000E-01 0.0000E-01 0.0000E-01 2.5553E 02

MATRIX 'M' 12 x 12: OUTBOARD SURFACE MECHANIZATION

```
ROW 1
 7.8675E 02  4.8375E 01  6.3172E 00 -3.0039E 01 -4.1943E 00  2.0902E 01
 3.4121E 01 -2.4087E 02  4.3332E 01 -1.9281E 02  4.1346E 01 -6.2867E 01
ROW 2
 4.8375E 01  3.0265E 02  3.7696E 00 -2.0526E 01 -6.0701E 00  1.8437E 01
 1.1035E 01 -3.9796E 01  2.9538E 01 -1.0223E 02  3.6191E 01 -5.0941E 01
ROW 3
 6.3172E 00  3.7696E 00  4.8063E 02  1.7884E 00  5.2397E 01 -6.8867E 01
-4.5802E 01 -1.8365E 01 -3.2175E 01 -6.4271E 01  4.9542E 00 -5.5438E 01
ROW 4
-3.0039E 01 -2.0526E 01  1.7884E 00  1.0660E 02  3.1106E 01 -4.8080E 01
-6.4176E 00  1.3715E 02 -3.1614E 01  8.9813E 01 -9.5785E 00 -2.6748E 01
ROW 5
-4.1942E 00 -6.0701E 00  5.2397E 01  3.1106E 01  3.5404E 03 -4.6933E 02
-1.9838E 02 -9.0788E 02 -1.8632E 02 -6.0310E 02 -1.1190E 02 -1.0415E 02
ROW 6
 2.0901E 01  1.8437E 01 -6.8867E 01 -4.8080E 01 -4.6933E 02  7.9956E 02
 9.7208E 01  7.3279E 02  2.0682E 02  6.8965E 02  1.8020E 02  2.0033E 02
ROW 7
 3.4121E 01  1.1035E 01 -4.5802E 01 -6.4176E 00 -1.9838E 02  9.7208E 01
 3.4758E 02  0.0000E-01  0.0000E-01  0.0000E-01  0.0000E-01  0.0000E-01
ROW 8
-2.4087E 02 -3.9796E 01 -1.8365E 01  1.3715E 02 -9.0788E 02  7.3279E 02
 0.0000E-01  4.0587E 03  0.0000E-01  0.0000E-01  0.0000E-01  0.0000E-01
ROW 9
 4.3332E 01  2.9538E 01 -3.2175E 01 -3.1614E 01 -1.8632E 02  2.0682E 02
 0.0000E-01  0.0000E-01  2.8206E 02  0.0000E-01  0.0000E-01  0.0000E-01
ROW10
-1.9281E 02 -1.0223E 02 -6.4271E 01  8.9813E 01 -6.0310E 02  6.8965E 02
 0.0000E-01  0.0000E-01  0.0000E-01  1.6917E 03  0.0000E-01  0.0000E-01
ROW11
 4.1346E 01  3.6191E 01  4.9543E 00 -9.5785E 00 -1.1190E 02  1.8020E 02
 0.0000E-01  0.0000E-01  0.0000E-01  0.0000E-01  1.5570E 02  0.0000E-01
ROW12
-6.2867E 01 -5.0941E 01 -5.5438E 01 -2.6748E 01 -1.0415E 02  2.0033E 02
 0.0000E-01  0.0000E-01  0.0000E-01  0.0000E-01  0.0000E-01  2.5553E 02

COMPILE TIME=     0.51 SEC,EXECUTION TIME=     5.76 SEC,OBJECT CODE=     416
```

MACH 0.9

MATRIX 'D' 12 x 12

THIS MATRIX IS NULL.

MACH 0.9

MATRIX 'K' 12 x 12

| | | | | |
|---|---|---|---|---|
| ROW | 1 | COLUMN | 1 | 1.739400D 06 |
| ROW | 2 | COLUMN | 2 | 2.334800D 06 |
| ROW | 3 | COLUMN | 3 | 1.005800D 07 |
| ROW | 4 | COLUMN | 4 | 5.611200D 06 |
| ROW | 5 | COLUMN | 5 | 2.832599D 08 |
| ROW | 6 | COLUMN | 6 | 2.710200D 07 |

ROWS 7 THROUGH 12 ARE ZERO.

MATRIX '$C_1$' 12 X 12

ROW 1
9.5461E 03 5.5596E 03 7.0879E 03 3.8111E 02 7.3005E 03 -4.1397E 04
2.7884E 04 -3.6098E 04 7.0287E 03 -1.4390E 03 -4.5136E 03 1.7213E 04

ROW 2
4.4723E 03 4.0766E 03 3.9739E 03 -2.1366E 03 -7.5908E 03 1.7285E 04
7.3211E 03 1.8704E 04 -3.2236E 03 2.5318E 04 -3.6786E 02 1.1730E 04

ROW 3
-1.7074E 03 2.8625E 03 5.4510E 03 3.0292E 03 -1.5231E 04 4.0480E 03
4.0344E 03 -8.2189E 04 9.7307E 03 -7.6626E 04 8.6543E 03 -5.7523E 04

ROW 4
7.6810E 02 6.7414E 02 1.2060E 03 3.0355E 03 -1.0989E 04 2.0540E 04
-5.6176E 03 -2.7928E 03 -6.1528E 03 -8.0503E 02 -6.7023E 02 -3.3526E 03

ROW 5
-7.5191E 03 2.8628E 03 1.6969E 04 2.1280E 04 -2.8545E 03 -2.9001E 05
9.0423E 04 -7.0943E 05 9.9519E 04 -5.7082E 05 2.3426E 03 -3.3593E 05

ROW 6
-2.6459E 03 -5.8633E 03 1.7116E 04 -8.1828E 03 8.6830E 04 3.5704E 04
-3.6882E 04 2.3279E 05 -3.5577E 04 1.4562E 05 9.5687E 03 1.0164E 05

ROW 7
1.7955E 03 -7.8678E 01 -7.0723E 03 -4.5973E 03 -7.5494E 02 9.0594E 04
-2.2752E 04 1.5858E 05 -6.8065E 03 1.2875E 05 -4.4554E 03 7.3911E 04

ROW 8
2.5366E 03 1.2065E 03 9.1141E 03 -2.0548E 03 1.3974E 04 5.0738E 04
-1.9501E 04 2.6721E 05 -4.4976E 04 1.4602E 05 -1.6760E 04 1.3157E 05

ROW 9
2.1330E 03 -8.1875E 02 -5.2956E 02 -4.0012E 03 1.6280E 04 4.8662E 04
-1.9643E 04 7.8151E 04 -2.5855E 03 7.8558E 04 -4.3871E 03 5.7091E 04

ROW 10
-5.6653E 03 -6.5935E 03 4.8514E 03 4.0797E 03 4.0065E 04 -1.2930E 04
-1.6154E 04 4.6378E 04 -2.1548E 04 5.0687E 04 2.4103E 03 1.8428E 04

ROW 11
8.5478E 02 4.9323E 01 8.0694E 02 -2.6278E 03 1.3012E 04 2.7233E 04
-1.5050E 04 5.9292E 04 -7.7007E 03 5.6722E 04 1.3131E 02 3.1074E 04

ROW 12
-4.9659E 03 -5.5028E 03 -2.2844E 03 -2.0469E 03 1.5074E 04 -4.1807E 03
-5.0668E 03 9.1340E 03 -4.5077E 03 -2.0700E 04 2.7251E 03 -8.3953E 03

MATRIX '$C_2$' 12 X 12

ROW 1
1.6705E 03 7.9264E 02 5.4130E 01 -1.4970E 01 1.3304E 03 -2.7772E 02
-1.8203E 03 -6.5752E 02 -7.9383E 02 -2.2632E 03 -2.9289E 02 -2.5975E 03

ROW 2
8.8848E 02 7.4688E 02 3.9029E 02 3.8410E 02 9.1696E 02 -2.9966E 03
-3.5372E 02 -1.7343E 03 -8.0198E 01 -2.3859E 03 -6.2382E 02 -1.7279E 03

ROW 3
3.4490E 02 4.4334E 02 7.9910E 02 2.5519E 02 2.3679E 03 -1.6540E 03
-1.4008E 01 5.5340E 03 -5.9770E 02 4.7989E 03 -9.9402E 02 2.5925E 03

ROW 4
-1.6831E 02 9.2801E 01 2.7861E 02 5.0808E 02 1.1302E 02 -1.9468E 03
4.8746E 02 2.0345E 03 7.2578E 02 1.7216E 03 -1.6800E 02 -3.3689E 02

ROW 5
9.9021E 02 -4.5048E 02 3.0612E 02 -2.0443E 03 1.1791E 04 1.2904E 04
-5.6282E 03 3.6540E 04 -5.4079E 03 2.9621E 04 3.1472E 02 1.9463E 04

ROW 6
-6.5211E 02 3.1337E 02 -1.1184E 03 1.3945E 02 -1.3139E 04 1.1394E 04
2.1516E 03 -8.3494E 03 1.2779E 03 -2.7962E 03 -7.8700E 02 -3.1175E 03

ROW 7
1.6465E 02 8.5615E 01 7.2780E 01 2.4389E 02 -1.5685E 03 -5.3703E 03
2.5817E 03 -1.0264E 04 3.7307E 02 -8.3874E 03 2.7486E 02 -4.8496E 03

ROW 8
-2.0028E 03 -4.7510E 02 -5.1813E 02 1.1778E 03 -6.5123E 03 1.0508E 01
1.5568E C3 2.1085E 04 2.7916E 03 -8.8453E 03 8.9505E 02 -9.5699E 03

ROW 9
1.9987E 02 2.7050E 02 -1.8201E 02 1.1540E 01 -2.4154E 03 -1.7568E 03
1.5317E 03 -5.3167E 03 1.0223E 03 -5.1715E 03 1.3303E 02 -3.7402E 03

ROW 10
-1.2489E 03 -5.6559E 02 -9.4995E 02 -1.3743E 01 -7.4048E 03 6.9657E 03
1.1489E 03 -1.5265E 03 1.2939E 03 1.6583E 04 2.0522E 02 -4.2349E 03

ROW 11
3.5147E 02 3.8958E 02 5.1264E 01 7.9649E 01 -1.9351E 03 -8.4662E 01
1.0868E 03 -3.1943E 03 7.3777E 02 -3.1029E 03 4.5643E 02 -1.5648E 03

ROW 12
-2.8029E 02 -1.1244E 02 -4.9631E 02 -2.4835E 02 -2.9284E 03 3.9663E 03
3.3752E 02 -1.6897E 03 2.6709E 02 1.5070E 03 -2.9931E 01 6.5071E 03

MATRIX '$C_3$' 12 X 12

ROW 1
7.6010E 00 -3.5711E 00 4.3557E 01 1.1287E 01 1.7535E 02 -2.7407E 02
-5.6567E-01 -4.3697E 02 6.5606E 00 -5.1503E 02 2.6547E 00 -4.6098E 02

ROW 2
3.4816E 00 -2.7536E 00 2.3084E 01 9.3326E 00 1.0747E 02 -1.5158E 02
-4.3322E 00 -1.4205E 02 -5.1231E 00 -2.6387E 02 2.0084E 00 -3.2716E 02

ROW 3
-6.1740E 00 -3.0211E-01 -6.4186E 00 6.9502E 00 -5.1282E 01 -8.0458E 00
1.6481E 01 1.9483E-01 2.9519E 01 -1.0736E 02 3.3536E 01 -2.6096E 02

ROW 4
-2.1837E 00 -3.4294E 00 -2.0895E 00 4.0230E-01 -2.0547E 01 3.2390E 01
-7.8802E 00 1.3042E 02 -2.1445E 00 1.0546E 02 1.8164E 01 -1.1626E 02

ROW 5
-2.5177E 01 -7.2157E-01 -5.8300E 01 -7.9895E 00 -4.3329E 02 2.2238E 02
1.2963E 02 -6.5390E 02 1.8493E 02 -7.1281E 02 1.7402E 02 -3.9391E 02

ROW 6
1.7939E 01 1.8220E 01 5.0111E 01 2.5803E 01 3.1127E 02 -4.1082E 02
-1.9063E 01 5.1092E 02 -1.3536E 02 7.6645E 02 -2.3061E 02 7.0130E 02

ROW 7
3.5358E 00 -3.8162E 00 1.6843E 01 -6.4372E 00 1.1436E 02 -2.1478E 01
-4.8563E 02 -3.0861E 01 -3.0157E 01 -2.5608E 01 -4.5816E 00 -1.5379E 01

ROW 8
-7.8735E-01 1.5306E 00 -1.1515E 01 -7.6126E-01 -1.6044E 01 6.4243E 01
-2.3768E 00 9.2418E 02 -6.2697E 00 4.6813E 02 -1.0459E 01 1.7828E 02

ROW 9
8.6889E 00 -4.5701E 00 2.4964E 01 -2.2376E 00 1.4891E 02 -1.0665E 02
-3.6251E 01 -4.2471E 01 -4.1502E 02 -3.5850E 01 -3.0731E 01 -2.1311E 01

ROW 10
2.3839E-01 2.6990E 00 -6.7166E 00 -1.1133E 00 -1.4352E 01 3.7953E 01
-9.7230E-01 2.7384E 02 -3.2616E 00 7.0704E 02 -8.8403E 00 3.0016E 02

ROW 11
8.3398E 00 1.5715E 00 2.8863E 01 1.1887E 01 1.4774E 02 -1.8468E 02
-4.2305E 00 -5.3389E 01 -3.4549E 01 -4.8901E 01 -3.7377E 02 -2.9798E 01

ROW 12
7.6270E-01 2.4018E 00 -2.4082E 00 -3.1765E-01 -4.1388E 00 1.0087E 01
-1.9160E-01 3.6560E 01 -7.1538E-01 9.8481E 01 -2.6988E 00 3.2455E 02

MATRIX '$D_1$' 12 X 12

ROW 1
-3.8963E-01 -2.6581E-02 7.4763E-02 5.8770E-01 -1.7933E 00 -5.3592E 00
1.0733E 00 -1.8130E 01 2.4185E 00 -1.7237E 01 1.3049E 00 -1.0905E 01

ROW 2
2.8259E-02 7.3967E-02 3.8757E-01 2.1889E-01 6.6017E-01 -3.4866E 00
6.3829E-01 -5.7048E 00 7.0565E-01 -3.4562E 00 -2.4847E-01 -4.3527E-01

ROW 3
-9.6866E-02 -3.9988E-03 -1.3268E 00 -2.6053E-01 -3.0646E 00 1.0054E 01
-1.7867E 00 1.0673E 01 -4.5425E-01 6.9562E 00 9.1848E-01 2.1138E 00

ROW 4
8.4695E-02 1.7019E-02 2.0733E-01 -4.9515E-02 5.0360E-01 -5.8009E-01
7.1957E-02 2.5413E-01 -2.9475E-01 8.1360E-01 -3.1209E-01 8.0377E-01

ROW 5
-2.3451E 00 -6.4414E-01 -8.4280E 00 -2.3052E-01 -2.6573E 01 4.7544E 01
-8.9257E 00 7.3517E 00 3.4887E 00 -2.1637E 01 1.1868E 01 -3.7099E 01

ROW 6
-2.9784E-01 2.2923E-01 1.7037E 00 7.2501E-01 3.9927E 00 -1.6180E 01
3.7764E 00 -1.8142E 01 1.4225E 00 -1.0432E 01 -1.8976E 00 -3.8878E 00

ROW 7
7.9961E-01 1.2310E-01 1.7484E 00 -3.3568E-01 6.8646E 00 -6.2642E 00
6.8414E-01 9.6328E 00 -2.2884E 00 1.5128E 01 -2.4364E 00 1.5876E 01

ROW 8
1.2416E-01 3.0556E-01 1.4521E 00 5.6885E-01 5.4383E 00 -1.0869E 01
1.6544E 00 -6.0650E 00 5.2786E-01 1.1074E 00 -2.1719E 00 6.6897E 00

ROW 9
3.5254E-01 -2.4632E-02 1.5462E 00 -1.0479E-01 4.0278E 00 -7.7825E 00
1.4881E 00 -4.9205E 00 -9.1957E-01 -5.6152E-01 -1.8100E 00 3.0364E 00

ROW 10
-2.8069E-02 1.3026E-02 6.5387E-01 1.4849E-01 2.4038E 00 -4.4033E 00
9.4530E-01 -2.2390E 00 6.1045E-03 9.8376E-01 -1.1272E 00 2.0941E 00

ROW 11
1.7776E-01 1.0151E-01 9.8143E-01 9.2114E-02 2.7845E 00 -6.5899E 00
1.2704E 00 -1.7813E 00 -2.1070E-01 1.1444E 00 -1.1267E 00 2.9155E 00

ROW 12
-1.2377E-02 -1.4488E-02 1.3403E-01 -8.9169E-05 4.4168E-01 -7.2738E-01
2.3903E-01 -4.2867E-01 -5.8060E-02 3.9188E-01 -2.7893E-01 4.4718E-01

MATRIX '$d_1$' 1 X 12

ROW 1

| | | | | | |
|---|---|---|---|---|---|
| 3.0000E-03 | 3.0000E-03 | 3.0000E-03 | 3.0000E-03 | 3.0000E-03 | 3.0000E-03 |
| 3.0000E-03 | 3.0000E-03 | 3.0000E-03 | 3.0000E-03 | 3.0000E-03 | 3.0000E-03 |

MATRIX '$D_2$' 12 X 12

ROW 1
1.4513E 01 3.2915E 00 1.5738E 01 -1.4290E C1 9.9497E 01 2.6848E 01
-1.0380E 01 4.4485E 02 -6.8389E 01 4.9389E 02 -5.6169E 01 3.7616E 02

ROW 2
4.3993E 00 4.6936E-01 -1.3576E 01 -1.0411E 01 3.9756E-01 1.4967E 02
-2.3812E 01 3.9244E 02 -3.7696E 01 3.4658E 02 -1.0769E 01 2.1586E 02

ROW 3
-8.7769E 00 -2.7055E 00 3.0759E 01 1.5446E 01 3.6979E 01 -3.2677E 02
5.9426E 01 -5.7547E 02 4.3259E 01 -5.1664E 02 4.7826E 00 -3.3679E 02

ROW 4
-1.5242E 00 -9.8026E-01 -6.3062E 00 3.0322E-01 -7.9325E 00 2.9946E 01
-5.2177E 00 2.9415E 01 4.9833E 00 8.8156E 00 8.1611E 00 -3.0872E-01

ROW 5
-8.6377E 00 -5.0649E 00 3.1711E 02 8.5604E 01 6.4598E 02 -2.5106E 03
4.2669E 02 -3.5323E 03 1.7024E 02 -2.7149E 03 -1.5237E 02 -1.4452E 03

ROW 6
2.1308E 01 -3.6342E 00 -4.1114E 01 -3.1982E 01 -1.3653E 02 4.8447E 02
-1.1331E 02 5.6909E 02 -5.3253E 01 4.0959E 02 4.9099E 01 2.2237E 02

ROW 7
-4.2653E 00 5.2496E 00 -9.2290E 01 -1.1134E 01 -2.0177E 02 6.1307E 02
-7.8175E 01 8.6153E 02 -1.2240E 00 6.6669E 02 1.5169E 01 3.4813E 02

ROW 8
6.7823E 00 -7.6610E 00 -4.4903E 01 -2.8469E 01 -1.5105E 02 4.1634E 02
-6.4421E 01 4.4428E 02 -4.7042E 01 2.3695E 02 4.5309E 01 -2.1259E 01

ROW 9
4.6182E 00 6.1454E 00 -5.9905E 01 -1.0686E 01 -9.3745E 01 4.4013E 02
-7.5779E 01 7.8273E 02 -2.0423E 01 6.7461E 02 2.2467E 01 4.2890E 02

ROW 10
6.6302E 00 1.2609E 00 -2.0685E 01 -9.3781E 00 -6.6337E 01 1.7413E 02
-3.7415E 01 2.0071E 02 -1.5159E 01 1.0172E 02 2.5506E 01 3.1361E 01

ROW 11
4.3949E 00 2.0971E-01 -3.6235E 01 -1.2319E 01 -7.6890E 01 3.1891E 02
-5.3938E 01 4.0033E 02 -2.2912E 01 3.3663E 02 9.4659E 00 2.0770E 02

ROW 12
1.7463E 00 8.8404E-01 -4.2975E 00 -9.9553E-01 -1.1254E 01 3.0617E 01
-9.6478E 00 4.6580E 01 -1.7337E 00 1.9076E 01 6.7206E 00 8.5784E 00

MATRIX '$d_2$' 1 X 12

ROW 1

| | | | | | |
|---|---|---|---|---|---|
| 9.0000E-03 | 9.0000E-03 | 9.0000E-03 | 9.0000E-03 | 9.0000E-03 | 9.0000E-03 |
| 9.0000E-03 | 9.0000E-03 | 9.0000E-03 | 9.0000E-03 | 9.0000E-03 | 9.0000E-03 |

MATRIX '$D_3$' 12 X 12

ROW 1
-4.1001E 01 -8.5356E 00 -1.3365E 02 3.0157E 01 -5.7912E 02 4.9503E 02
-3.7458E 01 -8.8464E 02 2.3431E 02 -1.2067E 03 2.4141E 02 -1.0393E 03

ROW 2
-1.7746E 01 4.1547E 00 -2.9263E 00 3.6125E 01 -1.8744E 02 -2.5595E 02
6.7257E 01 -1.1862E 03 1.5974E 02 -1.0911E 03 7.0214E 01 -7.2060E 02

ROW 3
4.1318E 01 5.2318E 00 -4.3543E 01 -5.9188E 01 -6.2769E 00 8.3985E 02
-2.0159E 02 1.4728E 03 -1.7634E 02 1.3894E 03 -3.8601E 01 9.3225E 02

ROW 4
5.6176E 00 7.1805E 00 2.4934E 01 1.6915E 00 3.5982E 01 -1.2834E 02
2.4860E 01 -8.0951E 01 -2.0626E 01 7.3255E 00 -4.4439E 01 3.2904E 01

ROW 5
1.4432E 02 -2.5445E 01 -7.8839E 02 -4.1060E 02 -1.3081E 03 8.0301E 03
-1.7170E 03 1.1600E 04 -9.6005E 02 9.0615E 03 3.8217E 02 4.8568E 03

ROW 6
-1.1306E 02 1.6201E 01 9.8463E 01 1.6680E 02 5.8640E 02 -1.7514E 03
5.3704E 02 -1.3334E 03 3.0068E 02 -7.7404E 02 -2.2462E 02 -1.6100E 02

ROW 7
-1.4146E 01 -8.1473E 00 2.4280E 02 5.4049E 01 3.7930E 02 -1.9599E 03
3.4671E 02 -3.0370E 03 1.9418E 01 -2.4201E 03 3.1486E 01 -1.3323E 03

ROW 8
-6.2314E 01 2.6527E 01 1.6262E 02 1.5054E 02 6.0249E 02 -1.7249E 03
2.8194E 02 -2.0198E 03 2.7591E 02 -1.2339E 03 -1.4132E 02 -1.8575E 00

ROW 9
-3.3757E 01 -1.0847E 01 1.3141E 02 4.9288E 01 9.7467E 01 -1.2630E 03
3.1736E 02 -2.2366E 03 1.2327E 02 -2.0011E 03 -9.6342E 01 -1.3447E 03

ROW 10
-5.0625E 01 -1.3906E 01 7.3491E 01 5.1182E 01 2.3122E 02 -7.0332E 02
1.7606E 02 -1.0324E 03 1.0770E 02 -6.2517E 02 -8.3946E 01 -3.0074E 02

ROW 11
-2.8068E 01 8.2371E 00 7.4442E 01 5.8097E 01 1.7330E 02 -9.7675E 02
2.1927E 02 -8.9913E 02 1.2071E 02 -7.7190E 02 -6.0588E 00 -4.5589E 02

ROW 12
-1.2839E 01 -5.8845E 00 1.4336E 01 6.1077E 00 2.7504E 01 -1.1222E 02
4.7196E 01 -2.5649E 02 1.7967E 01 -1.2902E 02 -2.3873E 01 -7.7980E 01

MATRIX '$d_3$' 1 X 12

ROW 1

| | | | | | |
|---|---|---|---|---|---|
| 1.5000E-02 | 1.5000E-02 | 1.5000E-02 | 1.5000E-02 | 1.5000E-02 | 1.5000E-02 |
| 1.5000E-02 | 1.5000E-02 | 1.5000E-02 | 1.5000E-02 | 1.5000E-02 | 1.5000E-02 |

MATRIX '$D_4$' 12 X 12

ROW 1
2.4698E 01 6.2633E 00 1.5249E 02 -9.8617E 00 6.6995E 02 -7.2666E 02
8.4985E 01 6.3286E 02 -1.9936E 02 9.7672E 02 -2.4404E 02 9.2221E 02

ROW 2
1.0547E 01 -8.5182E 00 2.3376E 01 -2.8108E 01 2.6032E 02 6.9608E 01
-4.1052E 01 9.8037E 02 -1.5019E 02 9.1038E 02 -7.4982E 01 6.2376E 02

ROW 3
-4.5064E 01 -8.8073E 00 2.4608E 01 5.6734E 01 2.2151E 00 -6.8127E 02
1.8080E 02 -1.2040E 03 1.7815E 02 -1.1734E 03 4.9577E 01 -7.9061E 02

ROW 4
-5.6863E 00 -1.0229E 01 -2.7358E 01 -5.8881E 00 -6.0655E 01 1.5194E 02
-3.0626E 01 1.4945E 01 1.7770E 01 -7.9392E 01 5.7785E 01 -9.9247E 01

ROW 5
-1.9291E 02 2.0667E 01 6.2636E 02 4.2987E 02 1.0318E 03 -6.9596E 03
1.6618E 03 -1.0415E 04 1.0790E 03 -8.2129E 03 -2.8032E 02 -4.3607E 03

ROW 6
1.5449E C2 9.2314E 00 -9.5128E 01 -1.9228E 02 -5.8613E 02 1.7564E 03
-6.0236E 02 1.6778E 03 -4.2269E 02 1.1134E 03 1.6604E 02 3.1261E 02

ROW 7
2.3423E 01 5.4258E 00 -1.9617E 02 -5.3145E 01 -2.7970E 02 1.6662E 03
-3.7359E 02 2.7116E 03 1.0205E 01 2.1837E 03 -5.3675E 01 1.2245E 03

ROW 8
9.6640E 01 -1.2599E 01 -1.5650E 02 -1.7139E 02 -5.7696E 02 1.7171E 03
-2.8988E 02 2.3158E 03 -3.4044E 02 1.6162E 03 9.0735E 01 2.2684E 02

ROW 9
3.8510E 01 7.6309E 00 -1.0128E 02 -5.3275E 01 -7.0402E 01 1.0660E 03
-3.2352E 02 1.7796E 03 -1.6312E 02 1.6300E 03 1.1744E 02 1.1267E 03

ROW 10
7.3539E 01 2.6220E 01 -6.3283E 01 -5.5990E 01 -1.5952E 02 6.3736E 02
-1.9061E 02 1.2503E 03 -1.4412E 02 8.4979E 02 5.9075E 01 5.2484E 02

ROW 11
3.5752E 01 -5.7490E 00 -5.7555E 01 -6.1898E 01 -1.6771E 02 8.7524E 02
-2.1832E 02 6.9490E 02 -1.4062E 02 6.1838E 02 -2.8140E 01 3.4229E 02

ROW 12
1.8074E 01 8.5987E 00 -1.0649E 01 -6.2147E 00 1.3903E 00 8.0755E 01
-5.2434E 01 3.1915E 02 -2.6823E 01 1.7576E 02 1.9267E 01 1.2423E 02

MATRIX '$d_4$' 1 X 12

ROW 1

| | | | | | |
|---|---|---|---|---|---|
| 2.1000E-02 | 2.1000E-02 | 2.1000E-02 | 2.1000E-02 | 2.1000E-02 | 2.1000E-02 |
| 2.1000E-02 | 2.1000E-02 | 2.1000E-02 | 2.1000E-02 | 2.1000E-02 | 2.1000E-02 |

MATRIX 'C$_1$' 8 X 8

ROW 1
2.0201E 04 1.0501E 04 -8.8509E 02 -4.0262E 03 -1.4376E 04 2.1562E 04
5.1154E 03 6.9209E 03

ROW 2
1.0488E 04 8.3595E 03 2.5310E 03 -8.1365E 02 -1.2556E 04 1.9407E 04
2.6551E 03 7.9292E 03

ROW 3
1.8045E 03 5.0609E 03 7.8430E 03 2.7232E 03 5.7608E 03 4.4630E 03

-6.8414E 02 -1.2003E 03

ROW 4
-1.5160E 03 6.5038E 02 4.1986E 03 6.2190E 03 -4.7119E 00 -9.6726E 03
-2.7646E 03 5.5280E 02

ROW 5
6.4537E 03 1.9413E 03 9.0176E 03 -5.1823E 03 7.9361E 04 -6.6960E 04
-4.7343E 03 -4.4855E 04

ROW 6
-1.6705E 04 -5.7836E 03 -6.0567E 03 6.4927E 02 -6.8696E 04 1.1998E 05
1.6866E 04 6.8343E 03

ROW 7
1.5467E 02 -1.5942E 02 -1.0369E 03 -1.4290E 03 -5.7554E 03 1.8933E 04
9.1459E 03 4.4481E 03

ROW 8
-1.2004E 04 -6.7918E 02 -2.3800E 03 4.6653E 03 -1.9241E 04 1.9234E 04
-3.5203E 02 5.0081E 04

MACH 0.6

MATRIX 'C2' 8 X 8

ROW 1
-1.5698E 03 -6.4661E 02 9.5133E 02 3.1098E 02 5.7941E 03 -7.2531E 03
-9.4633E 02 -3.9740E 03

ROW 2
-7.3631E 02 -5.6176E 02 7.5104E 02 4.0109E 02 2.9654E 03 -4.8371E 03
-5.3004E 02 -2.5107E 03

ROW 3
-1.7231E 02 2.2122E 02 8.9028E 02 4.2083E 02 1.7420E 03 -2.7360E 03
2.1228E 02 -1.2695E 03

ROW 4
-2.2652E 02 -3.7073E 01 -5.9045E 01 3.3301E 02 -1.2215E 03 3.9574E 02
5.5631E 02 1.1814E 03

ROW 5
-1.0201E 03 -1.0461E 03 1.5973E 03 -1.6013E 02 9.2618E 03 -5.1488E 03
1.1920E 03 -7.7428E 03

ROW 6
1.8271E 03 1.4735E 03 4.0551E 02 -6.6489E 02 -4.3669E 03 9.3129E 03
-2.2974E 03 1.3192E 04

ROW 7
7.2438E 02 4.1441E 02 -4.0210E 02 -4.2103E 02 -2.0537E 03 1.5752E 03
-6.4399E 02 -8.9256E 01

ROW 8
-3.4428E 02 -1.3514E 02 -5.8172E 02 -1.5265E 02 -3.7766E 03 5.0806E 03
9.8691E 01 1.6300E 04

MATRIX '$C_3$' 8 X 8

ROW 1
6.7642E 00 -4.1394E-01 3.4064E 01 9.6679E 00 1.3903E 02 -2.1626E 02
3.2497E 00 -3.7638E 02

ROW 2
3.3889E 00 -4.9519E-01 1.9148E 01 9.0690E 00 8.7332E 01 -1.2966E 02
-3.7426E 00 -2.0471E 02

ROW 3
-5.4654E 00 1.1496E 00 -7.9788E 00 6.0104E 00 -5.2429E 01 3.3300E 00
2.5414E 01 -5.4585E 01

ROW 4
-2.0698E 00 -2.6563E 00 -2.4685E 00 5.3893E-01 -2.2143E 01 3.1169E 01
-3.2412E-01 8.9613E 01

ROW 5
-2.3920E 01 2.4171E 00 -6.5515E 01 -1.3170E 01 -4.1581E 02 2.8404E 02
1.6211E 02 -3.5907E 02

ROW 6
1.5483E 01 1.0824E 01 5.5762E 01 3.2458E 01 3.1415E 02 -4.4156E 02
-1.3092E 02 4.3382E 02

ROW 7
9.9408E 00 -3.7597E 00 2.8788E 01 -1.4385E 00 1.6807E 02 -1.3390E 02
-4.4658E 02 -5.9373E 01

ROW 8
-4.8859E-01 -4.9457E-01 -3.9125E 00 -5.7724E-01 -8.7666E 00 2.6031E 01
-3.8031E 00 5.2264E 02

MATRIX '$D_1$' 8 X 8

ROW 1
3.8814E-02 4.4426E-02 -8.2333E-02 -9.1808E-03 -3.5450E-01 -1.0764E-01
2.3468E-02 2.3795E-01

ROW 2
3.8685E-02 2.6344E-02 1.8294E-02 -1.9479E-02 5.0892E-02 1.1487E-01
-3.1710E-02 3.5812E-01

ROW 3
4.5372E-02 -3.4993E-03 6.9160E-03 -1.7116E-02 1.8608E-01 2.5142E-01
-2.0128E-02 1.7698E-01

ROW 4
-2.7566E-02 -8.8435E-03 8.1493E-03 1.0801E-02 -2.3766E-03 -8.5505E-02
1.2041E-02 -1.4347E-01

ROW 5
4.5345E-02 -4.2652E-02 -3.1703E-01 1.1621E-01 -5.5835E-01 -4.7284E-01
1.9788E-01 -1.3660E 00

ROW 6
1.2766E-01 1.4542E-02 -1.2867E-01 -1.5990E-01 -3.1998E-01 2.1220E 00
-4.8409E-02 2.3087E 00

ROW 7
2.0771E-02 1.3274E-02 3.5358E-02 -5.3653E-02 3.3928E-02 4.6261E-01
-4.4746E-02 7.3141E-01

ROW 8
-1.9350E-02 -1.2903E-02 9.5901E-03 -1.2150E-02 2.8153E-03 1.6662E-01
-3.2754E-03 4.7058E-02

MATRIX '$d_1$' 1 X 8

ROW 1
3.0000E-03 3.0000E-03 3.0000E-03 3.0000E-03 3.0000E-03 3.0000E-03
3.0000E-03 3.0000E-03

MATRIX '$D_2$' 8 X 8

ROW 1
-1.4591E 00 -7.7930E-01 -2.3938E 00 -1.1741E 00 -6.6840E 00 3.3461E 01
6.1977E-02 4.1557E 01

ROW 2
-1.4012E 00 -5.1221E-01 -4.2514E 00 3.1087E-01 -1.4409E 01 1.2857E 01
1.9281E 00 1.5056E 01

ROW 3
-2.0573E 00 -3.5197E-01 1.9999E 00 1.1976E 00 8.8318E-01 -2.3747E 01
6.0818E-01 -3.1990E 01

ROW 4
1.0949E 00 2.6345E-01 3.7977E-01 -3.5128E-01 2.6110E 00 1.1867E-01
-6.5304E-01 4.0047E-01

ROW 5
-3.5245E 00 -1.1603E 00 3.0588E 01 -1.6684E 00 8.4048E 01 -7.5624E 01
-1.0672E 01 -1.0539E 02

ROW 6
-5.2238E 00 7.6416E-01 -6.9120E 00 5.4090E 00 -2.9069E 01 -3.1609E 01
5.0433E 00 -6.7264E 00

ROW 7
-4.2203E-01 5.1212E-01 -8.5685E 00 1.1596E 00 -2.6250E 01 1.7225E 01
3.1605E 00 3.0805E 01

ROW 8
7.8461E-01 4.1376E-01 -1.6686E-02 5.4282E-01 1.4314E 00 -8.6161E 00
1.2943E-01 -5.8504E 00

MATRIX '$d_2$' 1 X 8

ROW 1
9.0000E-03 9.0000E-03 9.0000E-03 9.0000E-03 9.0000E-03 9.0000E-03
9.0000E-03 9.0000E-03

MATRIX '$D_3$' 8 X 8

ROW 1
9.1101E 00 7.4648E 00 -1.1235E 01 6.7143E 00 -3.6324E 01 -1.0097E 02

5.4819E 00 -8.7502E 01

ROW 2
7.0887E 00 4.6226E 00 1.2940E 01 -1.2379E 00 4.5880E 01 -3.5677E 01
-8.1043E 00 -1.6385E 01

ROW 3
1.1201E 01 9.8839E-02 5.7010E 00 -6.7336E 00 5.0195E 01 7.6944E 01
-8.7647E 00 9.1984E 01

ROW 4
-6.1335E 00 -1.8248E 00 -8.8866E-01 1.8653E 00 -1.1104E 01 -5.3644E 00
3.7001E 00 -1.3941E 01

ROW 5
2.6367E 01 -4.9133E 00 -1.0021E 02 6.5014E 00 -2.2181E 02 1.9556E 02
3.7237E 01 1.8167E 02

ROW 6
2.8929E 01 1.9345E 00 2.2368E 01 -3.0390E 01 1.1215E 02 2.5052E 02
-2.9107E 01 2.0766E 02

ROW 7
-9.2261E-01 1.3774E 00 2.4874E 01 -6.0340E 00 6.8356E 01 -1.5517E 01
-1.1896E 01 -2.3387E 01

ROW 8
-4.5385E 00 -2.3092E 00 2.4467E 00 -3.0591E 00 -2.2390E 00 3.9706E 01
-1.3037E 00 2.0643E 01

MATRIX '$d_3$' 1 X 8

ROW 1
1.5000E-02 1.5000E-02 1.5000E-02 1.5000E-02 1.5000E-02 1.5000E-02
1.5000E-02 1.5000E-02

MATRIX '$D_4$' 8 X 8

ROW 1
-1.2524E 01 -8.9449E 00 1.8970E 01 -8.7719E 00 5.6766E 01 1.1864E 02
-7.8498E 00 9.9696E 01

ROW 2
-7.1280E 00 -5.5393E 00 -1.6173E 01 6.1819E-01 -5.3511E 01 5.4080E 01
9.0806E 00 3.3630E 01

ROW 3
-1.4099E 01 -4.7029E-01 -1.4005E 01 8.8842E 00 -8.5686E 01 -8.5162E 01
1.4490E 01 -1.1190E 02

ROW 4
7.7479E 00 2.3785E 00 1.8585E 00 -2.2345E 00 1.6151E 01 3.5400E 00
-5.2161E 00 1.6665E 01

ROW 5
-4.9865E 01 4.3546E 00 1.1410E 02 -1.1378E 00 1.9274E 02 -2.9315E 02
-2.8203E 01 -3.4173E 02

MACH 0.6

ROW 6
-3.0277E 01 -3.0447E 00 -4.1630E 01 3.7872E 01 -1.6303E 02 -2.7053E 02
4.0927E 01 -2.1857E 02

ROW 7
3.4722E 00 -1.3549E 00 -3.0354E 01 6.0901E 00 -6.7895E 01 3.5904E 01
1.1309E 01 6.1649E 01

ROW 8
6.3647E 00 2.7219E 00 -3.6583E 00 3.8116E 00 4.2811E 00 -4.7258E 01
1.3847E 00 -2.0801E 01

MATRIX '$d_4$' 1 X 8

ROW 1
2.1000E-02 2.1000E-02 2.1000E-02 2.1000E-02 2.1000E-02 2.1000E-02
2.1000E-02 2.1000E-02

MATRIX '$C_1$' 8 x 8

| | | | | | | | |
|---|---|---|---|---|---|---|---|
| 2.60763E 03 | -3.63395E 02 | 3.83336E 03 | -4.29293E 02 | 9.03975E 03 | 1.36809E 04 | | |
| 3.86283E 04 | -2.51741E 04 | | | | | | |
| 1.49029E 03 | 4.17266E 01 | 2.10434E 03 | 1.10184E 02 | 7.31426E 02 | 1.66684E 04 | | |
| 2.88933E 04 | -1.49576E 04 | | | | | | |
| 7.37809E 02 | -4.56680E 01 | 2.78077E 03 | 1.11872E 03 | -2.16875E 03 | 6.86488E 03 | | |
| 2.55810E 04 | -1.32482E 04 | | | | | | |
| -2.02867E 02 | 6.17016E 02 | 1.39187E 03 | 1.89772E 03 | -3.56484E 03 | 1.96725E 03 | | |
| -7.29895E 03 | 4.27527E 03 | | | | | | |
| 2.15798E 03 | -3.93008E 03 | 6.34713E 03 | -1.69627E 03 | 4.60163E 03 | -9.21500E 03 | | |
| 1.21640E 05 | -7.16539E 04 | | | | | | |
| -2.87361E 03 | 4.64724E 03 | -6.53044E 03 | 1.64149E 03 | 1.35178E 04 | -2.35310E 04 | | |
| -1.65569E 05 | 9.11281E 04 | | | | | | |
| -4.88047E 01 | -3.71141E 02 | 1.37295E 03 | 5.98270E 02 | 9.24100E 03 | -6.46944E 03 | | |
| -7.16950E 03 | 0.00000E-01 | | | | | | |
| -1.11456E 03 | 6.03551E 03 | -1.92210E 03 | 5.14018E 03 | 8.00994E 03 | -3.08132E 04 | | |
| -1.53106E 05 | 6.63463E 04 | | | | | | |

MATRIX '$C_2$' 8 x 8

| | | | | | | | |
|---|---|---|---|---|---|---|---|
| 1.64448E 03 | 1.02248E 03 | 6.57634E 01 | -4.83633E 01 | -1.67707E 02 | -1.55206E 03 | | |
| -2.89467E 03 | 6.54098E 02 | | | | | | |
| 9.00389E 02 | 8.10383E 02 | 4.37531E 02 | 1.44464E 02 | -3.26790E 01 | -1.11998E 03 | | |
| -1.83612E 03 | 4.47359E 02 | | | | | | |
| 3.11561E 02 | 5.20115E 02 | 8.39647E 02 | 3.33012E 02 | 1.52932E 03 | -9.51102E 02 | | |
| -1.75689E 03 | 5.34977E 02 | | | | | | |
| -6.85388E 01 | 1.02049E 02 | 3.48672E 02 | 6.00313E 02 | -2.51956E 02 | -5.65560E 02 | | |
| 6.13703E 02 | 3.80528E 02 | | | | | | |
| 5.51588E 02 | 1.82339E 02 | 5.23090E 02 | -6.07225E 02 | 8.87192E 03 | -6.49887E 03 | | |
| -8.78829E 03 | 6.88676E 02 | | | | | | |
| -8.40573E 02 | -5.34677E 02 | 1.80301E 02 | -1.37225E 02 | -6.32260E 03 | 1.36913E 04 | | |
| 1.07202E 04 | -1.13918E 03 | | | | | | |
| 3.04983E 02 | 1.85453E 02 | -3.04648E 02 | -3.21030E 02 | -1.86298E 03 | 2.51455E 03 | | |
| 3.33013E 03 | 0.00000E-01 | | | | | | |
| -1.42941E 03 | -1.12432E 03 | -3.41231E 02 | 3.54416E 02 | -3.75207E 03 | 5.72328E 03 | | |
| 7.71624E 03 | 1.44666E 04 | | | | | | |

MATRIX '$C_3$' 8 x 8

| | | | | | |
|---|---|---|---|---|---|
| 1.17883E 01 | 8.20263E-01 | 4.40056E 01 | 1.06401E 01 | 2.18312E 02 | -2.71655E 02 |
| 1.03256E 01 | -3.52417E 02 | | | | |
| 4.25572E 00 | 1.04562E 00 | 2.07921E 01 | 9.77275E 00 | 1.09550E 02 | -1.49634E 02 |
| 5.67483E 00 | -2.02288E 02 | | | | |
| -5.23260E 00 | -1.40556E 00 | 2.00159E 00 | 7.71825E 00 | -3.33349E 01 | -6.07876E 01 |
| 3.12645E 01 | -1.48572E 02 | | | | |
| -4.66615E 00 | -5.03438E 00 | -5.45414E 00 | -1.71370E 00 | -4.54686E 01 | 5.49588E 01 |
| -6.95494E 00 | 1.16258E 02 | | | | |
| -1.79866E 01 | -6.30923E 00 | -1.19362E 01 | 1.10855E 00 | -2.61531E 02 | -3.46007E 01 |
| 2.06944E 02 | -1.01902E 03 | | | | |
| 2.22754E 01 | 1.91898E 01 | 2.93068E 01 | 1.64002E 01 | 2.87250E 02 | -2.28288E 02 |
| -1.93813E 02 | 1.25222E 03 | | | | |
| 8.10466E 00 | 3.37709E 00 | 1.65893E 01 | -5.66132E 00 | 1.31735E 02 | -6.31852E 01 |
| -5.21456E 02 | 0.00000E-01 | | | | |
| 4.31138E-03 | -1.34863E 00 | -1.18585E 01 | -8.20690E 00 | -2.26626E 01 | 1.03947E 02 |
| 2.70509E 00 | 1.30105E 03 | | | | |

MATRIX '$D_1$' 8 x 8

| | | | | | |
|---|---|---|---|---|---|
| -6.01543E-01 | 1.25028E 00 | -4.23218E 00 | 6.92064E-01 | -2.83688E 01 | -1.59500E 01 |
| -4.99637E 00 | -2.02172E 00 | | | | |
| 5.56593E-02 | 2.76872E-01 | -5.41037E-01 | -1.37821E-01 | -5.45951E 00 | -1.22214E 00 |
| -2.29530E-02 | -1.19718E 00 | | | | |
| 1.14602E-01 | 2.06167E-01 | -3.00507E-01 | 3.31097E-02 | -1.18254E 00 | 1.52362E 00 |
| -2.23379E 00 | -1.03559E 00 | | | | |
| 1.56940E-01 | -2.25980E-01 | 8.76395E-01 | -6.38037E-02 | 5.59713E 00 | 3.61562E 00 |
| 1.08394E 00 | 4.90011E-01 | | | | |
| -7.76629E-01 | 2.26827E 00 | -7.76216E 00 | 1.74479E 00 | -4.24894E 01 | -2.57048E 01 |
| -1.66068E 01 | -6.27648E 00 | | | | |
| -1.39204E-01 | -1.48819E 00 | 4.85370E 00 | -7.96204E-01 | 2.52071E 01 | 1.42224E 01 |
| 1.15399E 01 | 7.95609E 00 | | | | |
| -1.18915E-01 | -1.90161E-02 | -2.03780E-01 | 1.24083E-02 | -8.84319E-01 | -1.97269E 00 |
| -7.89703E-01 | 0.00000E-01 | | | | |
| -3.73591E-01 | -1.18334E 00 | 4.12853E 00 | -6.36521E-01 | 2.80687E 01 | 1.17362E 01 |
| -6.53250E 00 | 1.08902E 01 | | | | |

MATRIX '$d_1$' 1 x 8

| | | | | | |
|---|---|---|---|---|---|
| 3.00000E-03 | 3.00000E-03 | 3.00000E-03 | 3.00000E-03 | 3.00000E-03 | 3.00000E-03 |
| 3.00000E-03 | 3.00000E-03 | | | | |

MATRIX '$D_2$' 8 x 8

-4.87614E 00 -3.47124E 00 -1.47481E 00  8.94350E 00 -4.27613E 01 -4.80729E 01
 1.72727E 02  3.23918E 01
-3.56392E 00 -1.31093E 00 -3.97598E 00  5.60194E 00 -1.92228E 01 -5.29791E 01
 3.30220E 01  1.91318E 01
-1.79436E 00 -1.82138E 00 -1.99934E 00  2.63242E 00 -1.87961E 01 -1.55643E 00
 7.31272E 01  1.65784E 01
 2.82827E-01  6.50958E-01 -1.87524E 00 -1.39505E 00  2.68636E 00 -2.14256E 00
-2.89836E 01 -7.68763E 00
-9.33416E 00 -1.08333E 01  1.02551E 01  9.15584E 00 -5.17529E 01  1.31025E 02
 4.95320E 02  9.98726E 01
 1.52810E 01  1.20789E 01 -1.42953E 01 -8.16487E 00  8.46021E 00 -1.31313E 02
-4.11211E 02 -1.26776E 02
 1.09683E 00  4.43741E-01  4.67606E-01 -7.65747E-01 -1.33206E 01  1.10278E 00
 1.55701E 01  0.00000E-01
 2.24519E 01  6.57872E 00  1.70914E-01 -7.53121E 00  2.61084E 01 -1.21396E 01
-9.70886E 01 -1.70094E 02

MATRIX '$d_2$' 1 x 8

 9.00000E-03  9.00000E-03  9.00000E-03  9.00000E-03  9.00000E-03  9.00000E-03
 9.00000E-03  9.00000E-03

MATRIX '$D_3$' 8 x 8

 1.53866E 01  2.25197E 01 -3.12849E 01 -3.83271E 01 -9.19851E 01  4.34563E 02
-6.14016E 02 -1.53188E 02
 1.27996E 01  9.22968E 00  4.22620E 00 -2.69256E 01 -1.57161E 01  2.74316E 02
-1.69146E 02 -9.05120E 01
 9.69656E 00  7.42809E 00  1.26038E 01 -2.13696E 01  1.04441E 02  1.78813E 02
-3.48047E 02 -7.85183E 01
 1.80609E 00 -3.34052E 00  1.27782E 01  3.44589E 00  2.68556E 01 -7.04932E 00
 7.95573E 01  3.60098E 01
 3.91712E 01  5.23573E 01 -7.23960E 01 -6.52402E 01  8.62461E 01  3.33110E 02
-2.11105E 03 -4.71510E 02
-6.23351E 01 -6.07634E 01  7.96731E 01  7.26057E 01  3.96172E 01 -1.51063E 02
 2.07157E 03  5.98920E 02
-9.56210E 00 -1.53603E 00  2.44644E-01  3.76172E 00  4.36328E 01 -6.31541E 01
-8.33257E 01  0.00000E-01
-8.31611E 01 -3.99591E 01  2.55208E 01  5.22903E 01 -1.40327E 01 -3.12954E 02
 7.67320E 02  7.94371E 02

MATRIX '$d_3$' 1 x 8

-1.50000E-02  1.50000E-02  1.50000E-02  1.50000E-02  1.50000E-02  1.50000E-02
 1.50000E-02  1.50000E-02

MATRIX '$D_4$' 8 x 8

| | | | | | |
|---|---|---|---|---|---|
| -1.87441E 01 | -2.89824E 01 | 4.70626E 01 | 3.26071E 01 | 2.54066E 02 | -4.26439E 02 |
| 9.24390E 02 | 1.92697E 02 | | | | |
| -1.51028E 01 | -1.39148E 01 | -2.68585E-01 | 2.87650E 01 | 8.21414E 01 | -3.01765E 02 |
| 1.89868E 02 | 1.13859E 02 | | | | |
| -1.47287E 01 | -1.20029E 01 | -8.52344E 00 | 2.62240E 01 | -3.41777E 01 | -2.79057E 02 |
| 1.55973E 02 | 9.87056E 01 | | | | |
| -6.06224E 00 | 1.72990E 00 | -1.52033E 01 | 2.43790E-01 | -2.48373E 01 | -4.22410E 01 |
| -1.72546E 01 | -4.55228E 01 | | | | |
| -5.45781E 01 | -7.02356E 01 | 1.41562E 02 | 6.18513E 01 | 4.04977E 02 | -5.44191E 02 |
| 1.99698E 03 | 5.93844E 02 | | | | |
| 8.62983E 01 | 8.73069E 01 | -1.49466E 02 | -8.71603E 01 | -5.73137E 02 | 5.25359E 02 |
| -2.18603E 03 | -7.54455E 02 | | | | |
| 1.47298E 01 | 4.43855E 00 | -2.00677E 01 | 2.68570E-01 | -1.37137E 02 | 5.24299E 01 |
| 1.14031E 02 | 0.00000E-01 | | | | |
| 8.60750E 01 | 5.69818E 01 | -5.81238E 01 | -6.08999E 01 | -1.93887E 02 | 4.20399E 02 |
| -1.00173E 03 | -1.00818E 03 | | | | |

MATRIX '$d_4$' 1 x 8

| | | | | | |
|---|---|---|---|---|---|
| 2.10000E-02 | 2.10000E-02 | 2.10000E-02 | 2.10000E-02 | 2.10000E-02 | 2.10000E-02 |
| 2.10000E-02 | 2.10000E-02 | | | | |

## 3.0 SST WING MODEL CONTROL SURFACE MECHANIZATION

This section discusses the analyses, design, and laboratory testing accomplished on the mechanization of control surfaces for the SST wing model flutter suppression system. Actuation system components have been identified to provide the desired performance, but work remains in incorporating the systems into the model.

### 3.1 Introduction

Since 1970, Boeing-Wichita has provided support to the NASA-Langley Research Center Aeroelasticity Branch on a research program to demonstrate in the Langley transonic dynamics wind tunnel an active flutter suppression system on a 1/17 scale SST semispan wing model. The initial effort was directed toward mechanizing an electromechanical actuation system for the model trailing edge control surface (see Reference 2). This system was subsequently determined inadequate for the flutter suppression system demonstration, and in 1971 an effort began to develop electrohydraulic actuation systems for the model midspan leading and trailing edge control surfaces. The following paragraphs describe the work that has been accomplished on this development.

The design philosophy followed in this development is straightforward: establish performance requirements that will lead to a successful wind tunnel demonstration of the flutter suppression system, purchase and/or design and fabricate components that satisfy the performance requirements, and breadboard test the systems thoroughly before installation in the model.

The NASA-developed flutter suppression system was formulated on the assumption that ideal actuators would be used to drive the control surfaces. Based on this assumption, a dynamic requirement of minimum phase and gain variations was set in the frequency range 5 to 25 Hz, with the model flutter mode frequency about 12 Hz. A goal of no more than 15 degrees phase lag at 25 Hz was chosen.

The actuation systems must be capable of ± 10 degree amplitude up to 25 Hz, and produce at least 20 inch-pound maximum torque. No external leakage of hydraulic fluid can be permitted in either the model or the wind tunnel test section. The hydraulic actuators must mount close to the control surface hinge lines without violating the wing airfoil.

A subminiature rotary actuator was designed and fabricated to be used with high performance Moog servovalves to actuate the midspan leading and trailing edge control surfaces. Detailed discussions of the design, testing, and analyses accomplished to date are presented in Sections 3.2 and 3.3. Section 3.4 presents a discussion of work necessary to complete the control surface mechanization. Section 3.5 contains nomenclature and detail drawings.

## 3.2 Control Surface Actuation System Design

A survey of current "off the shelf" subminiature electrohydraulic components indicated that, while satisfactory servovalves were available, special actuators would have to be designed and fabricated to meet the requirements. Therefore, two single vane rotary actuators with 0.5 inch vane radius and length were designed and fabricated for installation at the control surface hinge lines without protruding into the airstream.

### 3.2.1 Actuator Design

The design torque requirement of at least 20 in-lb maximum was based on control surface hinge moment estimates. To insure satisfactory operation of the actuation systems during the wind tunnel tests, a design goal of achieving a higher maximum torque capability was set, within the geometric constraints of the model. A limit of 1000 psi was chosen for hydraulic supply pressure to minimize fluid sealing difficulty in the actuator and lines.

A detailed drawing of the final actuator design is shown in Section 3.5. The actuator body and end caps are 2024 aluminum, and the vane and shaft are 17-4PH high strength stainless steel. Vane sealing is provided by coating the vane with adiprene in conjunction with a straight segment of an AN 5227 O-ring behind the shaft. Gasket seal between the end caps and actuator body is accomplished with two loops of 3 mil copper wire set in a light adhesive around the vane cavity. The 1/8-inch precision shaft is supported by ball bearings in each end cap and AN 5227-1 O-rings provide fluid seal around the shaft. A photograph of one of the actuators prior to assembly is shown in Figure 3.1.

The two actuators were designed to be identical, with the actuator body and end cap thickness machined to lie within the airfoil at the inboard edge of the leading edge control surface. Layouts of a proposed installation at each surface are shown in Section 3.5. Special 1/8-inch tube fittings were designed and fabricated to provide O-ring seals at the actuator ports.

The actuators were designed to produce 41.0 in-lb torque with two-thirds of the 1000 psi supply pressure across the actuator vane. Usual actuator design procedures were followed (see Reference 3). A method of attaching the surfaces to the actuator shaft has not been determined. The use of a tapered pin would reduce the stress area of the shaft and aluminum tubing the surfaces are mounted on to the point where failure would occur at 30-35 in-lb.

### 3.2.2 Electrohydraulic Servovalve Selection

Servovalves were selected to produce 10 degree actuator amplitude capability up to 25 Hz in a no-load condition. The servovalves selected are Moog Series 30 flow control type (part number 030 A 17010 E 022 F4) rated at 1.7 $in^3$/sec no-load flow rate at 1000 psi supply pressure. With a load pressure of two-thirds the supply pressure, the maximum flow rate is 58% of the no-load flow rate. With the design torque load (41.0 in-lb) on the actuator, the servovalve can produce 10 degree actuator amplitude up to 14 Hz and 5.8 degrees at

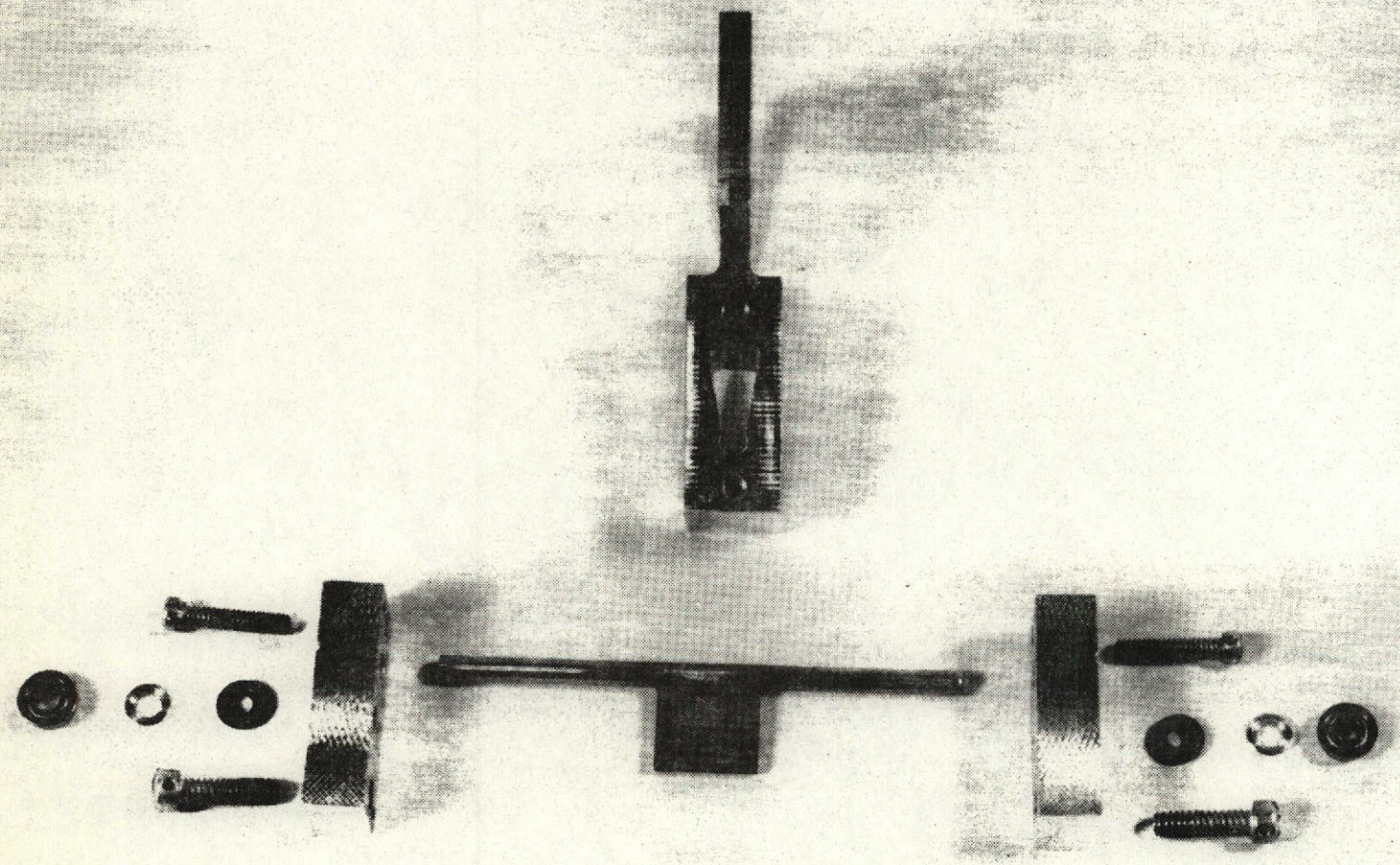

FIGURE 3.1 SUBMINIATURE ROTARY ACTUATOR

25 Hz. This capability was estimated with the assumption that the servovalve and actuator would be mounted close together, whereas in the model they will be separated by about 42 inches of stainless steel hydraulic tubing. Fluid compliance will degrade this estimated performance slightly, but the actual performance should be more than adequate to work the 12 Hz flutter mode.

The Moog Series 30 servovalves were selected primarily because of their high bandpass dynamic capability. The apparent undamped natural frequency (-90° phase point) is about 240 Hz with 0.50 damping ratio.

Port manifolds were designed and fabricated from 2024 aluminum to use with the servovalves (see Section 3.5). O-ring seals are used between the manifold and the servovalve ports. The manifolds (and servovalves) will mount on the wing mount plate within the fuselage fairing.

During the wind tunnel tests, the flutter suppression system will be mechanized on an analog computer. The error voltage to drive the servovalves (and subsequently the control surfaces) will be formed as the output of a computer operational amplifier. A servo amplifier has been designed and built using a 741 operational amplifier to accept the error voltage and produce current to drive the servovalve as a constant function of the error voltage, independent of frequency. A schematic of the servo amplifiers is shown in Figure 3.2. The servo amplifier will permit maximum current to the 500 ohm servovalve coils (in series) up to about 25 Hz. Thus, the maximum flow rate capability of the servovalves can be attained up to this frequency. The two servo amplifiers are mounted on a small circuit card and will mount close to the servovalves under the fuselage fairing.

Figure 3.3 shows a simplified plumbing diagram from the hydraulic supply pump to the servovalves, and return. The pump must supply MIL-H-5606 petroleum base fluid at 1000 ± 50 psi at a maximum flow rate of 3.4 $in^3$/sec (.88 GPM). A 5 micron nominal, 15 micron absolute filter is required in the pressure line. A 25 $in^3$ (or larger) accumulator, precharged to 500 psi, in the pressure line is recommended to damp out pressure transients or ripple from the pump, and to keep the pump from having to respond to high load frequencies.

### 3.2.3 Actuation System Installations

A sketch of the actuation system installations is shown in Figure 3.4. Two feet of 1/8-inch outside diameter stainless steel tubing will be used in each line, from the actuators inboard. The remaining distance will be 1/4-inch tubing. This choice of tubing sizes represents a compromise between pressure loss due to fluid friction at maximum flow and compliance in the lines between the servovalves and actuators. The hydraulic tubing will be set into channels cut into the balsawood, and bonded with epoxy to the aluminum alloy plate out to about one foot from the actuators, where an elastic adhesive will be used. The channels will be filled in over the lines before the wind tunnel tests.

Layouts showing details of the actuator installations at the leading and trailing edge control surfaces are included in Section 3.5. The actuators will mount on the model aluminum alloy plate. The actuator shafts will be attached

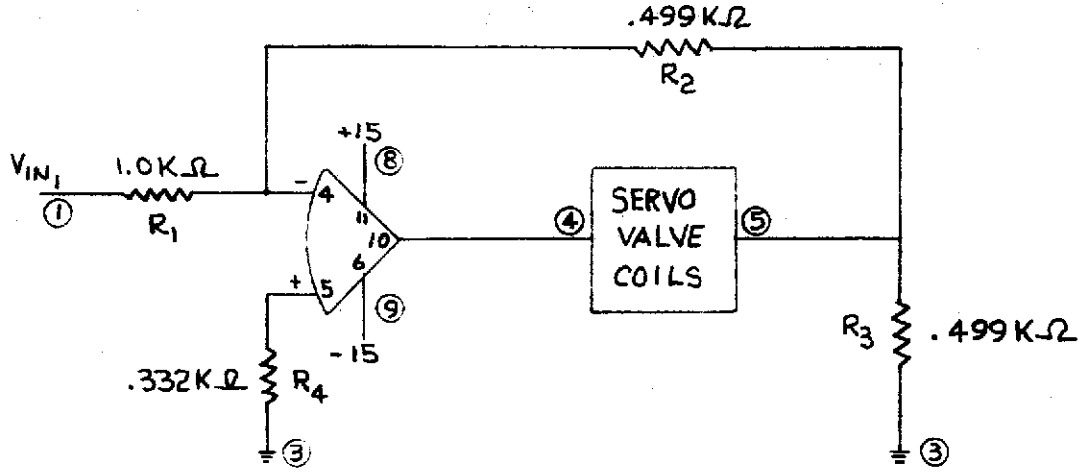


NOTE: CIRCLED NUMBERS REFER TO TERMINAL STRIP MARKING

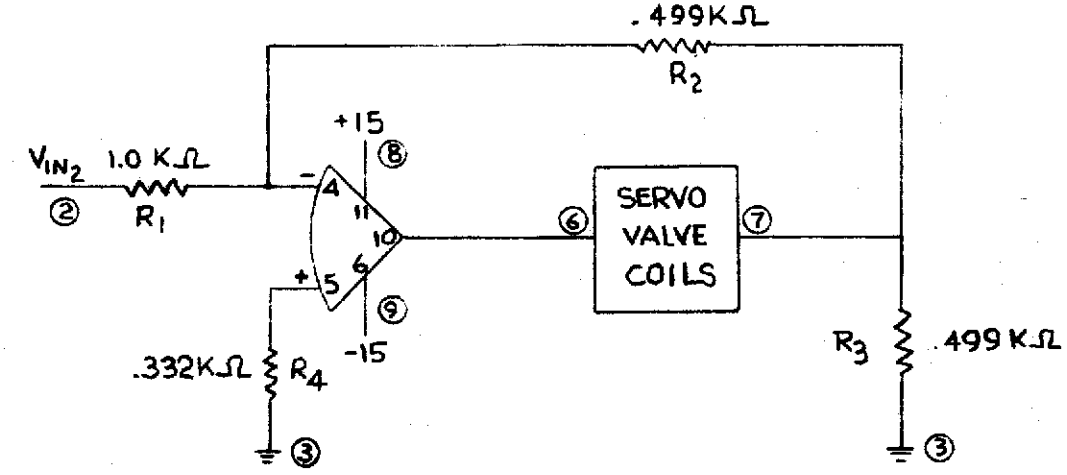


FIGURE 3.2

SERVO AMPLIFIERS

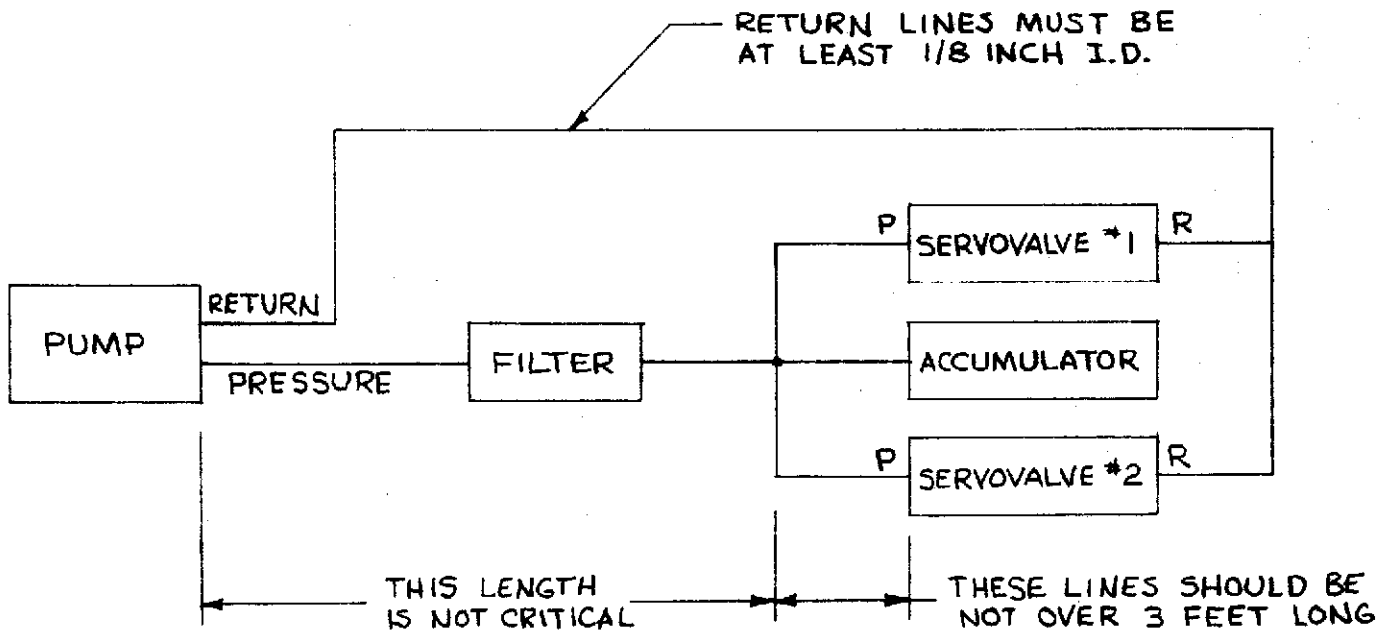


FIGURE 3.3

SIMPLIFIED PLUMBING DIAGRAM

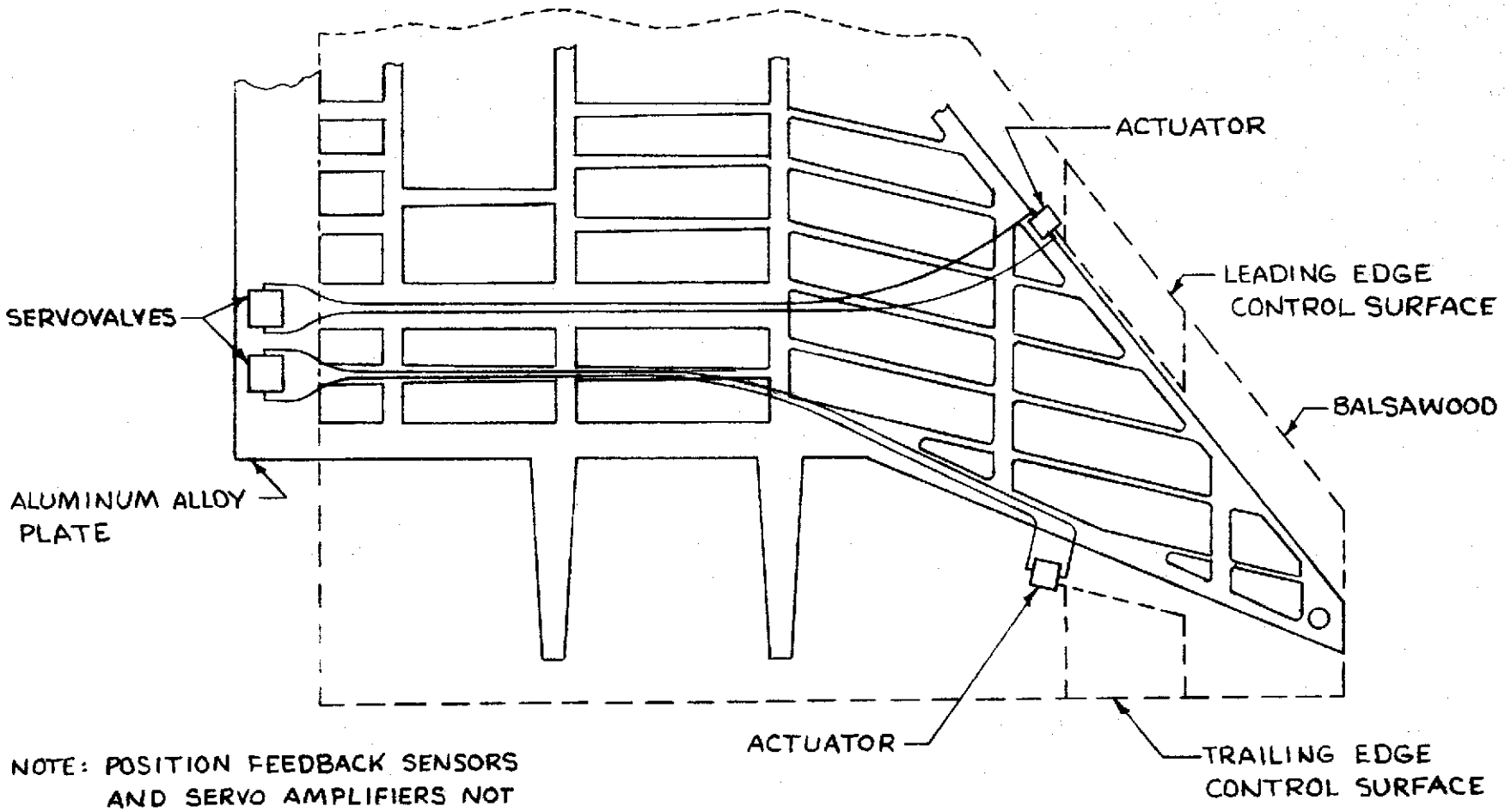


FIGURE 3.4

SKETCH OF ACTUATION SYSTEM INSTALLATIONS

directly to the aluminum tubing the balsawood control surfaces are mounted on, and will provide the inboard support for the surfaces. The outboard supports shown in the layouts will be used for laboratory testing of the actuation systems, but during wind tunnel tests pivot bearings must be used to prevent binding as the wing flexes.

An angular position sensor is being designed to mount on the actuator shaft on the side opposite the control surface. The sensor will use two silicon photocells mounted on a common brass base, with 0.010 inch gap between the cells. A semicircular area of light will be projected on the cells such that the differential voltage generated is proportional to the shaft angular position (see Reference 2).

## 3.3 Baseline System

### 3.3.1 Baseline System Testing

A baseline actuation system was assembled for breadboard testing to evaluate the hydraulic actuation systems. The baseline system, shown in Figure 3.5, has about 15 inches of 1/4-inch outside diameter stainless steel tubing and 4 inches of 1/8-inch tubing between the servovalve and actuator. A d.c. film type potentiometer provides the position feedback signal and the feedback loop is closed on an EAI TR-48 analog computer. Commands from the analog computer pass through the servo amplifier to the servovalve. The trailing edge control surface is used in the baseline system because it possesses higher inertia than the leading edge surface, resulting in a lower frequency surface-shaft mode. An MS 28797-1 accumulator is used in the pressure line to isolate the system from the pump in the hydraulic test bench.

The baseline system with position feedback only is unstable with the control surface connected to the actuator shaft. The instability appeared during testing as a sustained 55.9 Hz, 1.2 degrees peak to peak oscillation as the supply pressure was increased from zero at about 550 psi, with a nominal loop gain of 633.7/sec. This gain had been determined through testing of the baseline system without the control surface to provide less than 15 degrees phase lag at 25 Hz (see frequency response shown in Figure 3.6). The frequency response indicates a lightly damped peak at about 99 Hz. No attempt was made to determine the peak exactly during the laboratory testing due to the high amplitudes near the resonant frequency.

### 3.3.2 Baseline System Analysis

A simplified, linear mathematical model of the baseline actuation system was developed using the system sketch shown in Figure 3.7 and the frequency response of Figure 3.6. This mathematical model will be used to predict additional feedback compensation required to stabilize the baseline system.

Consider the sketch shown in Figure 3.7. This combination free body - flow diagram is drawn to represent the baseline system. Summing torque about the

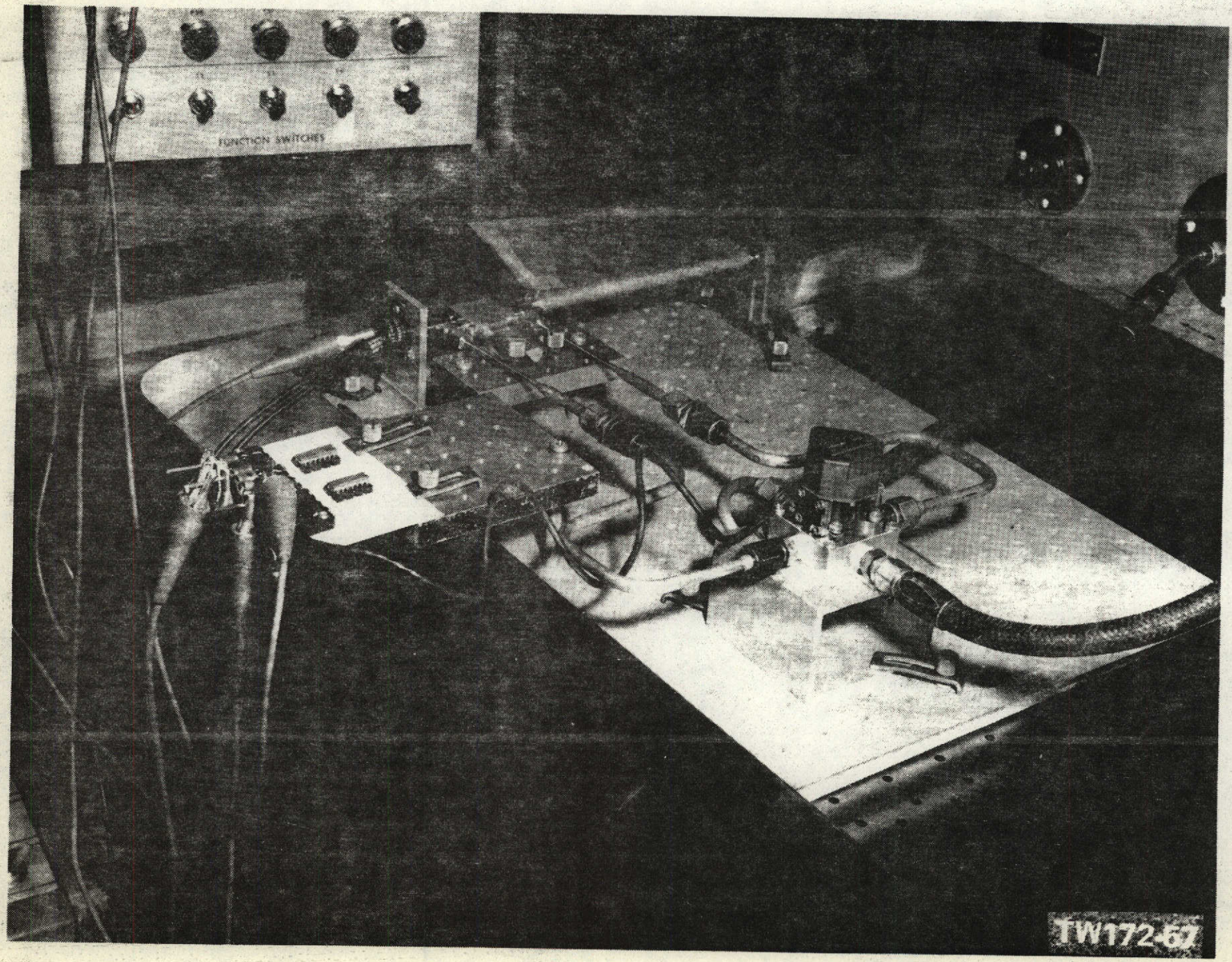


FIGURE 3.5 BASELINE ACTUATION SYSTEM

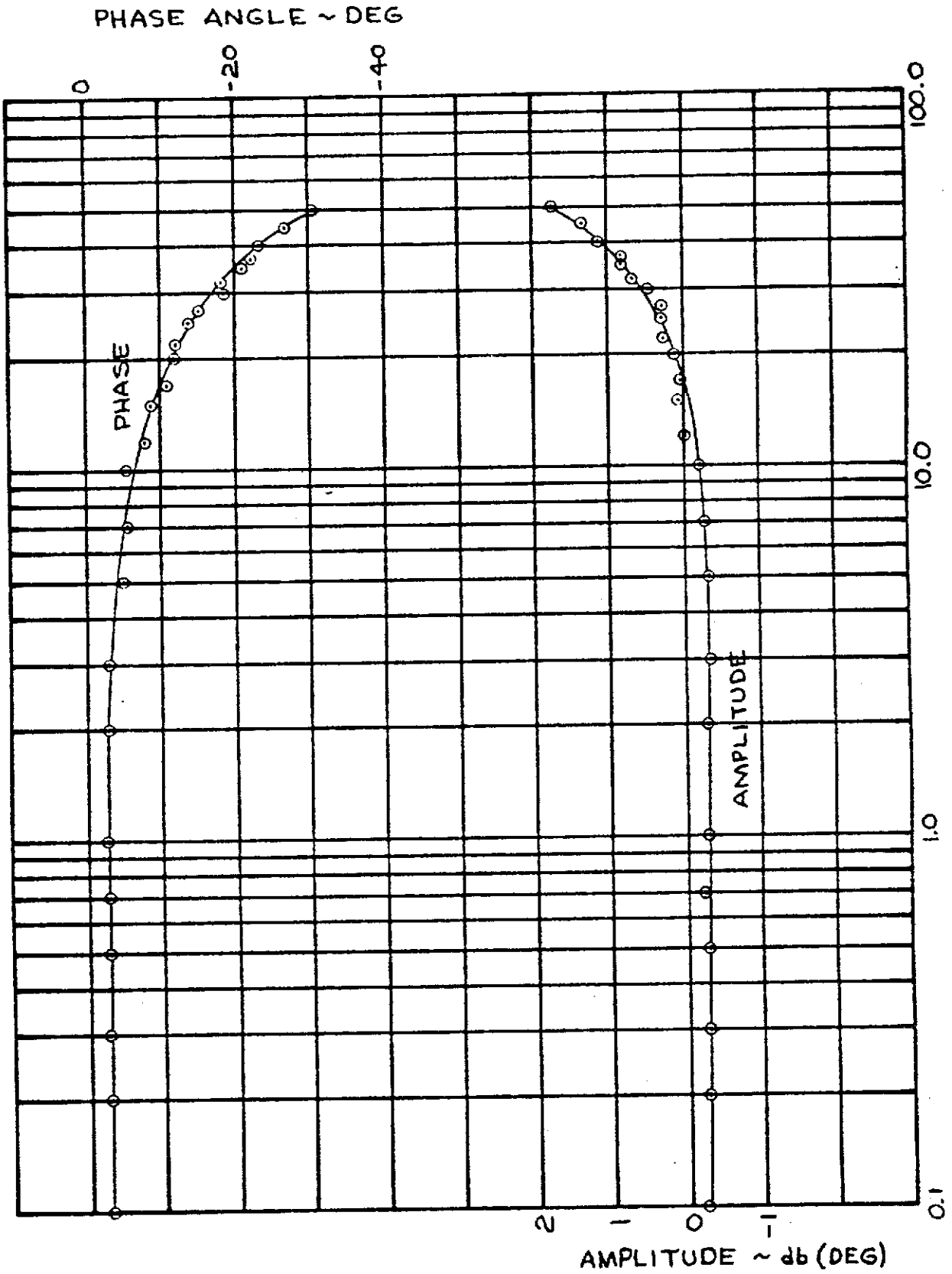


FIGURE 3.6 FREQUENCY RESPONSE OF BASELINE SYSTEM WITHOUT CONTROL SURFACE

NOTE: LOOP GAIN 633.7/SEC, 1.00 SIN $(2\pi f)t$ DEGREES INPUT COMMAND, POSITION FEEDBACK ONLY

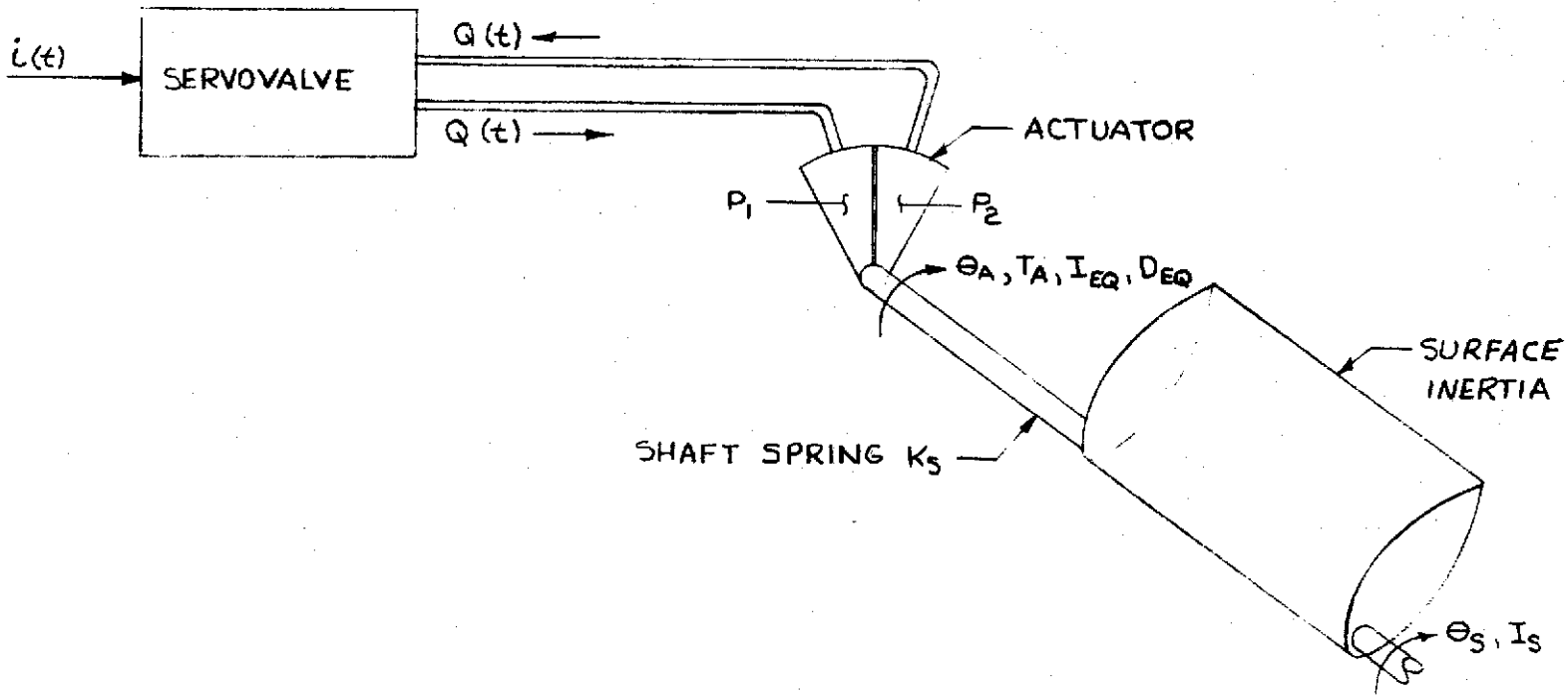


FIGURE 3.7

SKETCH OF BASELINE ACTUATION SYSTEM

actuator shaft produces the equation

$$I_{EQ} \frac{d^2\theta_A}{dt^2} + D_{EQ} \frac{d\theta_A}{dt} + K_S \theta_A - K_S \theta_S = T_A$$

where $I_{EQ}$ is the equivalent rotary inertia of the hydraulic fluid and the actuator vane, $D_{EQ}$ is an equivalent linear (viscous) damping coefficient and $T_A$ is the torque developed by the actuator. The developed torque can be determined by assuming the pressure acts on the vane area at the average radius:

$$T_A = (P_1 - P_2)\left[(r_D - r_S)\ell\right] \frac{r_D + r_S}{2} = \frac{1}{2}(P_1 - P_2)(r_D^2 - r_S^2)\ell = C_A(P_1 - P_2)$$

where $C_A$ is the actuator effectiveness coefficient with units of $in^3$.

The Moog servovalve dynamic characteristics can be assumed constant for low input commands and loads. The approximate servovalve equation of motion can be expressed as

$$\frac{d^2Q(t)}{dt^2} + 2\zeta_v \omega_{n_v} \frac{dQ(t)}{dt} + \omega_{n_v}^2 Q(t) = \omega_{n_v}^2 K_V i(t)$$

where i(t) is the coil current and $K_V = {}^{Q_{max}}/_{i_{max}}$. The flow rate of hydraulic fluid to the servovalve divides into damping flow ($Q_D$) due to leakage across the spool, flow due to fluid compressibility ($Q_H$), and actuator flow ($Q_A$). The damping flow is accounted for in the approximate servovalve equation given above. The flow in the line from the servovalve to the actuator is

$$Q(t) = Q_H(t) + Q_A(t) \quad .$$

The compressibility flow can be determined from the definition of the fluid bulk modulus

$$\beta = \frac{\Delta P}{\Delta V/V} \quad , \quad \text{or} \quad \frac{\beta}{V} \Delta V = \Delta P$$

where $\Delta V$ is an incremental change in fluid volume due to an incremental change in pressure, $\Delta P$, and V is the fluid volume on either side of the actuator vane. Both sides of the equation can be divided by an incremental time, $\Delta t$, and in the limit

$$\lim_{\Delta t \to 0} \left[\frac{\beta}{V} \frac{\Delta V}{\Delta t}\right] = \lim_{\Delta t \to 0} \frac{\Delta P}{\Delta t}$$

produces

$$\frac{\beta}{V} \frac{dV}{dt} = \frac{dP}{dt} \quad , \quad \text{or} \quad \frac{dP}{dt} = \frac{\beta}{V} Q_H(t) \quad .$$

The actuator flow can be obtained by recognizing the flow rate is the rate of change of volume in the actuator on one side of the vane due to an angular displacement, $\theta_A$.

$$Q_A = \frac{d}{dt}\left[\frac{1}{2}(r_D^2 - r_S^2)\ell\right]\theta_A = C_A \frac{d\theta_A}{dt} .$$

Then,

$$Q(t) = \frac{V}{\beta}\frac{dP}{dt} + C_A \frac{d\theta_A}{dt} .$$

The load pressure $P_1 - P_2$ is twice the pressure $\Delta P$ since pressure increases on one side of the actuator vane by $\Delta P$ and decreases by the same amount on the other side as the servovalve opens. Then the flow equation may be written as

$$Q(t) = \frac{V}{2\beta}\frac{d(P_1 - P_2)}{dt} + C_A \frac{d\theta_A}{dt} .$$

This equation can now be used to obtain the actuator torque as a function of servovalve flow rate. Integrating from some time $t_o$ to time $t$ gives the form

$$(P_1 - P_2)(t) = \frac{2\beta}{V}\int_{t_o}^{t} Q(\tau)d\tau - \frac{2\beta}{V} C_A \theta_A(t)$$

where it is assumed $(P_1 - P_2)(t_o) = 0$ and $\theta_A(t_o) = 0$. From the torque equation above,

$$T_A(t) = \frac{2\beta}{V} C_A \int_{t_o}^{t} Q(\tau)d\tau - \frac{2\beta}{V} C_A^2 \theta_A(t) .$$

Substitution of this equation into the actuator equation of motion gives

$$I_{EQ}\frac{d^2\theta_A}{dt^2} + D_{EQ}\frac{d\theta_A}{dt} + K_S\theta_A - K_S\theta_S = \frac{2\beta}{V} C_A \int_{t_o}^{t} Q(\tau)d\tau - \frac{2\beta}{V} C_A^2 \theta_A$$

or,

$$I_{EQ}\frac{d^2\theta_A}{dt^2} + D_{EQ}\frac{d\theta_A}{dt} + \left(\frac{2\beta}{V} C_A^2 + K_S\right)\theta_A - K_S\theta_S = \frac{2\beta}{V} C_A \int_{t_o}^{t} Q(\tau)d\tau .$$

The other equation of motion required to describe the baseline system dynamic behavior can be obtained by summing torque about the surface shaft.

$$-K_S\theta_A + I_S\frac{d^2\theta_S}{dt^2} + K_S\theta_S = 0 .$$

Assuming zero initial conditions, the Laplace transformation of the two equations produces

$$\left(I_{EQ}\,S^2 + D_{EQ}\,S + \frac{2\beta}{V}C_A^2 + K_S\right)\Theta_A(S) - K_S\,\Theta_S(S) = \frac{2\beta}{V}C_A\left(\frac{1}{S}\right)Q(S)$$

$$-K_S\,\Theta_A(S) + \left(I_S\,S^2 + K_S\right)\Theta_S(S) = 0 \quad .$$

The transfer function $\Theta_A(S)/Q(S)$ can be determined by applying Cramer's rule

$$\frac{\Theta_A}{Q}(S) = \frac{\frac{2\beta}{V}C_A\left(I_S\,S^2 + K_S\right)}{S\left[\left(I_{EQ}\,S^2 + D_{EQ}\,S + \frac{2\beta}{V}C_A^2 + K_S\right)\left(I_S\,S^2 + K_S\right) - K_S^2\right]} \quad .$$

This transfer function for the baseline system without the surface inertia can be obtained by setting $I_S = 0$ and $K_S = 0$ in the transformed equations.

$$\frac{\Theta_A}{Q}(S) = \frac{\frac{2\beta}{V}C_A}{S\left[I_{EQ}\,S^2 + D_{EQ}\,S + \frac{2\beta}{V}C_A^2\right]} \quad .$$

The block diagram shown in Figure 3.8 represents the baseline actuation system without the control surface. The frequency response of this system, Figure 3.6, indicates a resonant peak at about 99 Hz and 0.30 damping ratio. This mode is the closed loop equivalent hydraulic fluid-actuator inertia mode. The closed loop transfer function is

$$\frac{\Theta_A}{V_C}(S) = \frac{57.3\,K_{AMP}\,K_V\,\omega_{n_V}^2\,(2\beta C_A/VI_{EQ}) \qquad (\text{DEG/VOLT})}{S\left(S^2 + 2\mathcal{J}_V\omega_{n_V}S + \omega_{n_V}^2\right)\left(S^2 + \frac{D_{EQ}}{I_{EQ}}S + \frac{2\beta C_A^2}{VI_{EQ}}\right) + 57.3\,K_F\,K_{AMP}\,K_V\,\omega_{n_V}^2\left(\frac{2\beta C_A}{VI_{EQ}}\right)}$$

where the fifth order denominator has two pair of complex conjugate roots and one real root. The closed loop denominator can be written in terms of open loop quantities:

$$\left(S^2 + 2\mathcal{J}_1\omega_{n_1}S + \omega_{n_1}^2\right)\left(S^3 + a_1S^2 + a_2S + a_3\right) = S\left(S^2 + 2\mathcal{J}_V\omega_{n_V}S + \omega_{n_V}^2\right)\left(S^2 + \frac{D_{EQ}}{I_{EQ}}S + \frac{2\beta C_A^2}{VI_{EQ}}\right)$$

$$+ 57.3\,K_F\,K_{AMP}\,K_V\,\omega_{n_V}^2\left(\frac{2\beta C_A}{VI_{EQ}}\right)$$

where $\mathcal{J}_1 \approx .01$ and $\omega_{n_1} \approx (2\pi)(99)$. Five linear simultaneous equations in the five unknown coefficients $\left(a_1, a_2, a_3, \frac{D_{EQ}}{I_{EQ}}, \text{and } \frac{2\beta C_A^2}{VI_{EQ}}\right)$ can be obtained by substituting the known quantities in the above equation and equating coefficients of like powers of S. The solution of these equations gives the open loop hydraulic fluid-actuator inertia mode as

$$S^2 + \frac{D_{EQ}}{I_{EQ}}S + \frac{2\beta C_A^2}{VI_{EQ}} = S^2 + 4.777\times10^3\,S + 3.080\times10^6 = (S+768.4)(S+4008.3)$$

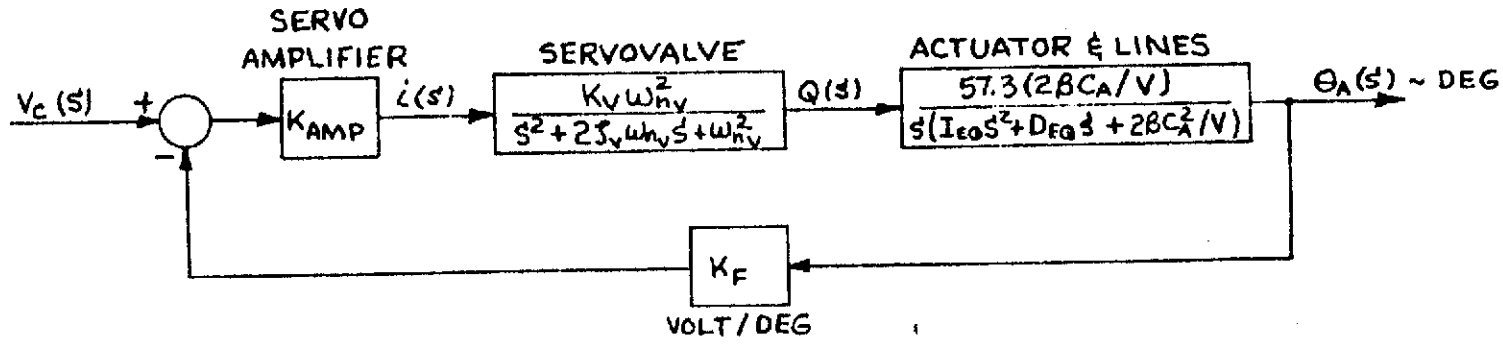


FIGURE 3.8

BLOCK DIAGRAM OF BASELINE SYSTEM WITHOUT CONTROL SURFACE

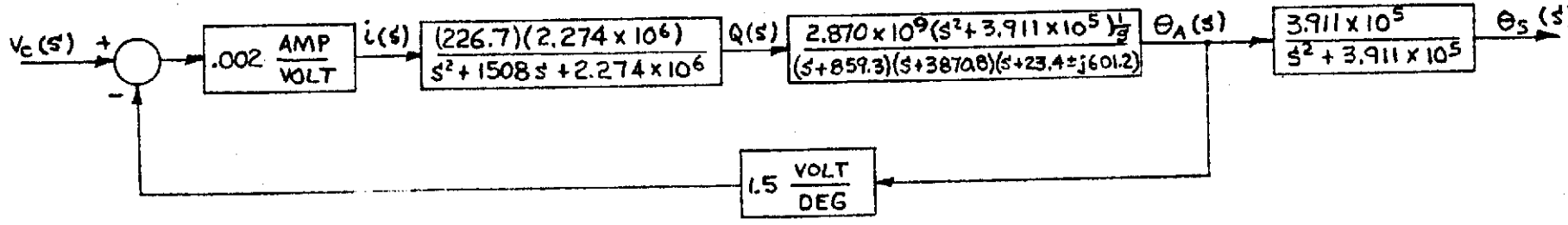


FIGURE 3.9

BLOCK DIAGRAM OF BASELINE SYSTEM WITH CONTROL SURFACE

indicating that this mode is overdamped. This appears reasonable due to the friction between the actuator vane and body, and between the shaft and O-rings. The equivalent damping and inertia are $D_{EQ} = 4.012 \frac{\text{in-lb}}{\text{rad/sec}}$ and $I_{EQ} = .00084$ in-lb-sec$^2$.

The transfer function $\Theta_A(S)/Q(S)$ with the control surface included (derived above) may be written in the form

$$\frac{\Theta_A}{Q}(S) = \frac{\frac{2\beta C_A}{VI_{EQ}}\left(S^2 + \frac{K_S}{I_S}\right)(57.3) \quad \left(\frac{\text{DEG}}{\text{IN}^3/\text{SEC}}\right)}{S\left[\left(S^2 + \frac{D_{EQ}}{I_{EQ}}S + \frac{2\beta C_A^2}{VI_{EQ}} + \frac{K_S}{I_{EQ}}\right)\left(S^2 + \frac{K_S}{I_S}\right) - \frac{K_S^2}{I_{EQ}I_S}\right]} .$$

The shaft spring rate was estimated at 368.9 in-lb/rad, considering both the actuator shaft and the aluminum tubing that the surface is mounted on. The hydraulic fluid-actuator inertia mode becomes

$$S^2 + \frac{D_{EQ}}{I_{EQ}}S + \frac{2\beta C_A^2}{VI_{EQ}} + \frac{K_S}{I_{EQ}} = S^2 + 4.777\times10^3 S + 3.080\times10^6 + \frac{368.9 \text{ IN-LB/RAD}}{.00084 \text{ IN-LB-SEC}^2}$$

$$= S^2 + 4.777\times10^3 S + 3.519\times10^6$$

$$= (S + 910.1)(S + 3866.6) .$$

The midspan trailing edge surface inertia was supplied by NASA and is $9.432 \times 10^{-4}$ in-lb-sec$^2$. The surface inertia-shaft mode is

$$S^2 + \frac{K_S}{I_S} = S^2 + \frac{368.9 \text{ IN-LB/RAD}}{9.432\times10^{-4} \text{ IN-LB-SEC}^2} = S^2 + 3.911\times10^5 .$$

The transfer function denominator then becomes

$$S\left[(S^2 + 4.777\times10^3 S + 3.519\times10^6)(S^2 + 3.911\times10^5) - \frac{(368.9)^2}{(.00084)(.0009432)}\right]$$

$$= S(S^4 + 4777\,S^3 + 3.910\times10^6 S^2 + 1.868\times10^9 S + 1.204\times10^{12})$$

$$= S(S + 859.3)(S + 3870.8)(S + 23.43 \pm j601.2)$$

and the numerator is

$$\frac{2\beta C_A}{VI_{EQ}}(57.3)\left(S^2 + \frac{K_S}{I_S}\right) = \frac{2(1.9\times10^5 \text{ LB/IN}^2)(.0615 \text{ IN}^3)(57.3 \text{ DEG/RAD})}{\frac{1.111}{2} \text{ IN}^3 (.00084 \text{ IN-LB-SEC}^2)}(S^2 + 3.911\times10^5)$$

$$= 2.870\times10^9 (S^2 + 3.911\times10^5) .$$

The block diagram of the baseline system with the control surface included is shown in Figure 3.9, with the position feedback loop closed. Additional feedback compensation must be determined to stabilize the system, and the analysis extended to the actuation systems as installed in the model. The compensation that stabilizes the baseline system should also stabilize the actual systems. The compensation will be incorporated into the breadboard system and performance verified through laboratory testing.

Several simplifying assumptions were made in the above derivation. The most significant is the assumption that the servovalve behavior can be described by a constant coefficient, linear ordinary differential equation. The change in flow gain due to load pressure has been neglected, but since this is reflected as a loss in loop gain, the mathematical model is conservative. The servovalve apparent undamped natural frequency and damping ratio were taken from a Moog brochure for the Series 30 servovalve. Combining the hydraulic fluid mass with the actuator vane mass into an equivalent inertia is not new (see Reference 4). The correctness of all assumptions will be determined through laboratory testing of the breadboard system, with the analytically identified compensation incorporated.

## 3.4 Remaining Work

Components have been selected for the electrohydraulic actuation systems, but work remains in integrating these components into stable systems meeting all the performance requirements. The primary item to be accomplished is the determination of feedback compensation (in addition to actuator shaft angular position feedback) required to stabilize the systems. A mathematical model of the baseline system has been developed to permit analytical determination of the required compensation. The compensation will be tested on the breadboard baseline system to verify the analysis results. The breadboard system will be modified to include the line length dictated by the wing geometry. When the systems have been proven through breadboard testing, they will be installed in the model and retested to verify performance.

Some effort must also be spent in perfecting the silicon photocell angular position sensor. The concept has been proven through laboratory testing, but the design for this particular application must be perfected to provide a reliable actuator shaft position feedback signal.

Provisions have already been made to install the midspan trailing edge surface actuator in the model, but nothing has been done to the model toward installing the leading edge surface actuator.

## 3.5 Nomenclature and Drawings

This section includes nomenclature and detail drawings of fabricated hardware required for the control surface actuation systems.

3.5.1 Nomenclature

Symbols used in the mathematical development in Section 3.3.2 are listed below.

| SYMBOL | DEFINITION | UNITS |
|---|---|---|
| $C_A$ | Actuator torque effectiveness coefficient ($C_A = 1/2\ (r_D^2 - r_S^2)\ell$) | $in^3$ |
| $D_{EQ}$ | Equivalent viscous damping coefficient of actuator and hydraulic fluid | $\frac{in\text{-}oz}{rad/sec}$ |
| i | Servovalve coil current | amp |
| $I_{EQ}$ | Equivalent rotary inertia of actuator vane and hydraulic fluid | $in\text{-}lb\text{-}sec^2$ |
| $I_S$ | Rotary inertia of control surface with respect to its hinge line | $in\text{-}lb\text{-}sec^2$ |
| $K_F$ | Actuator shaft angular position feedback gain | volt/deg |
| $K_S$ | Torsional spring constant of actuator shaft and surface tubing | in-lb/rad |
| $K_V$ | No-load flow gain of servovalve | $\frac{in^3/sec}{amp}$ |
| $\ell$ | Length of actuator vane (= .50 inch) | inches |
| P | Hydraulic fluid pressure | $lb/in^2$ |
| Q | Hydraulic fluid flow rate from servovalve | $in^3/sec$ |
| $r_D$ | Actuator vane radius, measured from shaft axis (= .50 inch) | inches |
| $r_S$ | Actuator shaft radius | inches |
| S | Laplace transform operator | 1/sec |
| $T_A$ | Torque developed by actuator | in-lb |
| V | Volume of hydraulic fluid on one side of actuator vane (from servovalve to vane) | $in^3$ |
| $\beta$ | Bulk modulus of hydraulic fluid (taken as $1.9 \times 10^5$ $lb/in^2$ for MIL-F-5606 fluid) | $lb/in^2$ |

| SYMBOL | DEFINITION | UNITS |
|---|---|---|
| $\zeta_v$ | Apparent damping ratio of open loop servovalve | - |
| $\theta_A$ | Actuator shaft angular displacement | radian |
| $\theta_S$ | Control surface angular displacement | radian |
| $\omega_{n_v}$ | Apparent undamped natural frequency of open loop servovalve | rad/sec |

3.5.2 Detail Drawings

Copies of detailed drawings of the actuator (2 sheets) and servovalve port blocks, and layouts of the actuator installations in the model, are presented in this section.

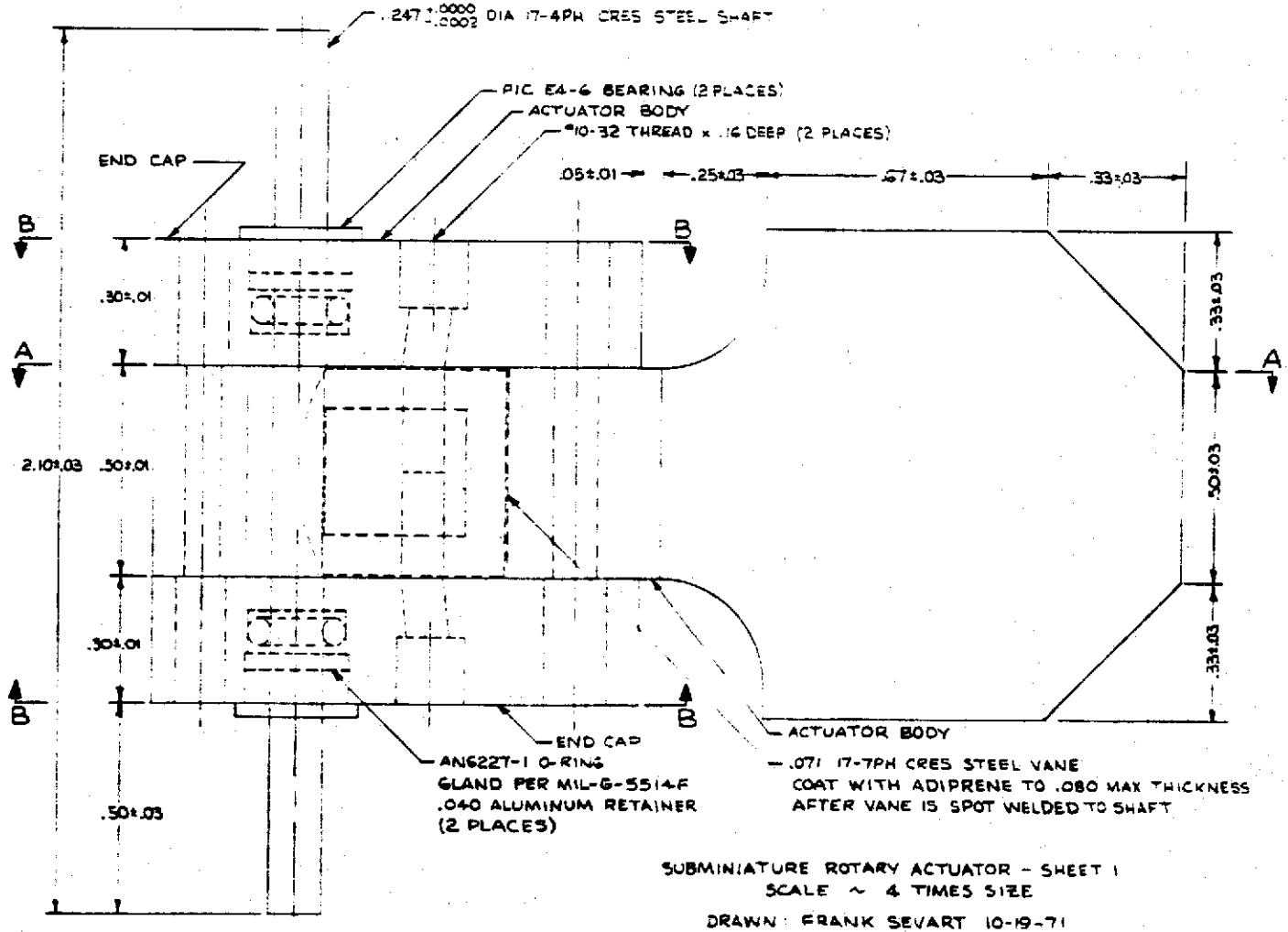


NOTES
1. THE TWO END CAPS ARE IDENTICAL
2. SLOT MUST BE DRILLED FROM EACH PORT TO AREA OF ACTUATOR BODY BEHIND VANE IN MAXIMUM DISPLACEMENT POSITIONS
3. ACTUATOR BODY AND END CAPS TO BE FABRICATED FROM 2024 ALUMINUM ALLOY
4. ACTUATOR WILL OPERATE AT 1000 PSI MAX PRESSURE, USING MIL-F-5606 FLUID
5. SEE SHEET 2 FOR SECTION VIEWS

SUBMINIATURE ROTARY ACTUATOR - SHEET 1
SCALE ~ 4 TIMES SIZE

DRAWN: FRANK SEVART 10-19-71

BOEING NO. D4-PAPL
SHEET PAGE 21

12

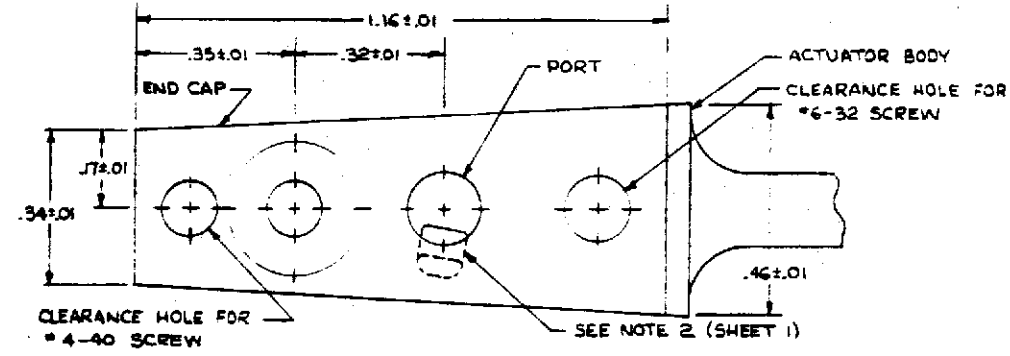


SECTION B-B

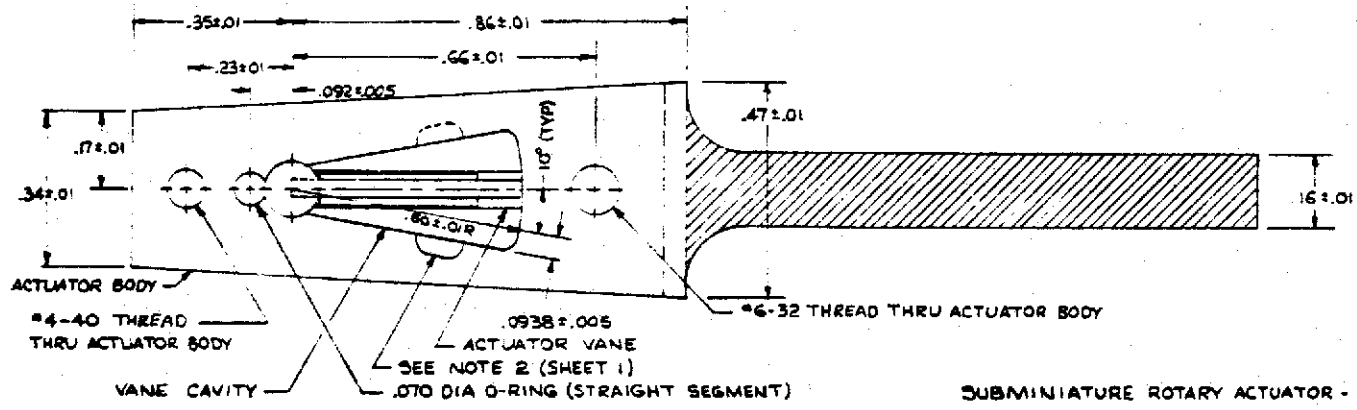


SECTION A-A

SUBMINIATURE ROTARY ACTUATOR - SHEET 2

SCALE ~ 4 TIMES SIZE

DRAWN: FRANK SEVART 10-19-71

BOEING NO. D[illegible]

SHCT PAGE 72

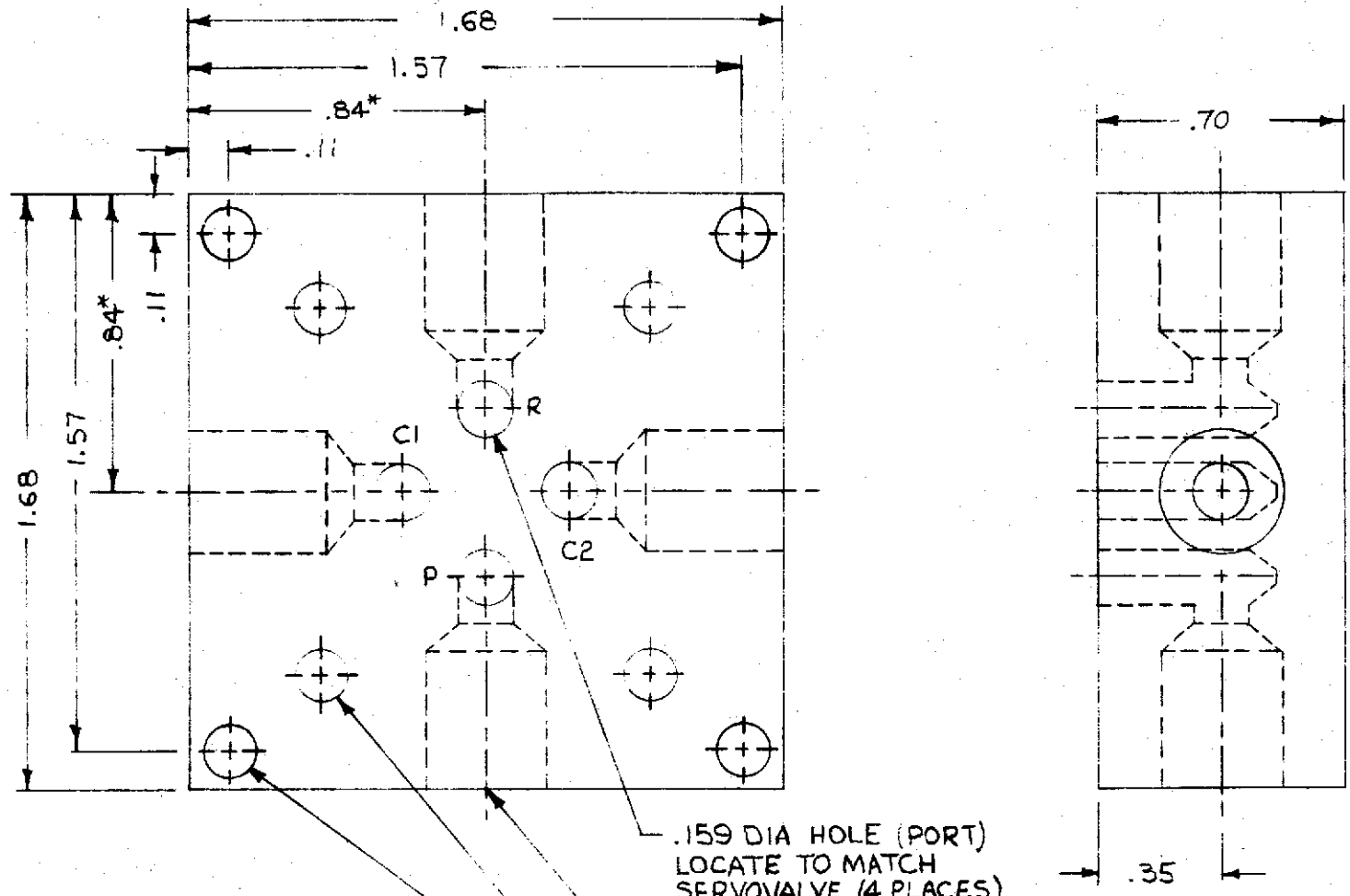


SCALE: 2/1

* REFERENCE DIMENSION

# PORT MANIFOLD

2024 ALUMINUM

BOEING NO. D3-8884

SECT PAGE 73

DRAWN: F. SEVART 12/13/71

# ACTUATOR INSTALLATION
# TRAILING EDGE SURFACE

SCALE ~ FULL SIZE

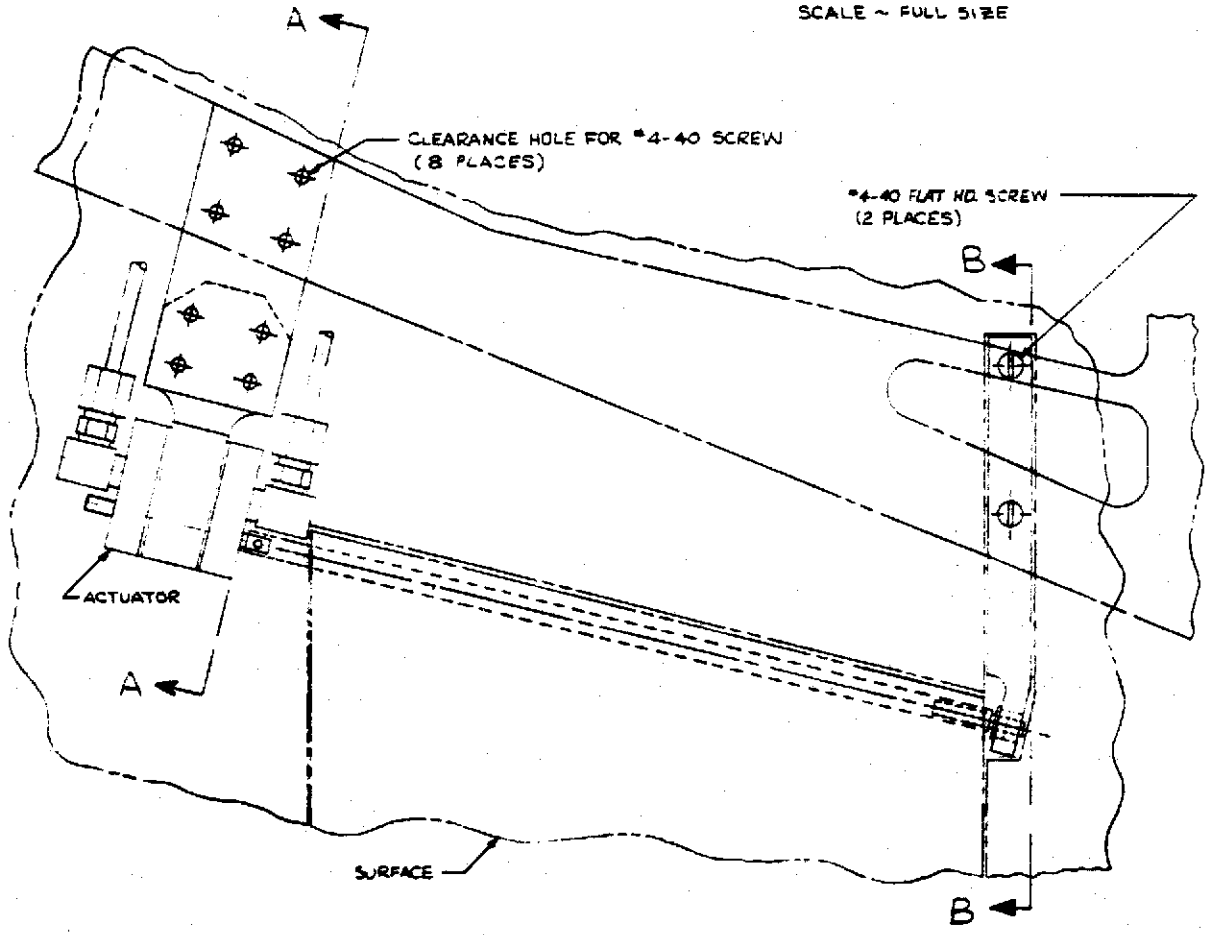


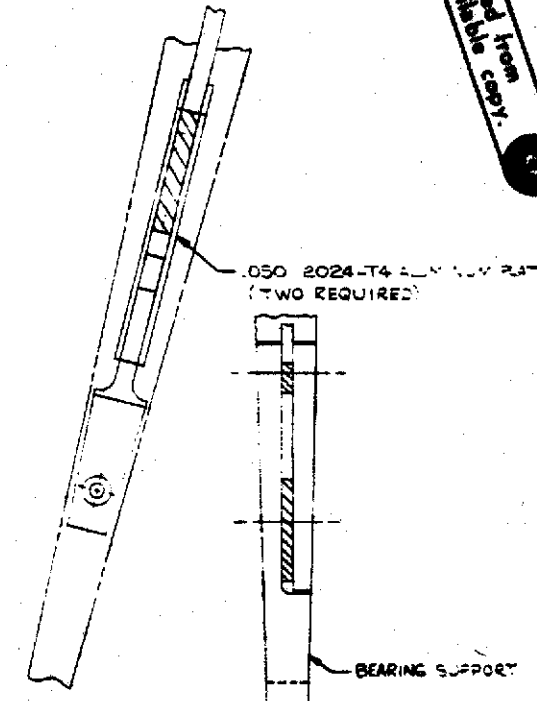


A-A




B-B

DRAWN: FRANK SEVART

BOEING



74

# ACTUATOR INSTALLATION
# LEADING EDGE SURFACE

SCALE ~ FULL SIZE

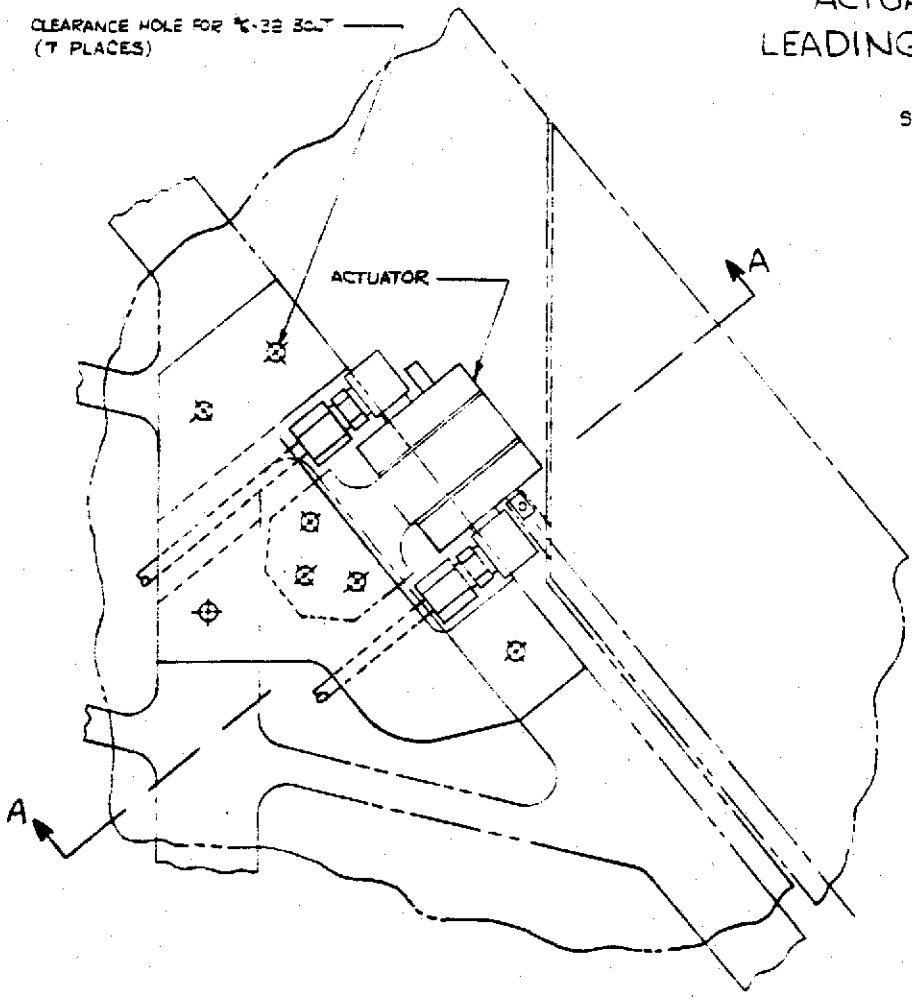


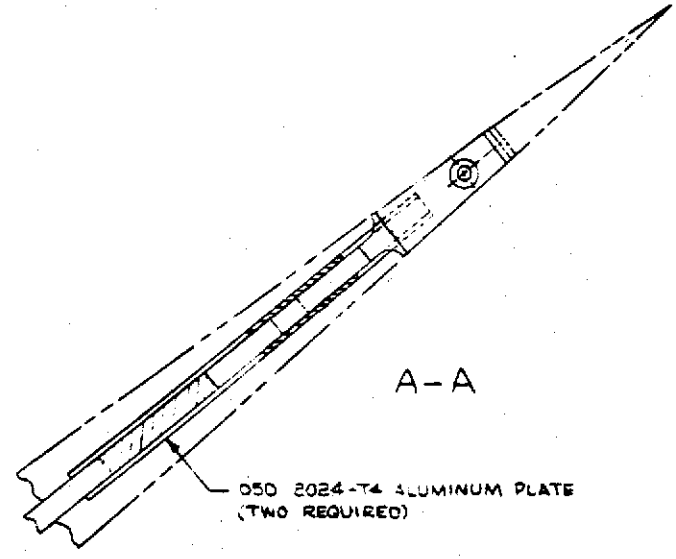




DRAWN: FRANK SEVART 11-1-71

BOEING NO. [illegible]
SECT PAGE

SU 75

# OUTBOARD BEARING INSTALLATION
## LEADING EDGE SURFACE

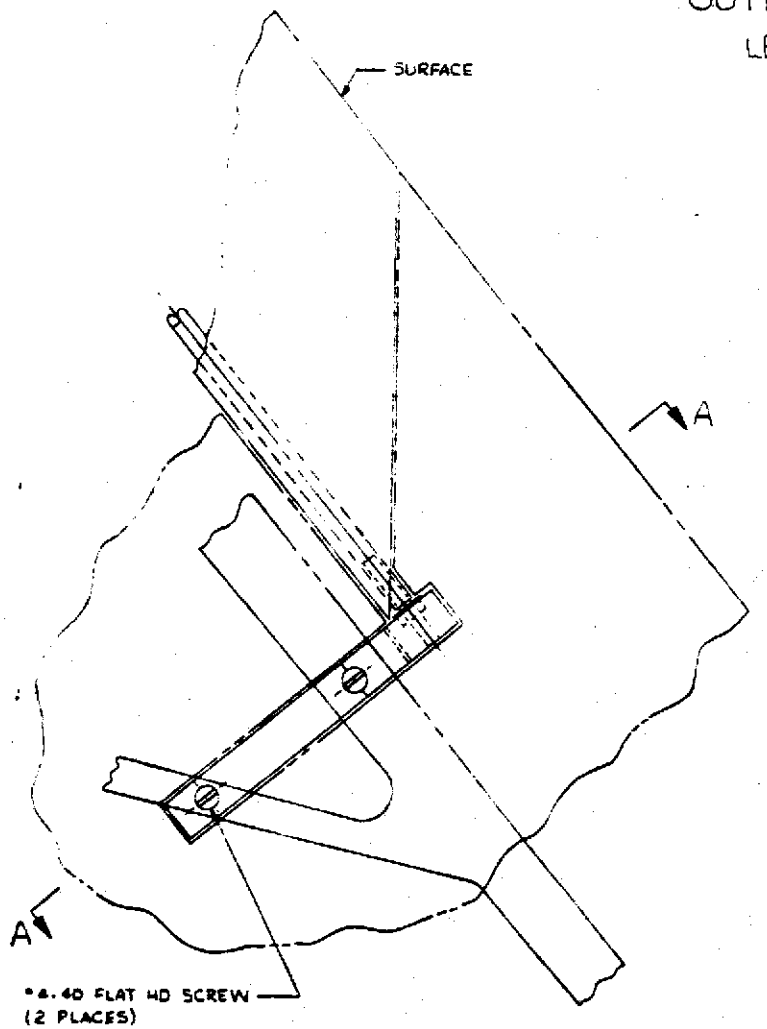


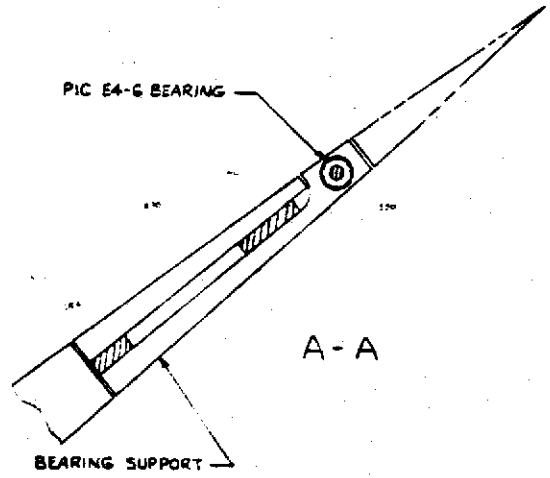




| BOEING | NO. |
|---|---|
| SECT | PAGE |

DRAWN: F. SEVART 1-22-72

## 4.0 B-52 AEROELASTIC MODEL RIDE CONTROL SYSTEM SYNTHESIS

The synthesis of a ride control system for the NASA one-thirtieth scale B-52E aeroelastic model is described in this section. The final system produces more than 30 percent reduction in rms vertical acceleration (airplane response to random atmospheric turbulence) along the entire model fuselage, using forward body horizontal canards, inboard wing flaperons, and elevator control surfaces. This system will be mechanized on the model and demonstrated in the Langley transonic dynamic tunnel.

### 4.1 Introduction

A three phase study to design a ride control system for the B-52 aeroelastic model was formulated in 1970 and reported in Boeing Document D3-8390-2 (Reference 5). This document is included as Section 3 of D3-8390-4 (Reference 2).

The objective of this study was to design and evaluate a ride control system (RCS) for the B-52 aeroelastic model with maximum performance for minimum model modifications. During Phase I, the ride improvement attainable using the existing elevator and aileron control surfaces was evaluated. These surfaces were capable of producing no more than a five percent reduction in rms vertical acceleration ($\bar{A}$) at the pilot station (BS 172) for a random vertical gust disturbance. Performance attainable with canard and canard/elevator systems was investigated during Phase II. Satisfactory $\bar{A}$ reduction was obtained at the pilot station, but mid and aft body reductions did not meet the design goal of thirty percent. A ride control system was designed and evaluated during Phase III using canard, flaperon, and elevator control surfaces. This system produces $\bar{A}$ reductions in excess of thirty percent over the length of the model fuselage.

The remaining work includes using updated cable-mounted model equations of motion for evaluating the system performance, refining the system design and for generating system responses for correlation with wind tunnel data.

### 4.2 Design of Ride Control System

The objective of this study was to analytically demonstrate feasibility of improving passenger/pilot ride using active controls. The control surfaces, and surface locations, considered in the study are shown in Figure 4.1. The system design goal was to obtain a minimum of 30 percent reduction in fuselage rms vertical accelerations in a random atmospheric turbulence environment.

The design study was conducted using model equations of motion that did not include the cable mount effects on the model dynamic behavior. All data shown in the following pages is model scale, but wing and body station designations are airplane scale. The mathematical model included the first 14 symmetric degrees-of-freedom for wind tunnel test condition 1 (Reference 6). The model equations included lift growth effects and the Von Karman gust spectrum. The characteristic gust length used in Phase I and II was 16.67 feet and 83.3 feet (equivalent to 500 feet and 2500 feet in airplane scale) was used in Phase III. Phase III was believed to be more representative of actual flight conditions. Actuator dynamics

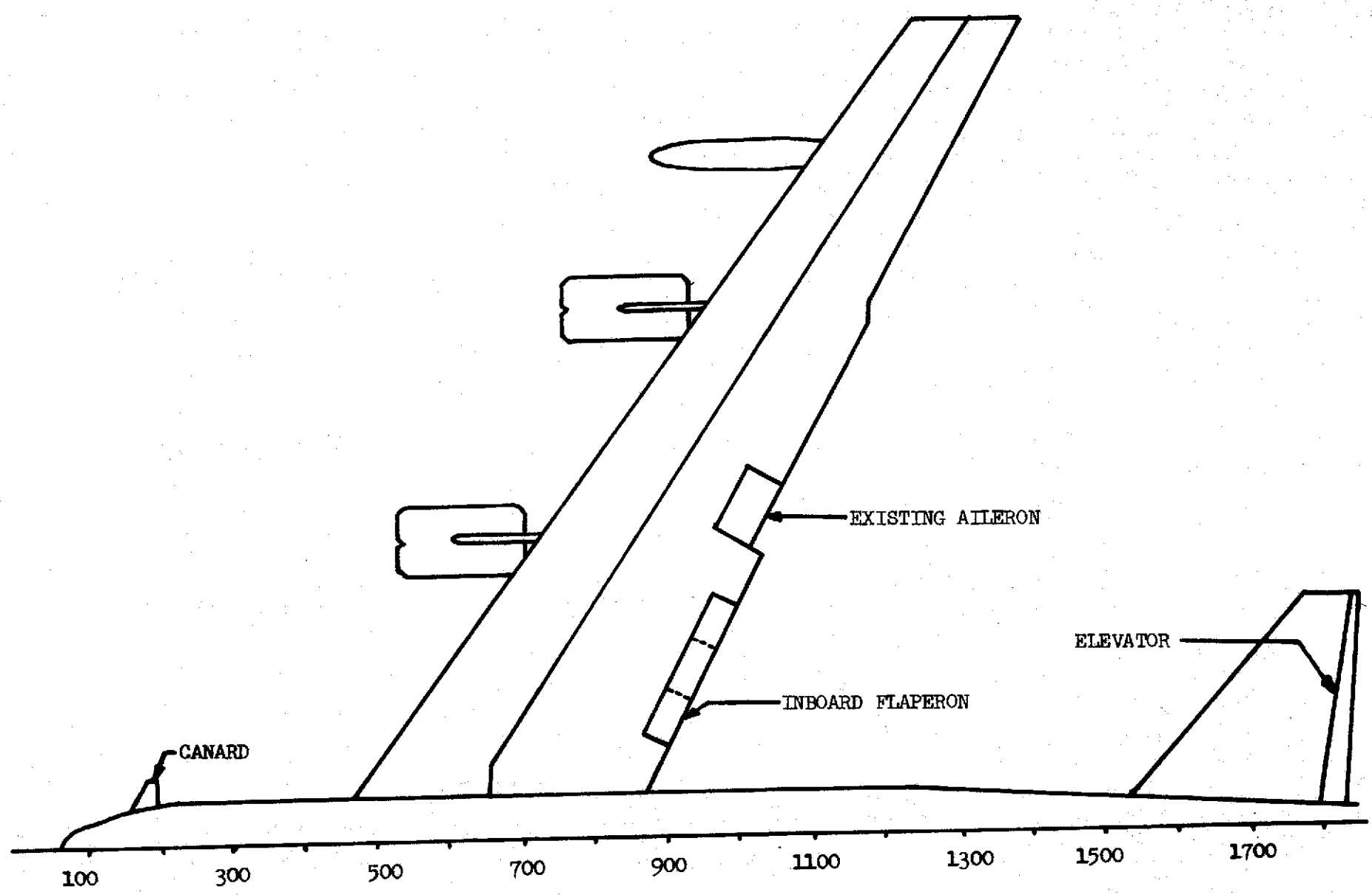


B-52 CONTROL SURFACES AND LOCATIONS

FIGURE 4.1

in Phase I and II were represented by a first order lag, while Phase III included the actual second order actuator dynamic behavior.

The RMS-PSD analyses conducted in this study included the full 0-40 cps frequency range of the model equations. All percentage reductions in vertical acceleration presented in this section are based on the full frequency range.

4.2.1 Phase I - Existing Control Surfaces

The B-52 aeroelastic model was originally constructed with elevator and aileron control surface actuation systems. The objective of this phase was to determine the ride improvement attainable with these control surfaces.

Figure 4.2 shows the effects of elevator and aileron ride control systems on rms vertical acceleration along the model fuselage. Corresponding results tabulated as percent change in rms vertical acceleration are given in Table I. The results show that the elevator can significantly reduce mid and aft body vertical accelerations, but the ailerons are considerably less effective. The two systems were synthesized independently to produce the maximum vertical acceleration reductions attainable with the elevator and ailerons. Block diagrams of the elevator and aileron ride control systems are shown in Figures 4.3 and 4.4. Results with both loops closed simultaneously show that the elevator system alone is better. Since the aileron system alone was not effective in reducing fuselage vertical acceleration, no attempt was made to refine the aileron system with the elevator loop closed.

TABLE I

EFFECTS OF ELEVATOR AND AILERON RIDE CONTROL SYSTEMS ON RMS VERTICAL ACCELERATION

| Body Station | Percent Change in RMS Vertical Acceleration | | |
|---|---|---|---|
| | Elevator RCS | Aileron RCS | Elev. & Aileron RCS |
| 172 | -4.4 | +3.3 | -1.0 |
| 860 | -16.7 | -1.7 | -11.4 |
| 1655 | -20.7 | -9.3 | -20.2 |

Figures 4.5 through 4.16 show PSD and RMS data which support the results given in Figure 4.2 and Table I. Some of the accumulative RMS plots are not complete out to 40 cps, but under each plot a final RMS value (corresponding to 40 cps) is printed. The units for the PSD and RMS axes respectively are $(g's/ft/sec)^2/rad$ and g's/ft/sec. These plots are all with respect to a 1 ft/sec RMS vertical gust on the model. Due to velocity scaling, a 1 ft/sec gust has the

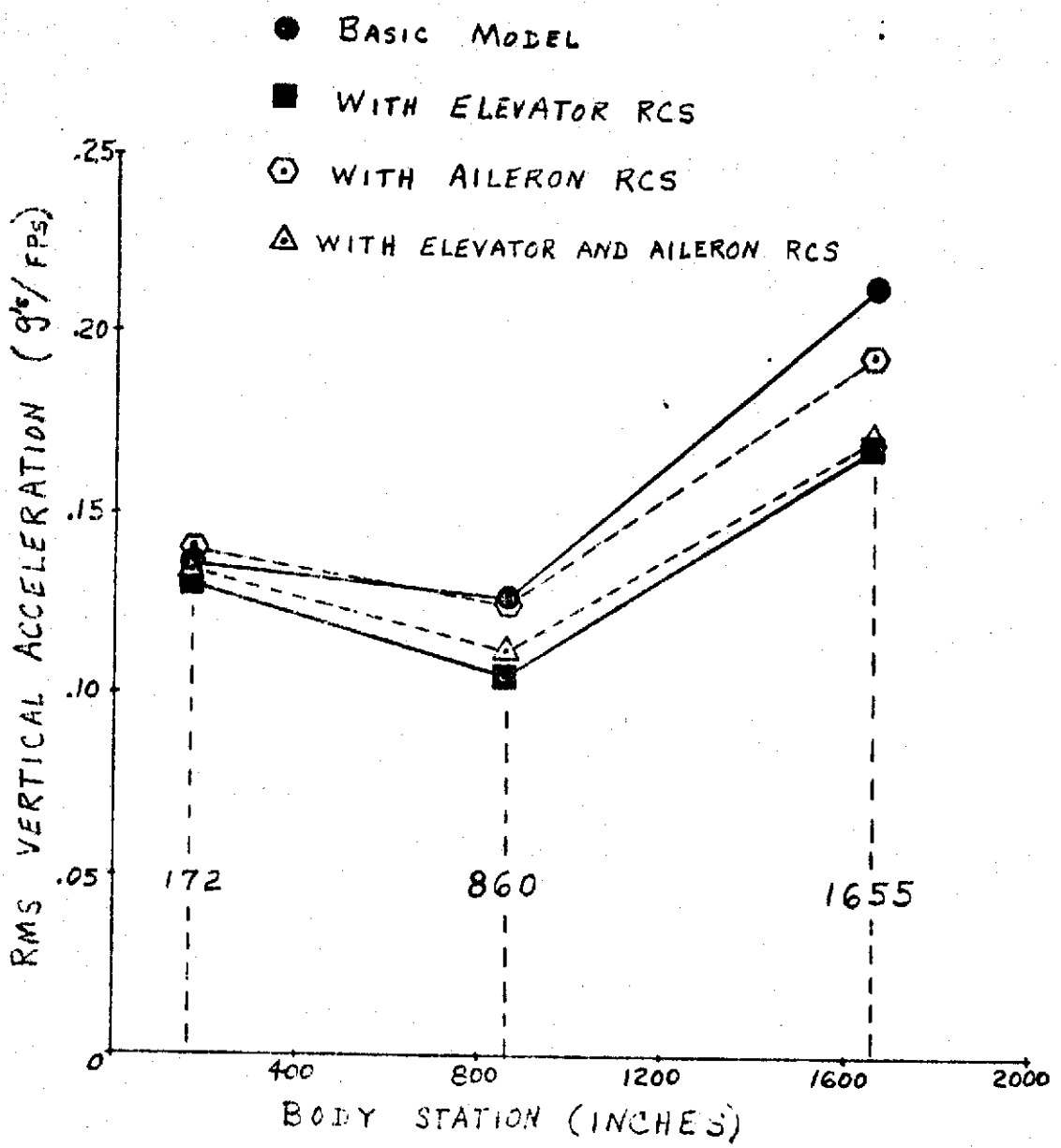


EFFECTS OF ELEVATOR AND AILERON RCS
ON RMS VERTICAL ACCELERATION

FIGURE 4.2

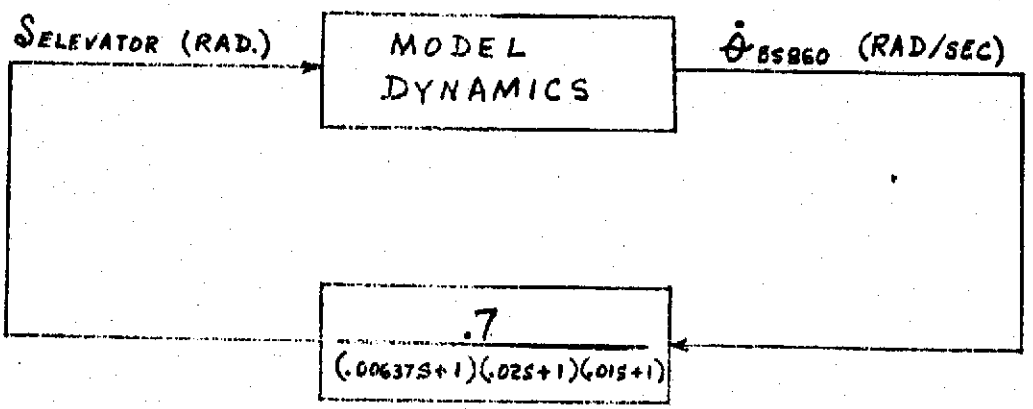


ELEVATOR RIDE CONTROL SYSTEM BLOCK DIAGRAM

FIGURE 4.3

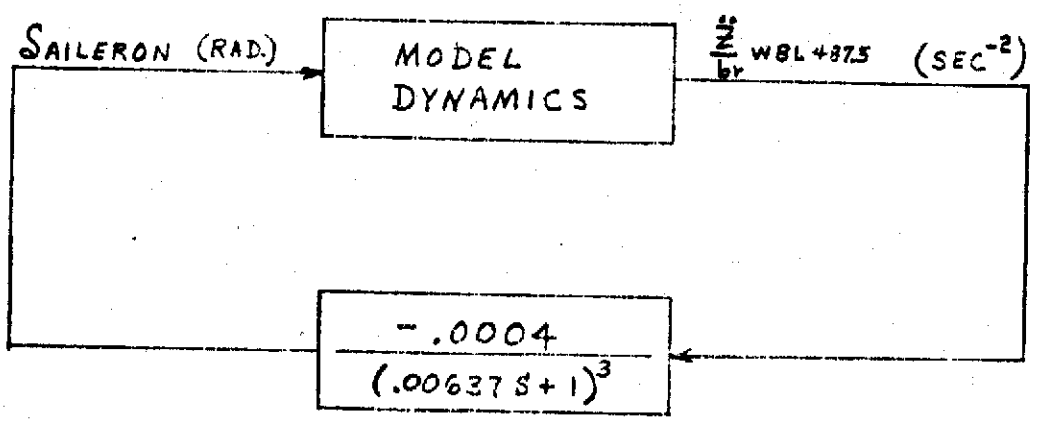


AILERON RIDE CONTROL SYSTEM BLOCK DIAGRAM

FIGURE 4.4

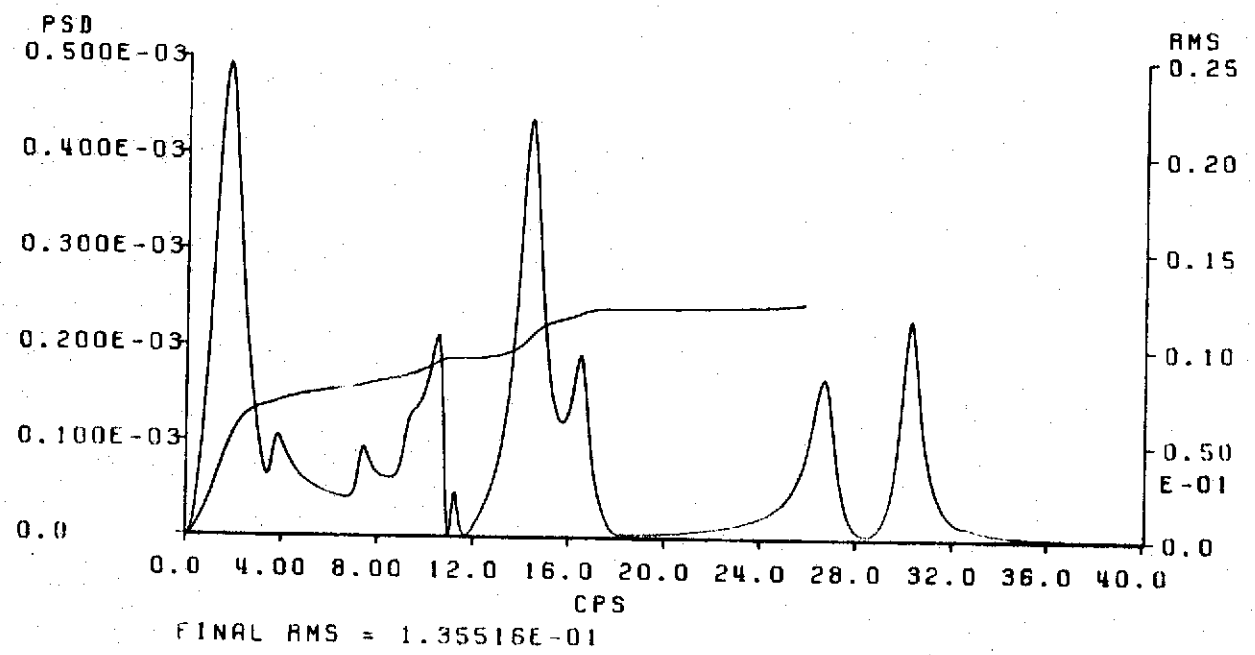


BS 172 VERTICAL GUST RESPONSE
SYSTEM OFF

FIGURE 4.5

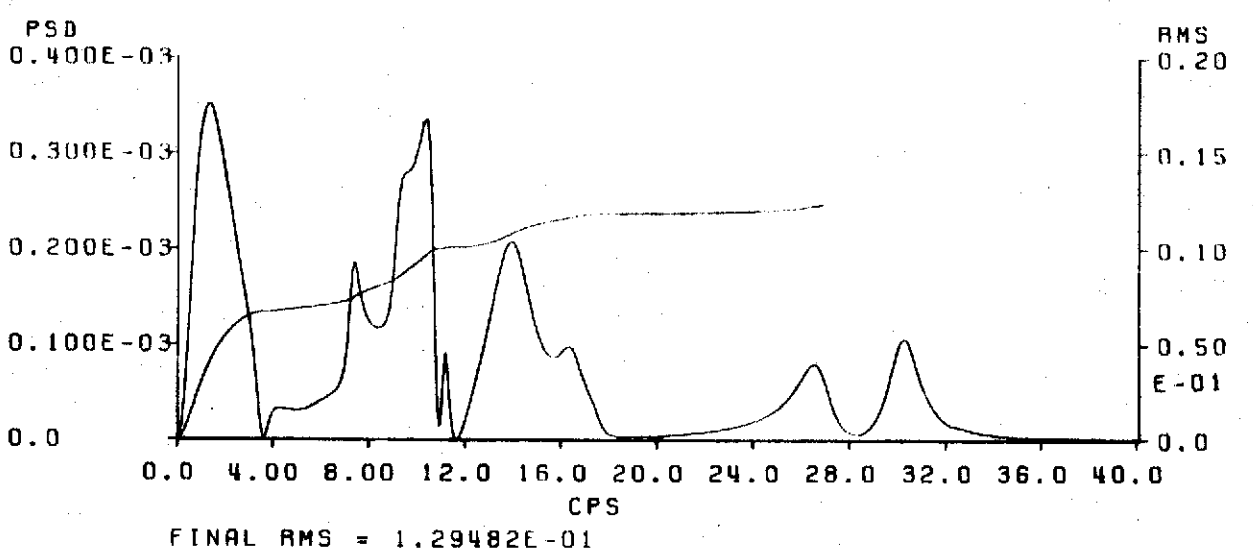


BS 172 VERTICAL GUST RESPONSE
SYSTEM ON

FIGURE 4.6

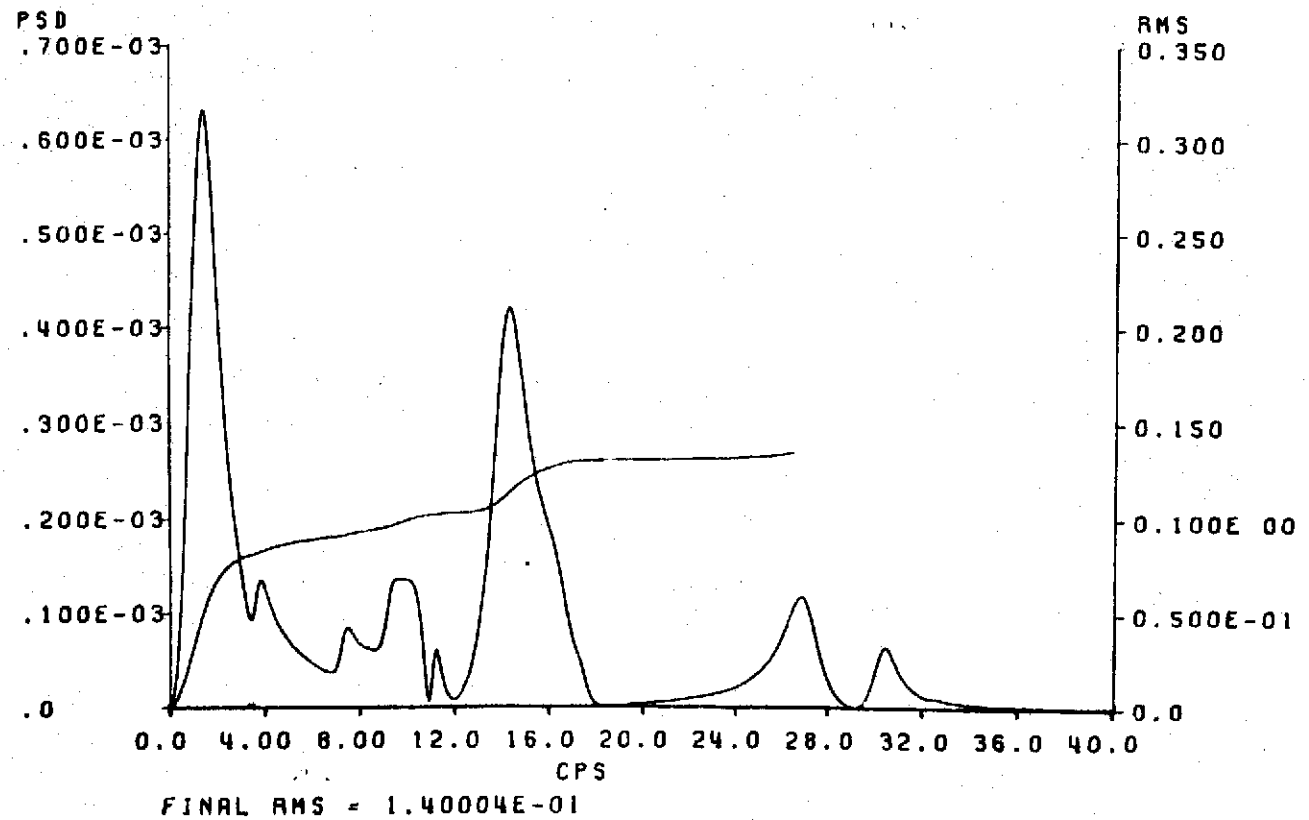


BS 172 VERTICAL GUST RESPONSE
AILERON SYSTEM ON

FIGURE 4.7

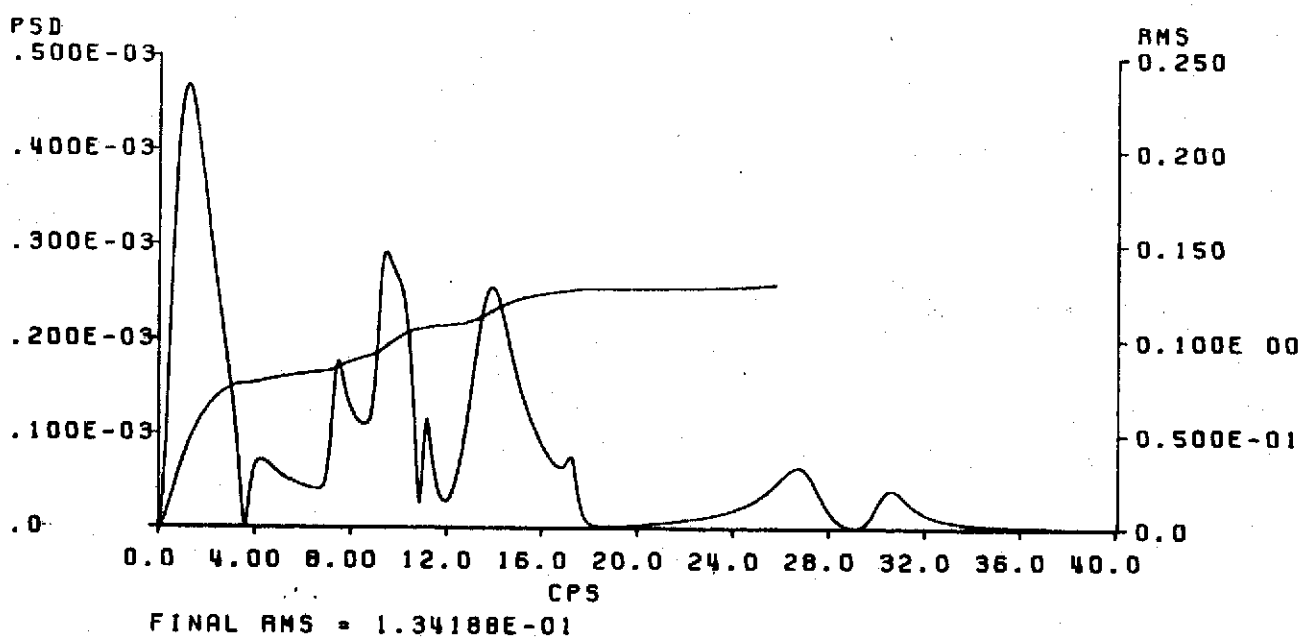


BS 172 VERTICAL GUST RESPONSE
ELEVATOR AND AILERON SYSTEM
ON
FIGURE 4.8

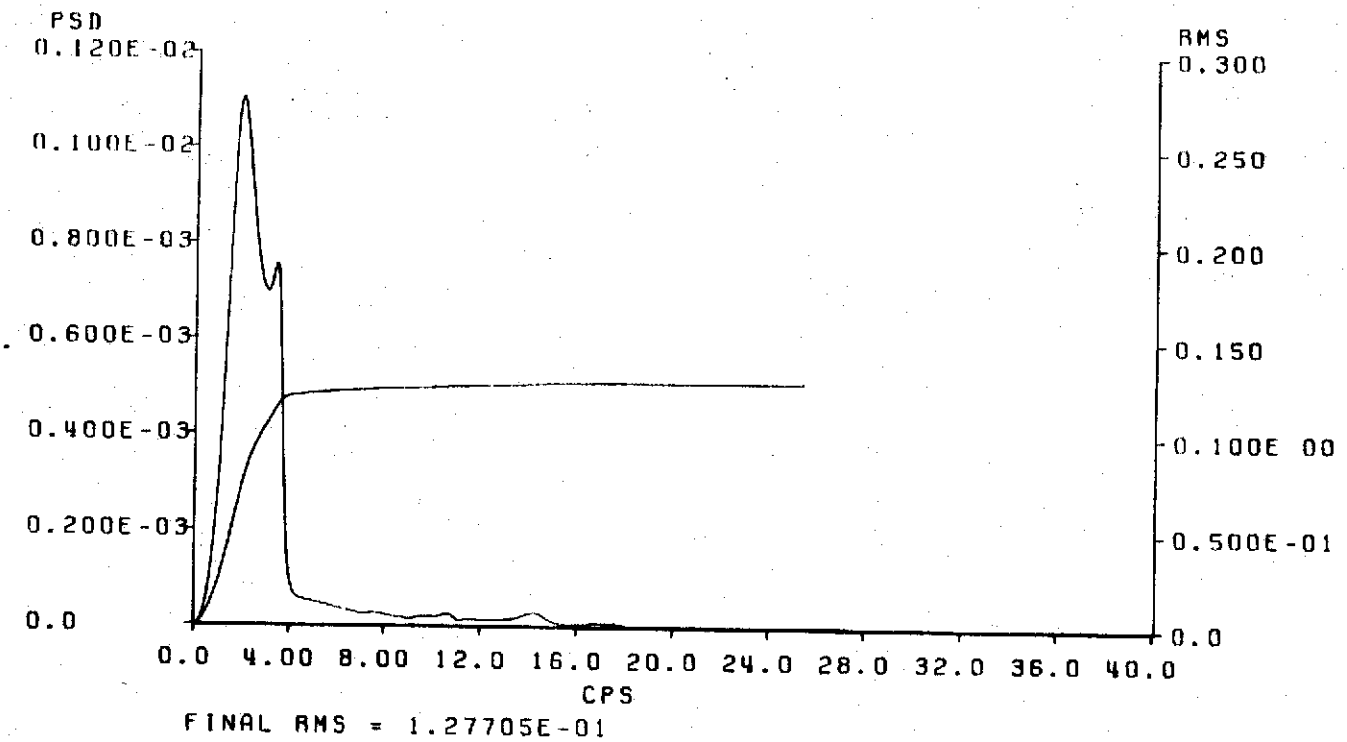


BS 860 VERTICAL GUST RESPONSE
SYSTEM OFF

FIGURE 4.9

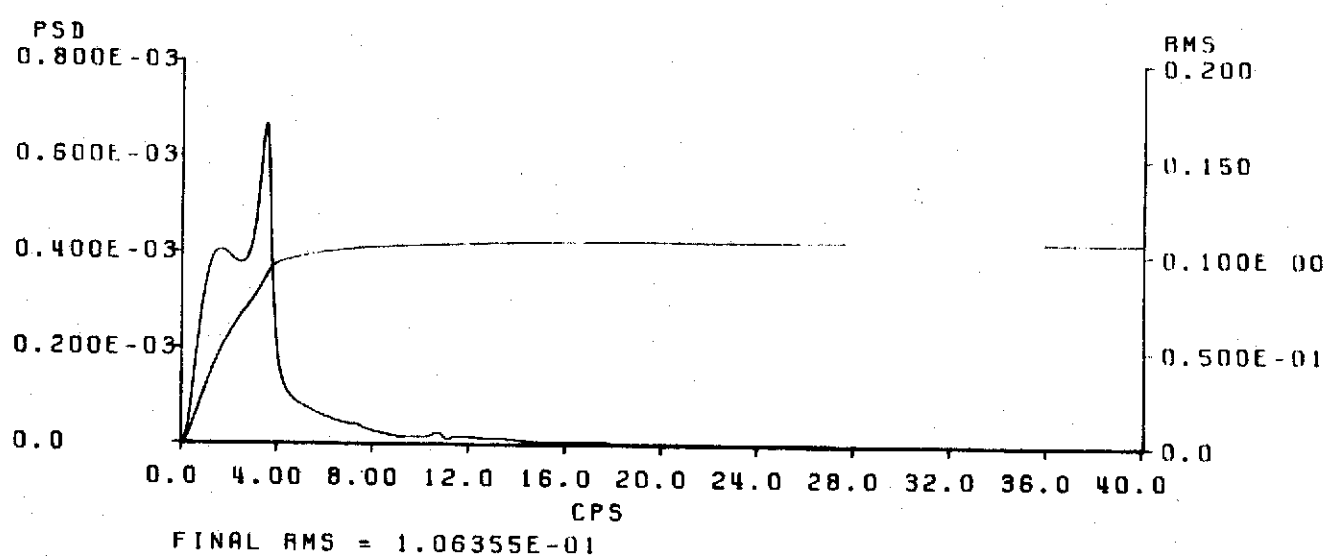


BS 860 VERTICAL GUST RESPONSE
ELEVATOR SYSTEM ON

FIGURE 4.10

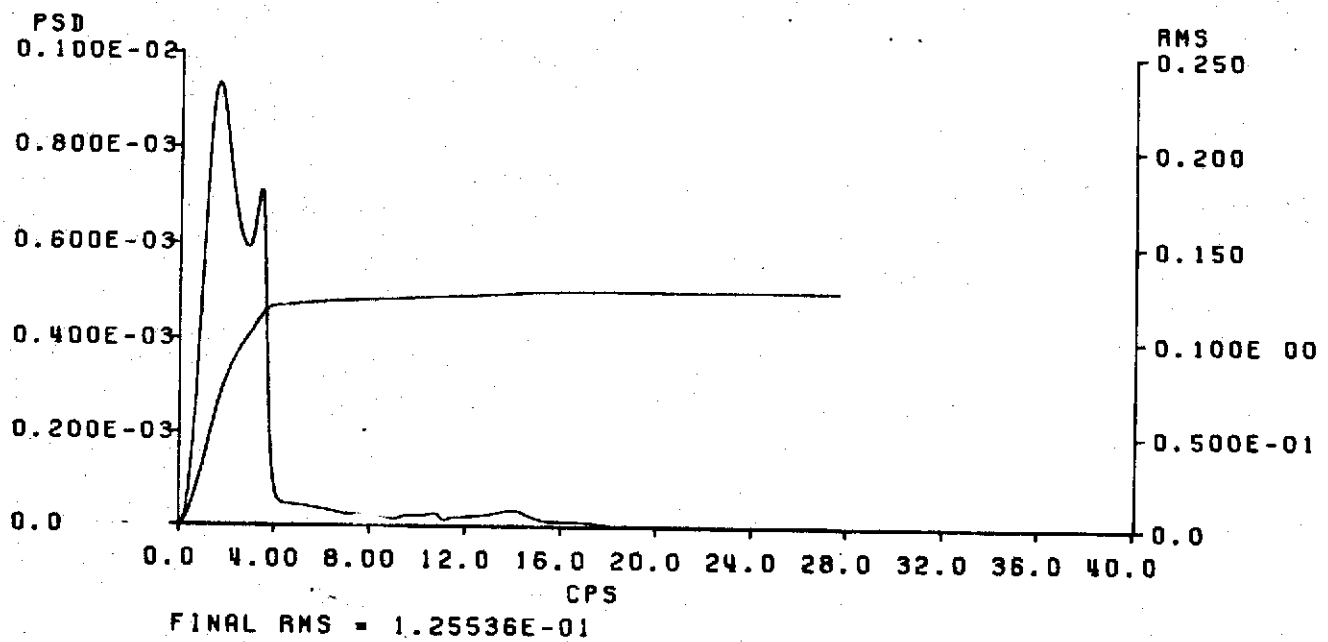


BS 860 VERTICAL GUST RESPONSE
AILERON SYSTEM ON

FIGURE 4.11

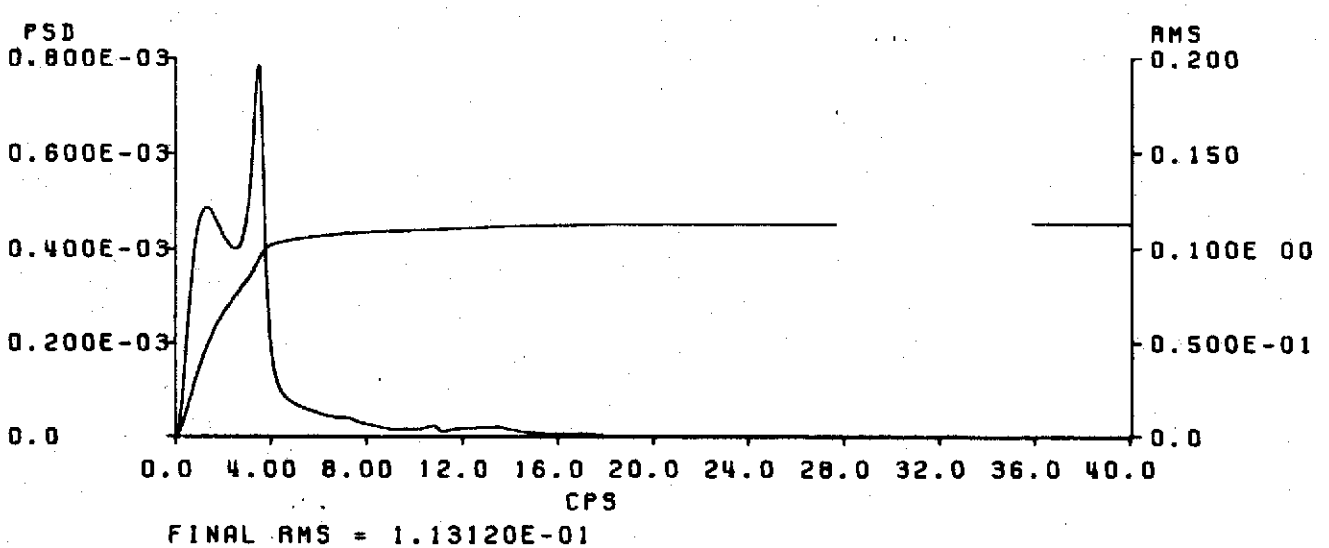


BS 860 VERTICAL GUST RESPONSE
ELEVATOR AND AILERON SYSTEM
ON
FIGURE 4.12

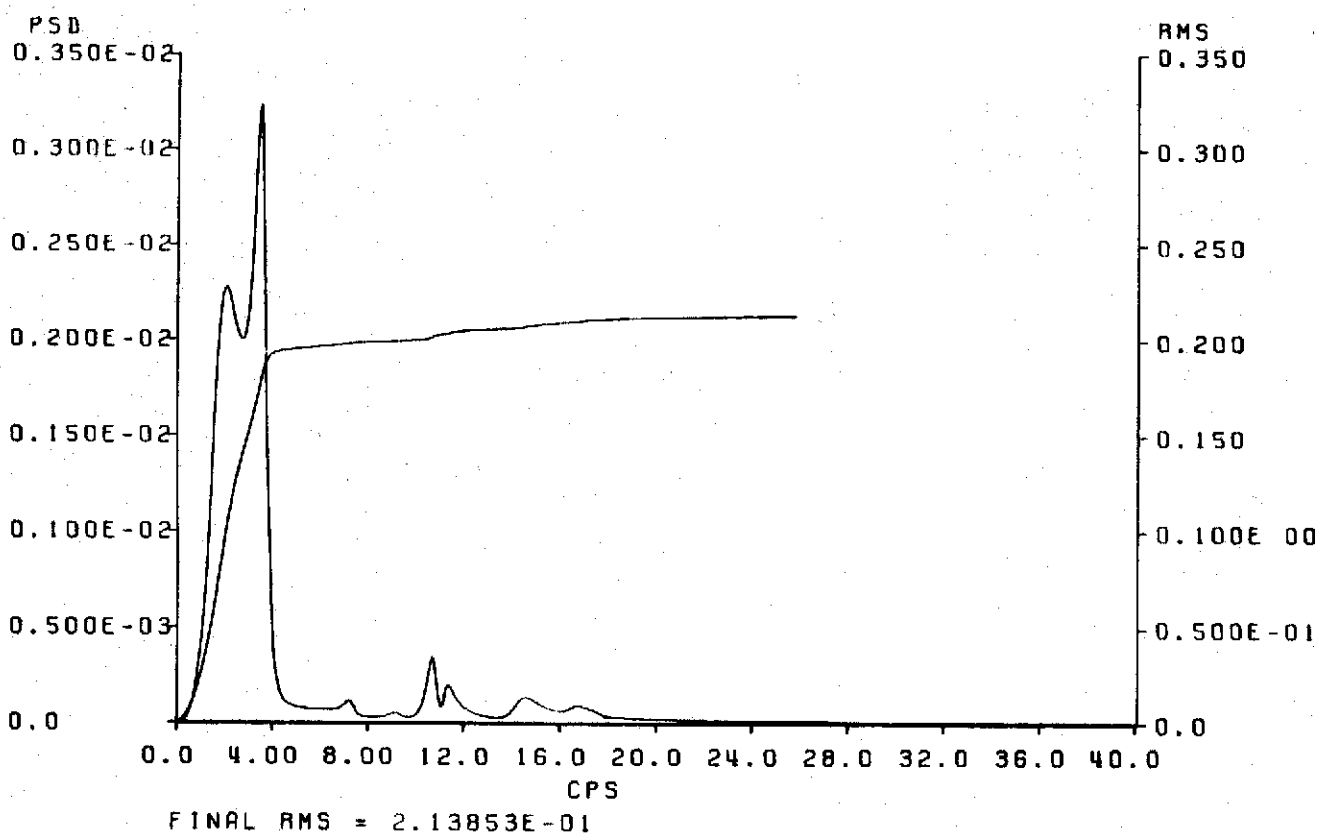


BS 1655 VERTICAL GUST RESPONSE
SYSTEM OFF

FIGURE 4.13

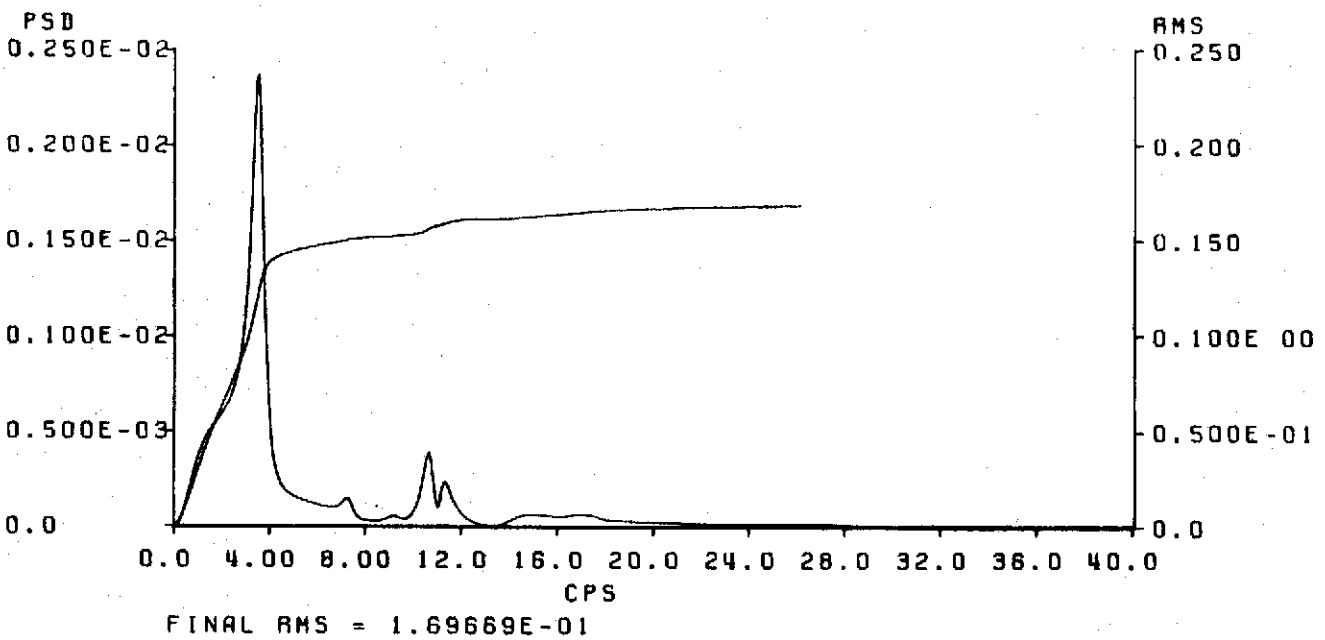


BS 1655 VERTICAL GUST RESPONSE
ELEVATOR SYSTEM ON

FIGURE 4.14

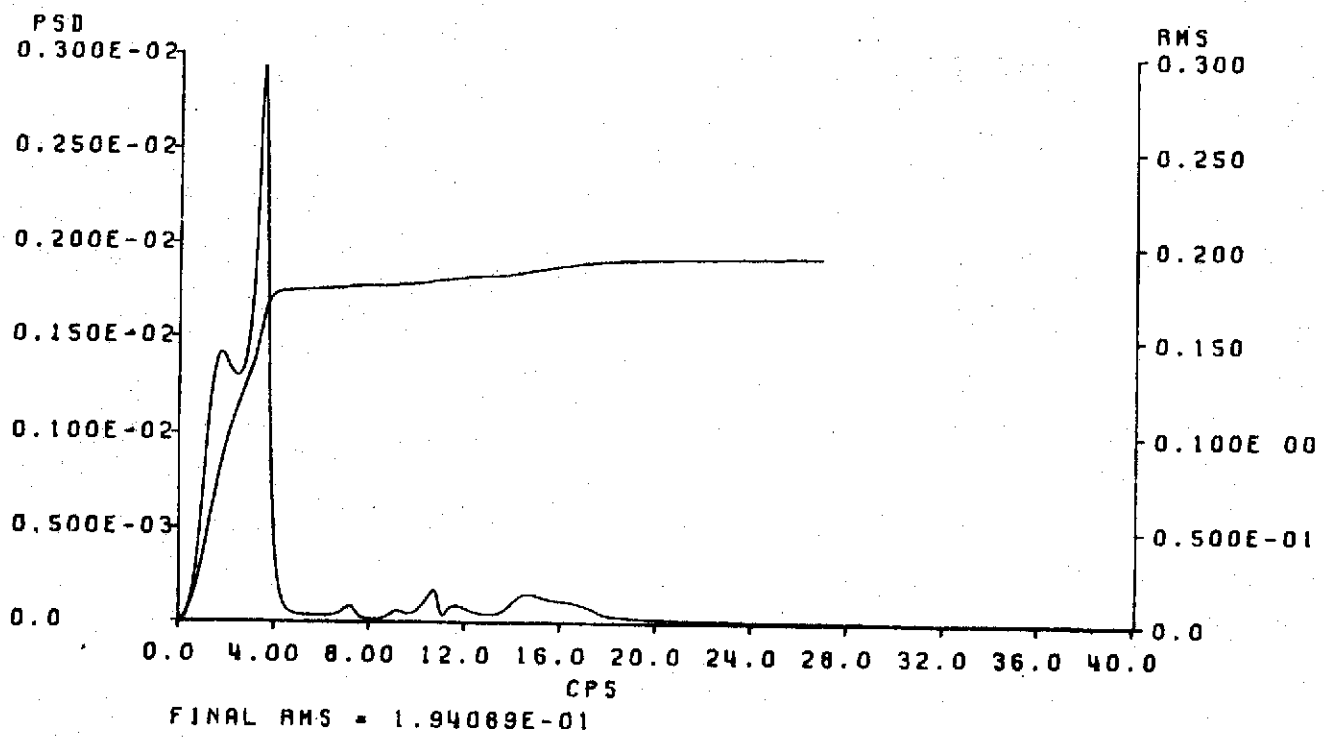


BS 1655 VERTICAL GUST RESPONSE
AILERON SYSTEM ON

FIGURE 4.15

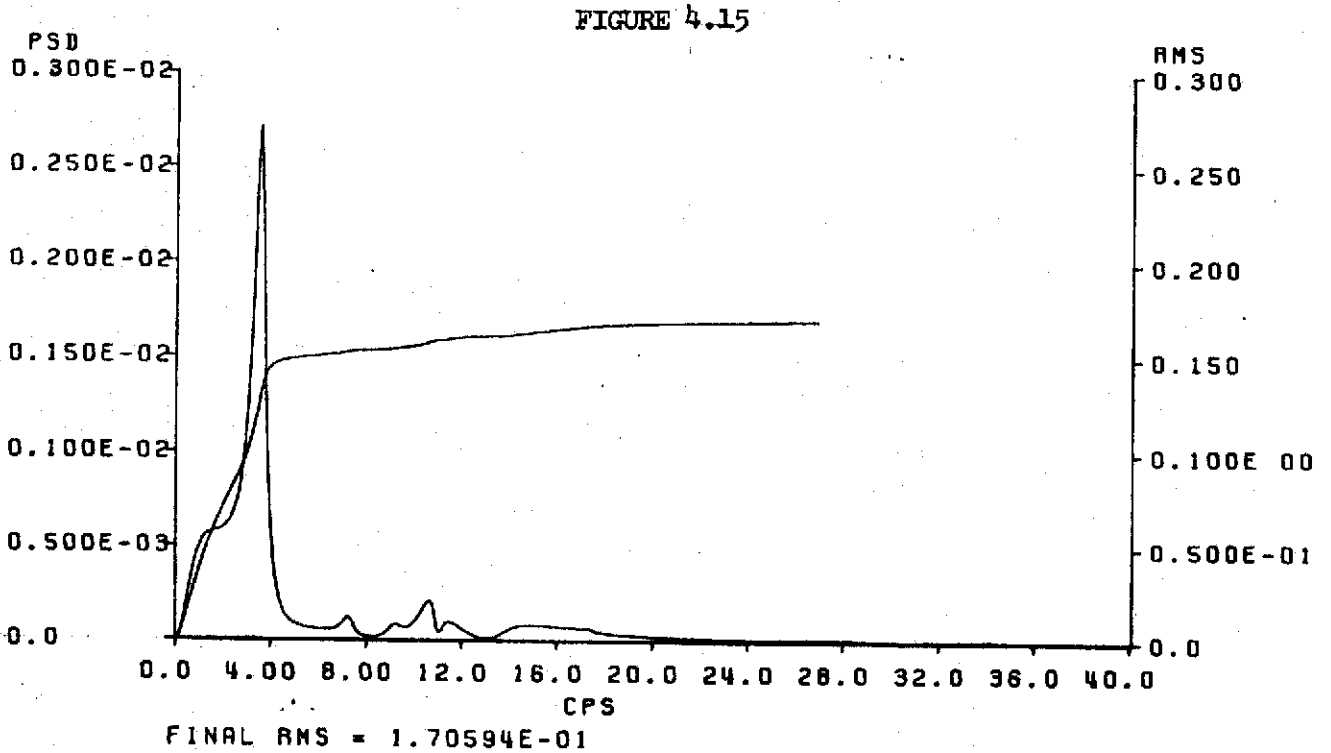


BS 1655 VERTICAL GUST RESPONSE
ELEVATOR AND AILERON SYSTEM
ON

FIGURE 4.16

same effect on the model as a 5.48 ft/sec gust has on the full scale airplane. Equivalent airplane values can be obtained by dividing the model RMS values by 5.48. Ride performance was evaluated at three stations along the fuselage: BS 172 (pilot's station), BS 860 (approximate cg), and BS 1655 (aft fuselage).

The PSD's in Figures 4.5 through 4.8 show that the model gust response at BS 172 has contributions from rigid body motions and several structural modes and that neither the elevator nor the aileron ride control system changes the response significantly.

Figures 4.9 through 4.16 show that the model gust response at BS 860 and BS 1655 are similar in that they both indicate predominant rigid body and first structural mode contributions. The elevator ride control system is effective in reducing rigid body response but neither the elevator nor the aileron effectively couples with the first structural mode.

Pitch rate feedback from BS 860 is used in the elevator ride control system as depicted in Figure 4.3. Its effect on model dynamics may be observed in the root locus of Figure 4.21a. Primary coupling is with the short period mode. Figures 4.17 and 4.18 indicate model elevator displacement and rate in a gust environment. Equivalent airplane surface activity may be obtained by dividing displacement by 5.48 and rate by $(5.48)^2$.

The aileron ride control system shown in Figure 4.4 uses acceleration feedback from the wing (WBL 487.5 which is near the aileron). Root loci for this system used alone and in support of the elevator system are shown in Figures 4.21b and 4.21c. Aileron surface activity is shown in Figures 4.19 and 4.20.

The 12th structural mode showed no coupling with the systems and was omitted from the root loci in Figure 4.21.

The systems presented have at least 6 db gain margins and 60 degrees phase margins.

4.2.2 Phase II - Canard Surfaces

Phase I results indicated that a control surface on the forward body would be necessary to improve ride at the pilot station. For preliminary analysis purposes, a point force (P.F.) representation of canards at BS 172 was added to the equations of motion. The canard coefficients were obtained by transposing the BS 172 Z-modal coefficient row.

Phase II included evaluation of a canard ride control system and a canard/elevator system. Effects of these ride control systems on RMS vertical acceleration are given in Table II.

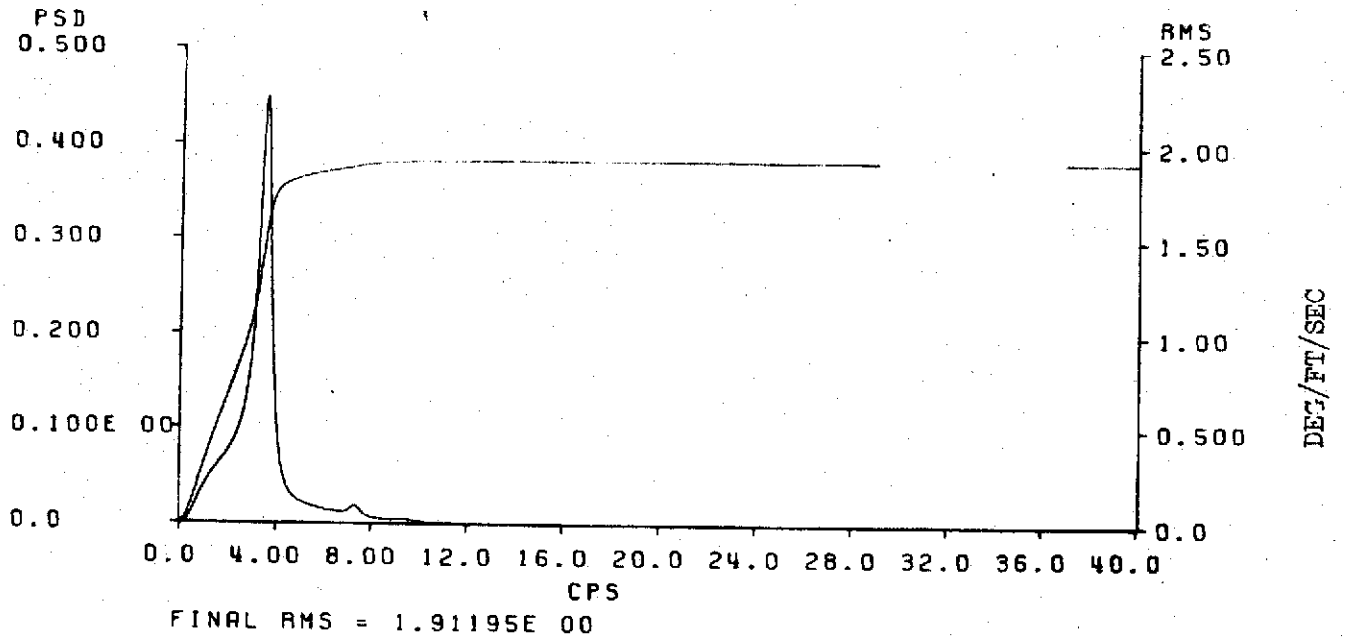


ELEVATOR DISPLACEMENT/VERTICAL GUST

FIGURE 4.17

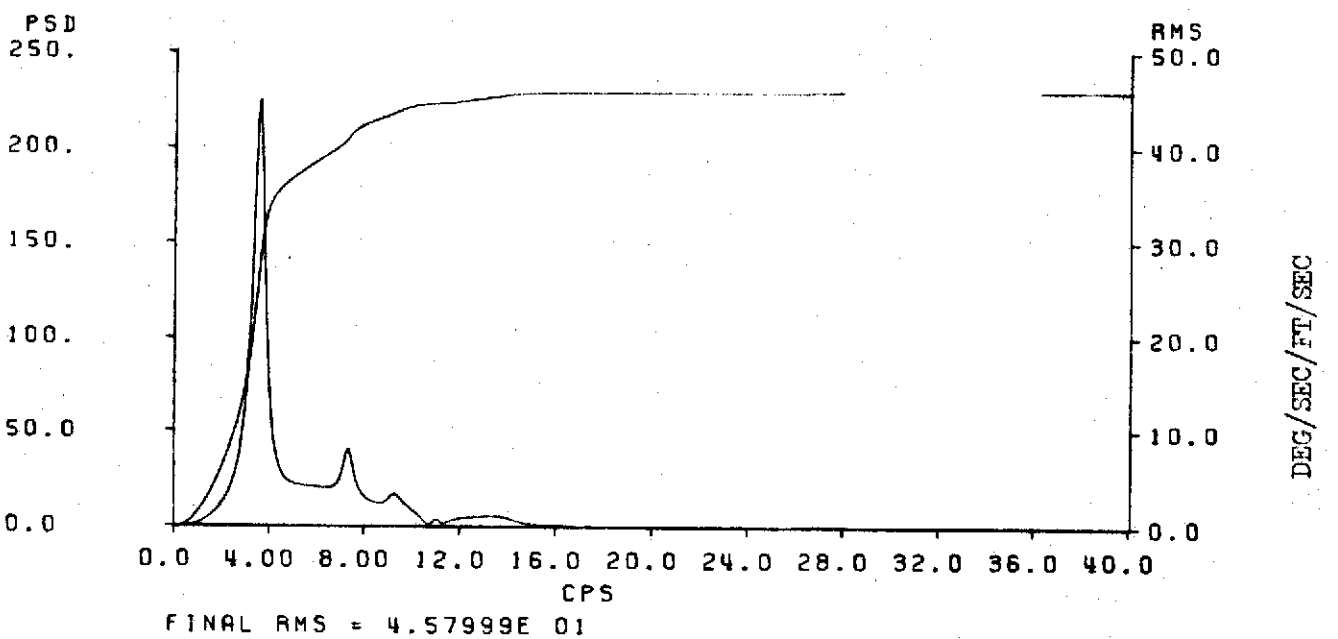


ELEVATOR RATE/VERTICAL GUST

FIGURE 4.18

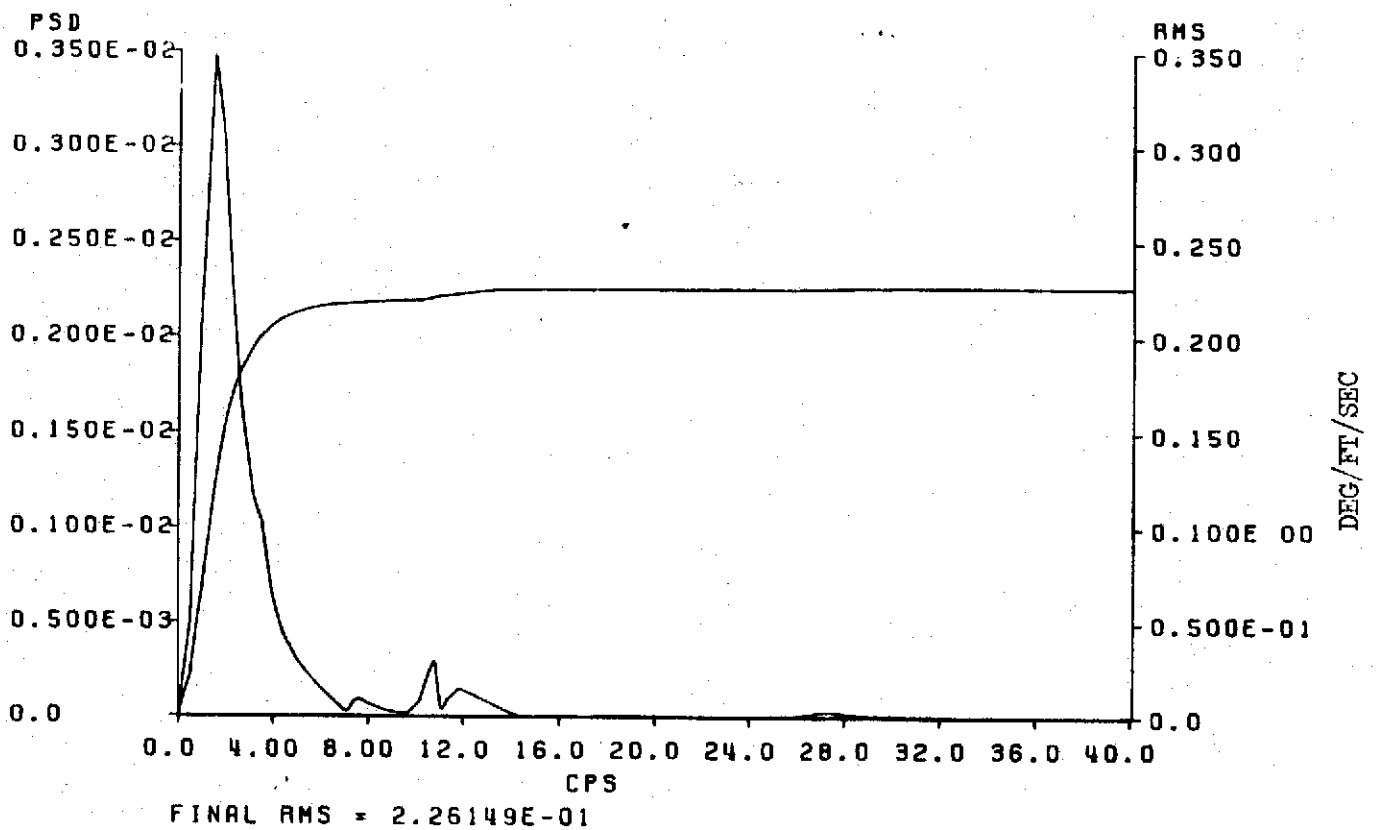


AILERON DISPLACEMENT/VERTICAL GUST

FIGURE 4.19

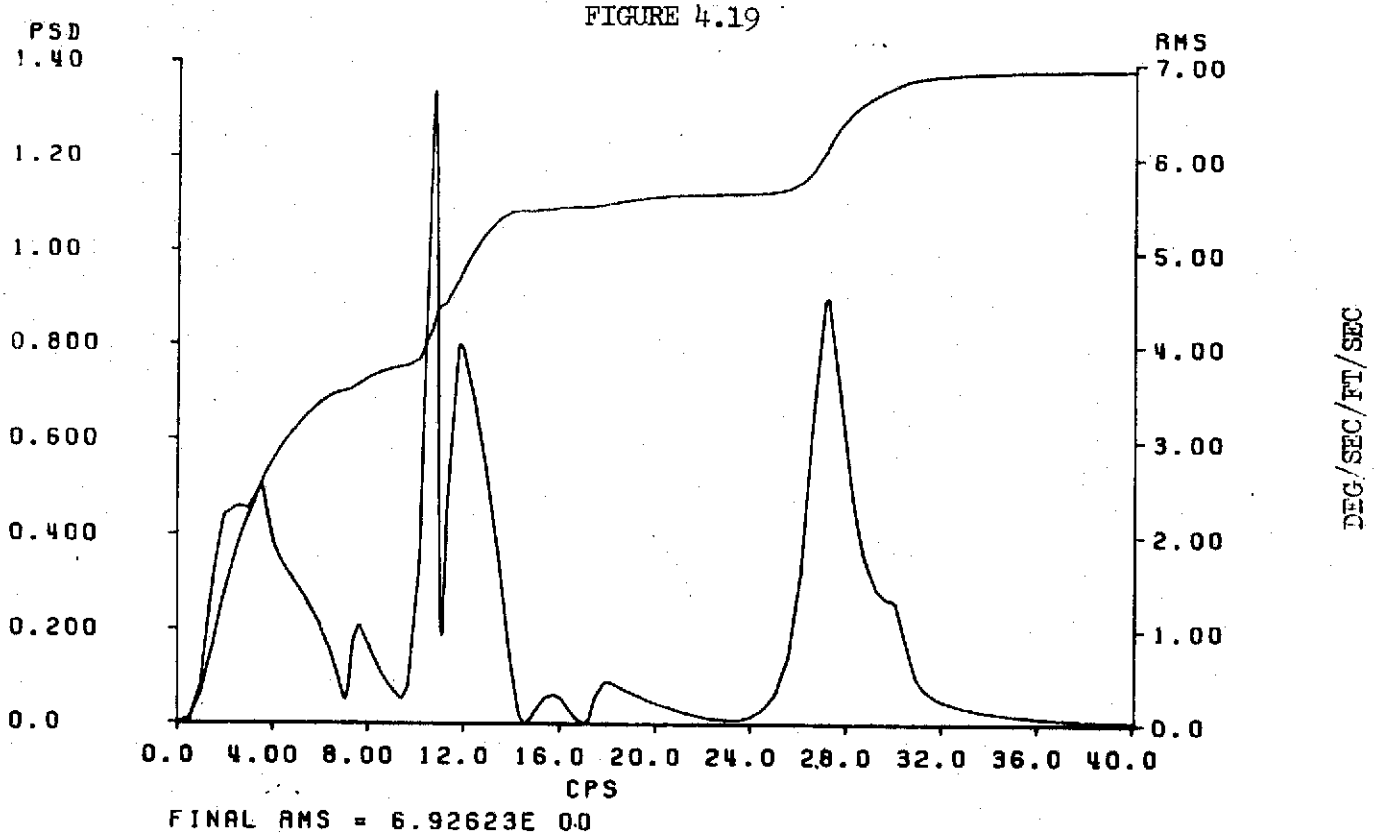


AILERON RATE/VERTICAL GUST

FIGURE 4.20

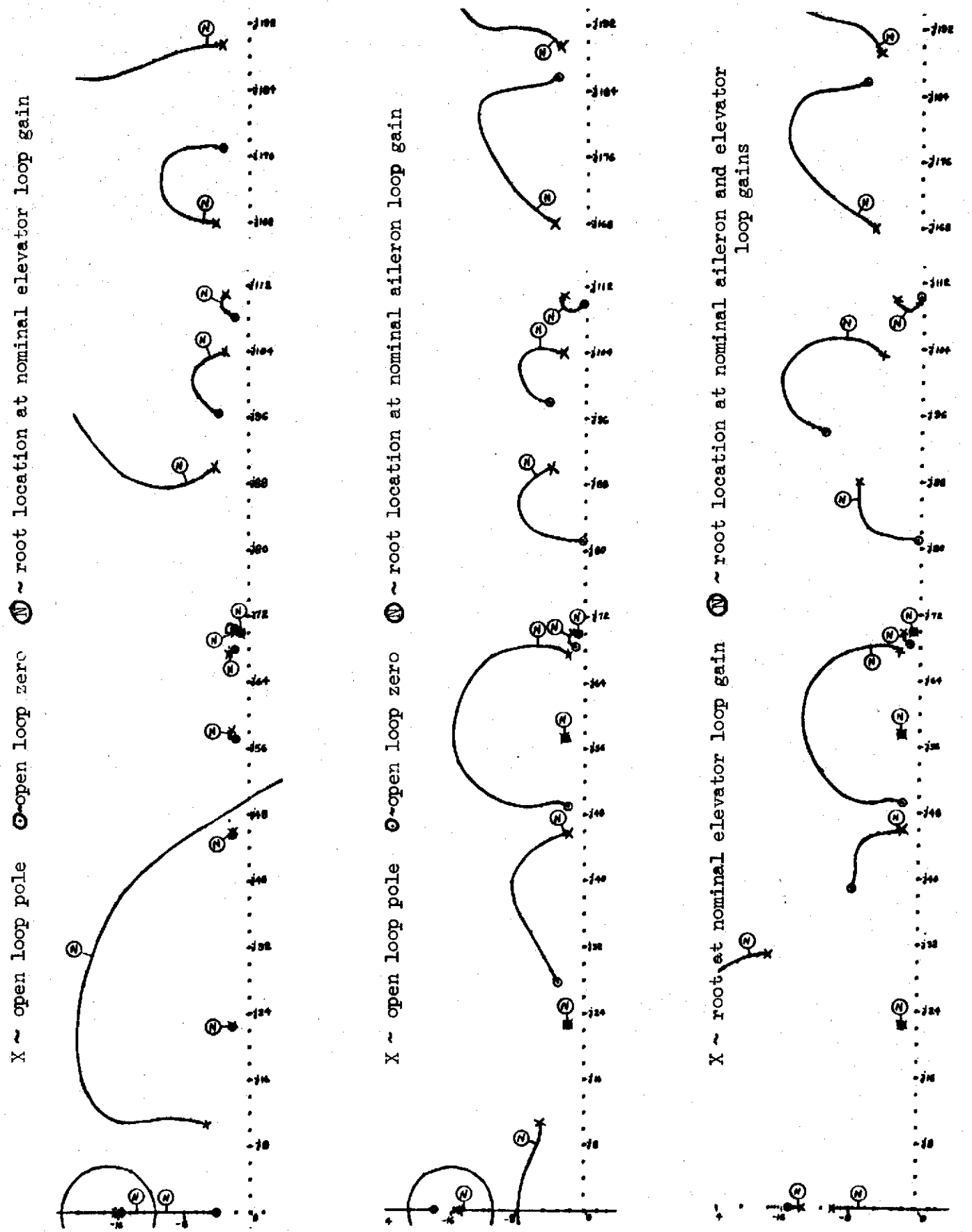


a) Elevator RCS

b) Aileron RCS

c) Aileron RCS with Elevator Loop Closed

RIDE CONTROL SYSTEMS ROOT LOCI

FIGURE 4.21

TABLE II

EFFECTS OF CANARD AND ELEVATOR RIDE CONTROL SYSTEMS ON RMS VERTICAL ACCELERATION

| Body Station | Percent Change in RMS Vertical Acceleration | |
|---|---|---|
| | Canard (P.F.) RCS | Canard (P.F.) and Elevator RCS |
| 172 | -37.9 | -35.0 |
| 860 | -10.2 | -23.7 |
| 1655 | + 1.5 | -12.2 |

$\ddot{Z}$ at BS 172 was sensed and fed back to the canard through the feedback transfer function

$$\frac{-.0001S}{(.00637S + 1)(.02S + 1)^2} .$$

The elevator system was the same as presented in Section 2.1 for Phase I.

Figures 4.22 through 4.27 show the PSD and RMS data from which Table II was derived. The canard system provides adequate vertical acceleration reduction at the pilot station and some reduction at the mid body station. Comparing Figures 4.14 and 4.27, it is evident that the canard excited the aft body 1st structural mode and the 10 cps mode. With both the canard and elevator loops closed, the reduction at the mid and aft body is lower than the reduction obtained with the elevator system only. The canard system was designed independent of the elevator to produce the maximum vertical acceleration reduction possible with the forward body canards.

Figure 4.28a presents a root locus of the canard system and Figure 4.28b shows the effect of the elevator system on the closed loop canard system. The canard system is a wide bandpass system that causes large movements of the higher frequency structural mode poles.

None of the systems presented thus far significantly improved the 1st mode response at the mid and aft body stations nor indicated adequate potential for reducing vertical accelerations by 30 percent over the length of the fuselage.

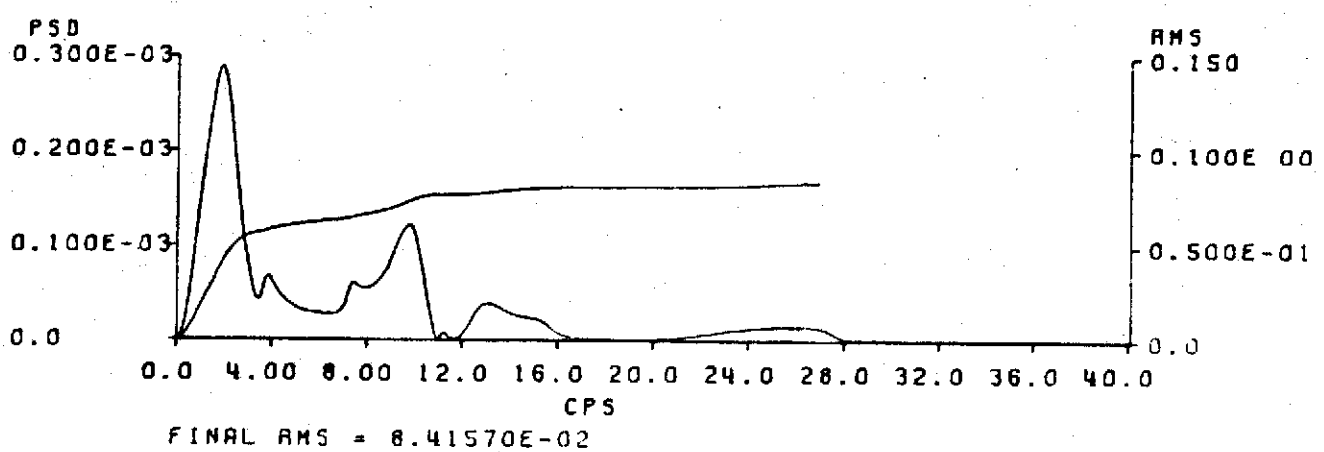


BS 172 VERTICAL GUST RESPONSE
CANARD SYSTEM ON

FIGURE 4.22

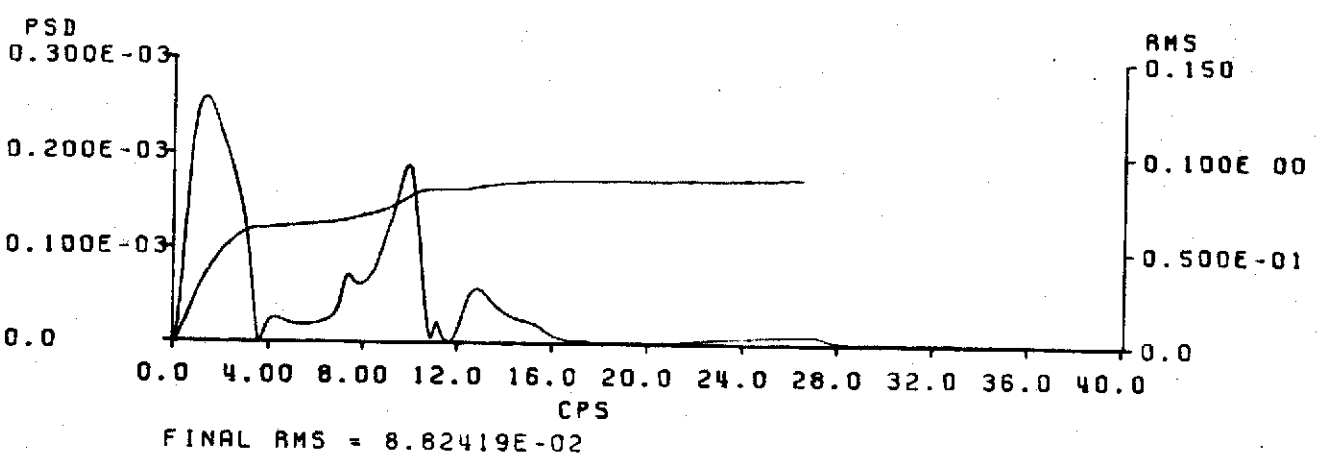


BS 172 VERTICAL GUST RESPONSE
CANARD AND ELEVATOR SYSTEM
ON
FIGURE 4.23

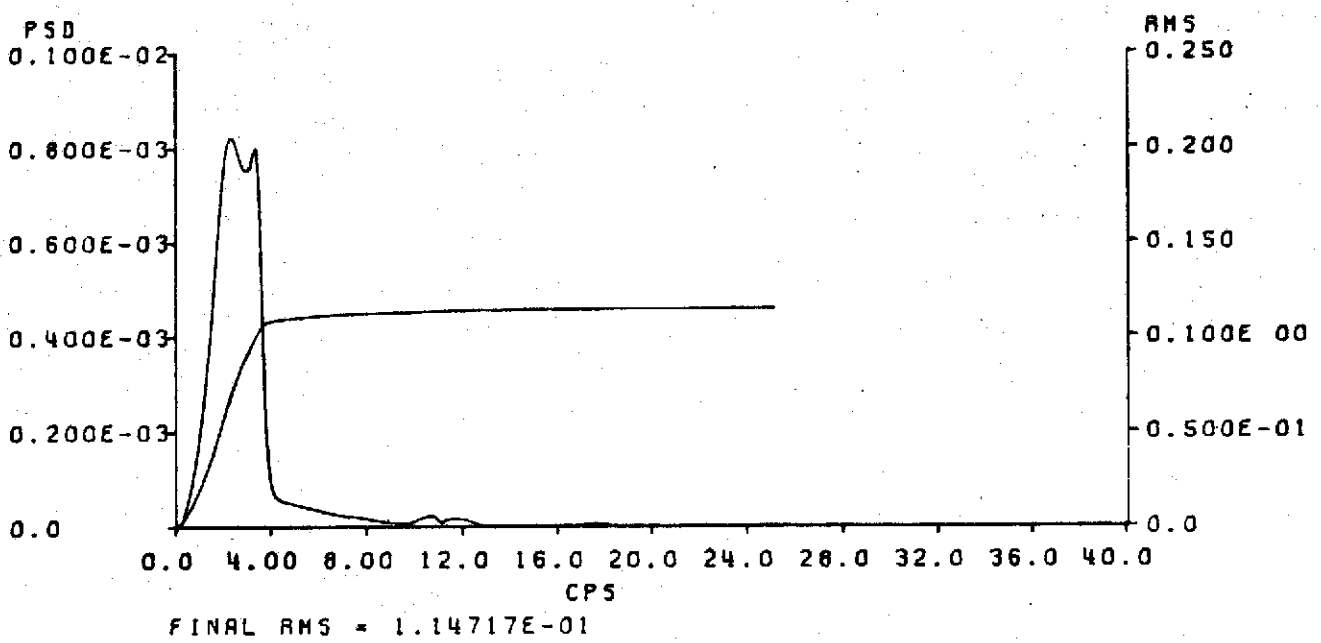


BS 860 VERTICAL GUST RESPONSE
CANARD SYSTEM ON

FIGURE 4.24

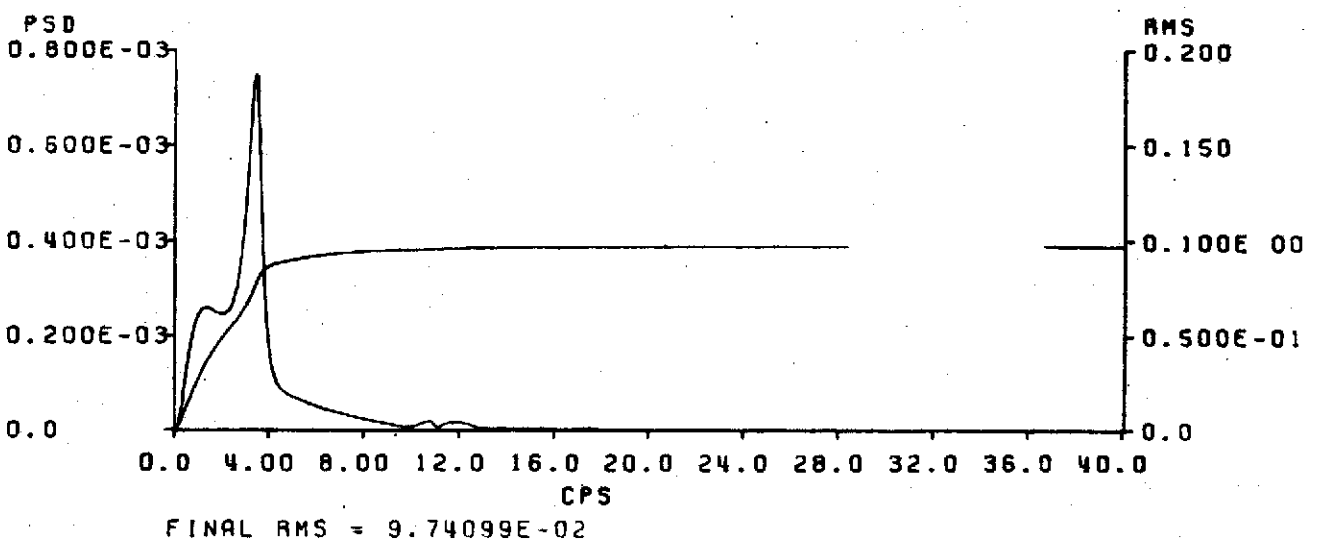


BS 860 VERTICAL GUST RESPONSE
CANARD AND ELEVATOR SYSTEM
ON
FIGURE 4.25

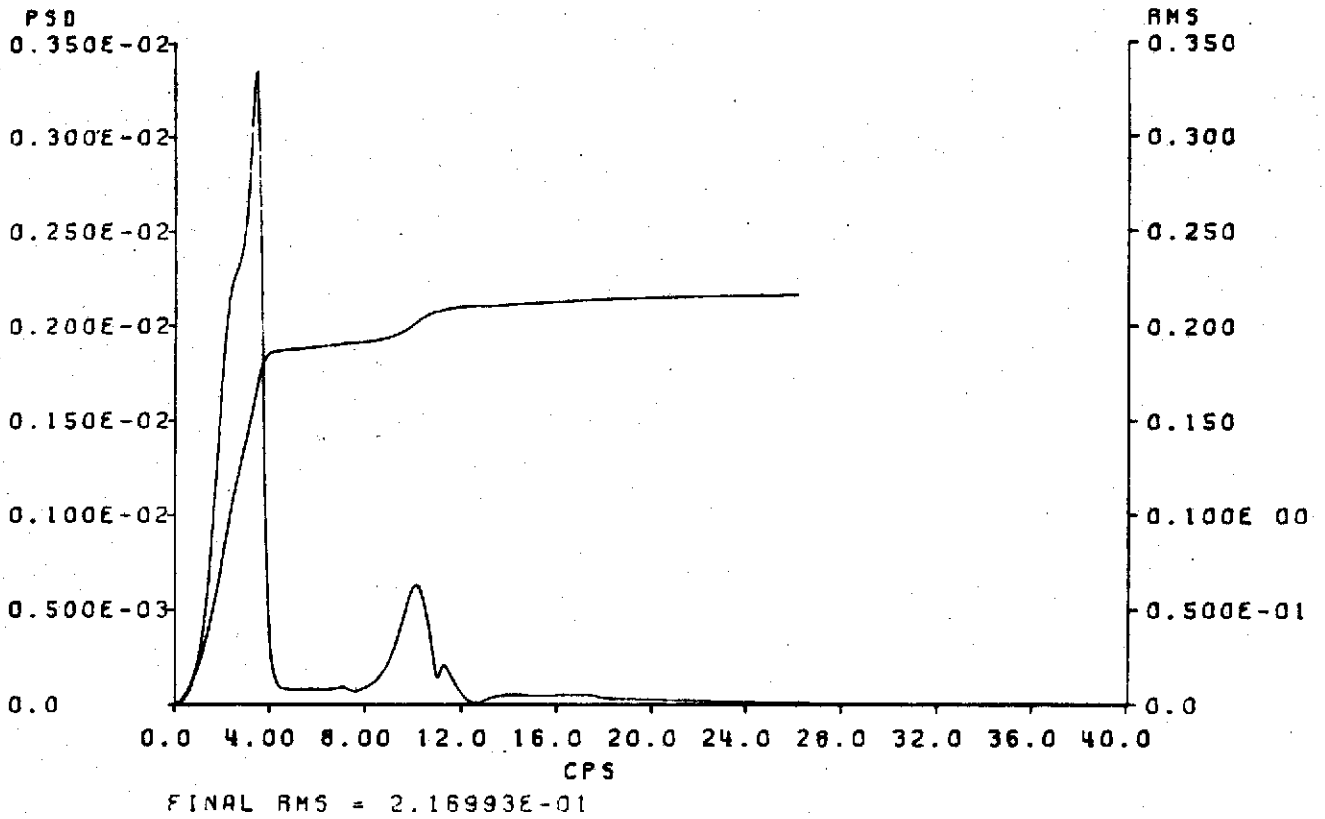


BS 1655 VERTICAL GUST RESPONSE
CANARD SYSTEM ON

FIGURE 4.26

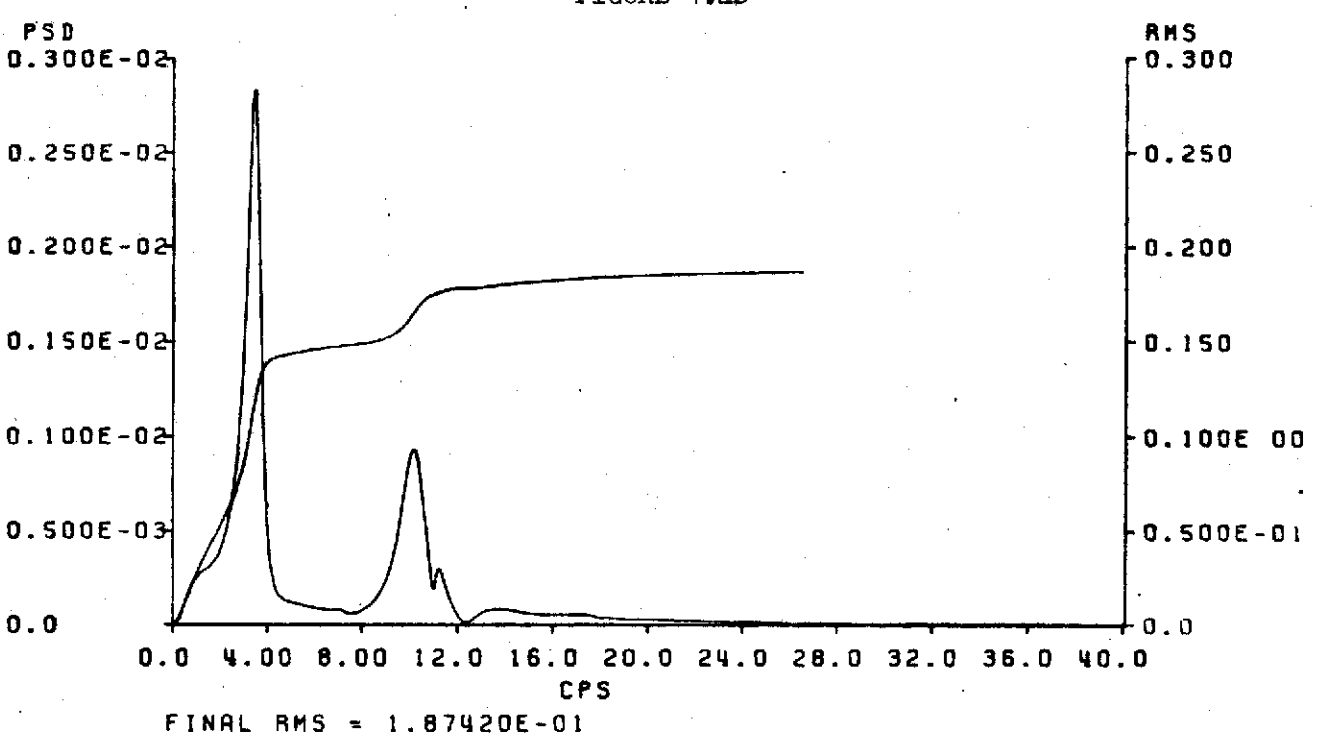


BS 1655 VERTICAL GUST RESPONSE
CANARD AND ELEVATOR SYSTEM
ON

FIGURE 4.27

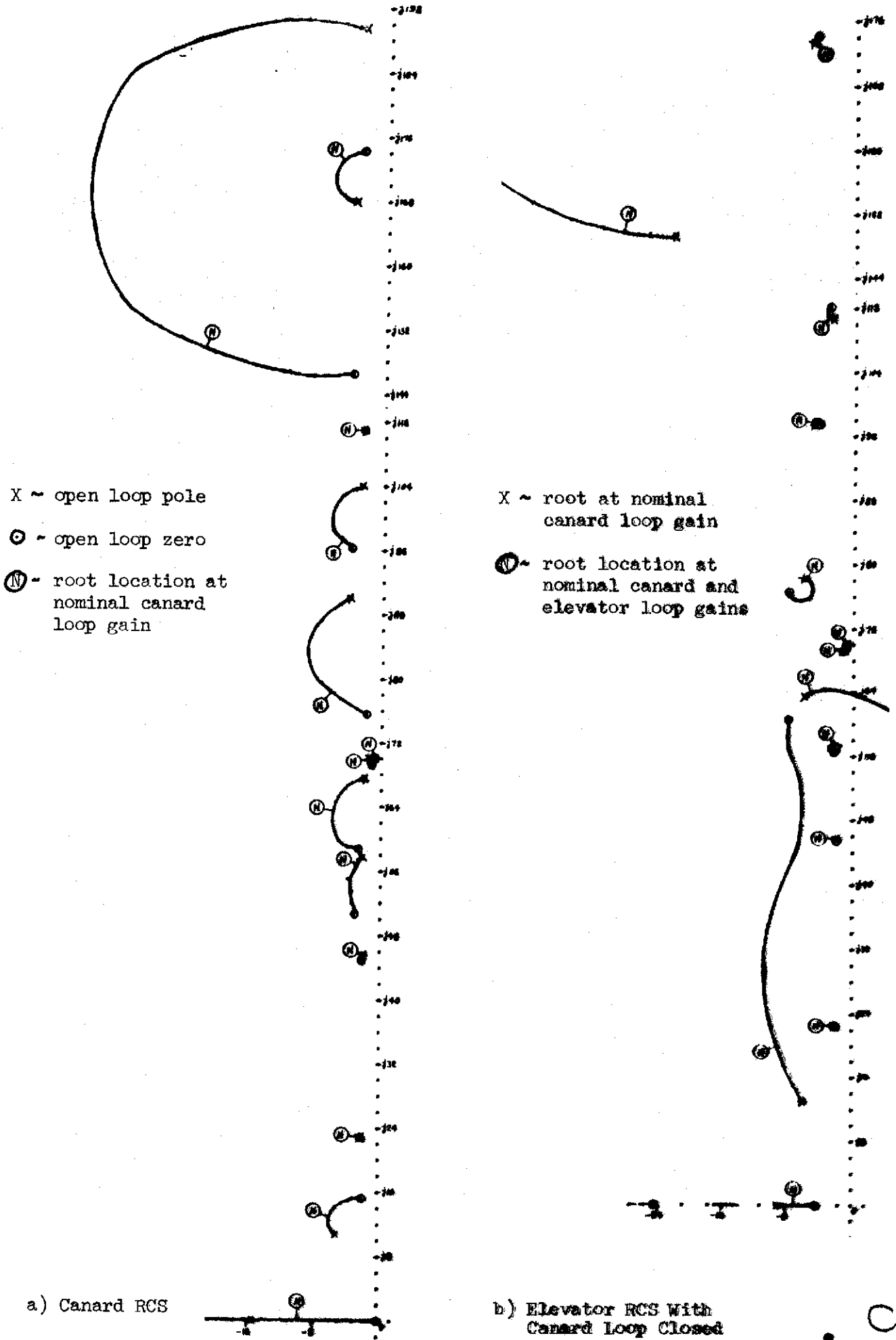


a) Canard RCS

b) Elevator RCS With Canard Loop Closed

RIDE CONTROL SYSTEMS ROOT LOCI
FIGURE 4.28

### 4.2.3 Phase III - Canard-Flaperon-Elevator Surfaces

The results of Phases I and II indicated that a three surface control system would be required to achieve the design goal of 30 percent vertical acceleration reduction over the length of the model fuselage. Table III presents the percent reduction obtained with a canard-flaperon-elevator system.

TABLE III

EFFECTS OF CANARD-FLAPERON-ELEVATOR RIDE CONTROL SYSTEM ON RMS VERTICAL ACCELERATION

| Body Station | Percent Change in RMS Vertical Acceleration |
|---|---|
| 172 | -36.4 |
| 510 | -35.6 |
| 860 | -39.2 |
| 1237 | -32.7 |
| 1655 | -31.0 |

These reductions were computed using the Von Karman gust spectrum with a characteristic length of 2500/30 = 83.3 ft. The numerical values as a function of body station are shown in Figure 4.29. Figures 4.30 and 4.34 present the RMS-PSD data supporting Table III.

Figure 4.30 indicates that the short period mode has been effectively suppressed at the pilot station, the 1st structural mode shows an insignificant increase and the 2nd through 10th structural modes have been suppressed.

Aft from the pilot station, the basic airplane short period and 1st structural mode response increase monotonically and the higher frequency structural mode responses become nearly insignificant by comparison. Using the elevator and flap system, the short period and 1st mode can be controlled. The increased response shown by Figures 4.31 through 4.34 in the frequency range of 4 to 12 cps results from the flap and canard systems.

For Phase III, the mathematical representation of the canard was updated to include canard aerodynamics. Aerodynamic flaperon representation was also used. Second order actuator dynamics based on control surface moments of inertia were used as shown in Figure 4.35. A significant difference between this system and the previous systems is that the elevator is driven with $\ddot{Z}$ sensed at the aft body station which permits significant reduction of the 1st structural mode response.

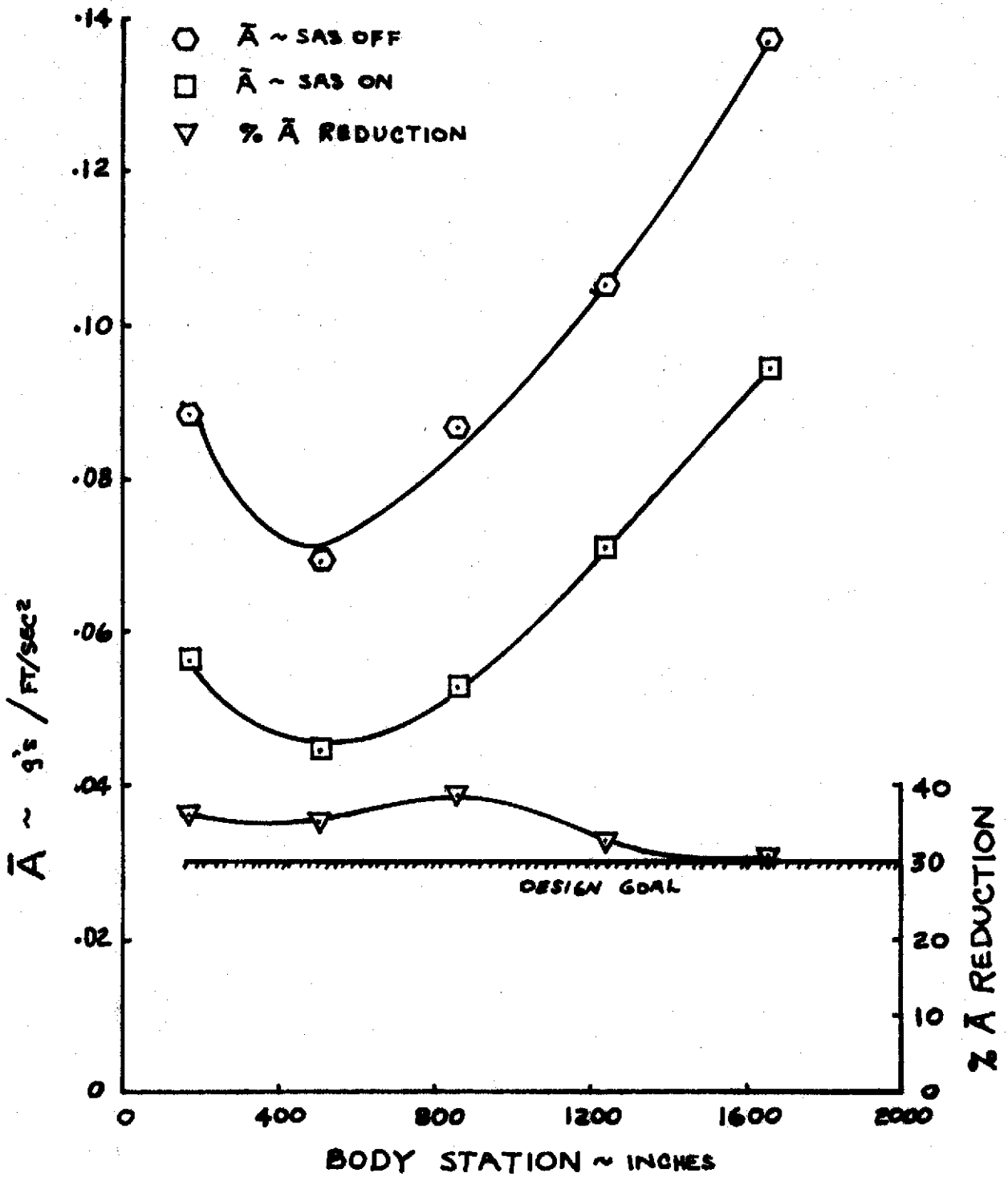


EFFECTS OF CANARD-FLAPERON-ELEVATOR RCS ON RMS VERTICAL ACCELERATION

FIGURE 4.29

| | | | | |
|---|---|---|---|---|
| CALC | WW | | REVISED | DATE |
| CHECK | | | | |
| APPD | | | | |
| APPD | | | | |

REV LTR:

E 1196 R6

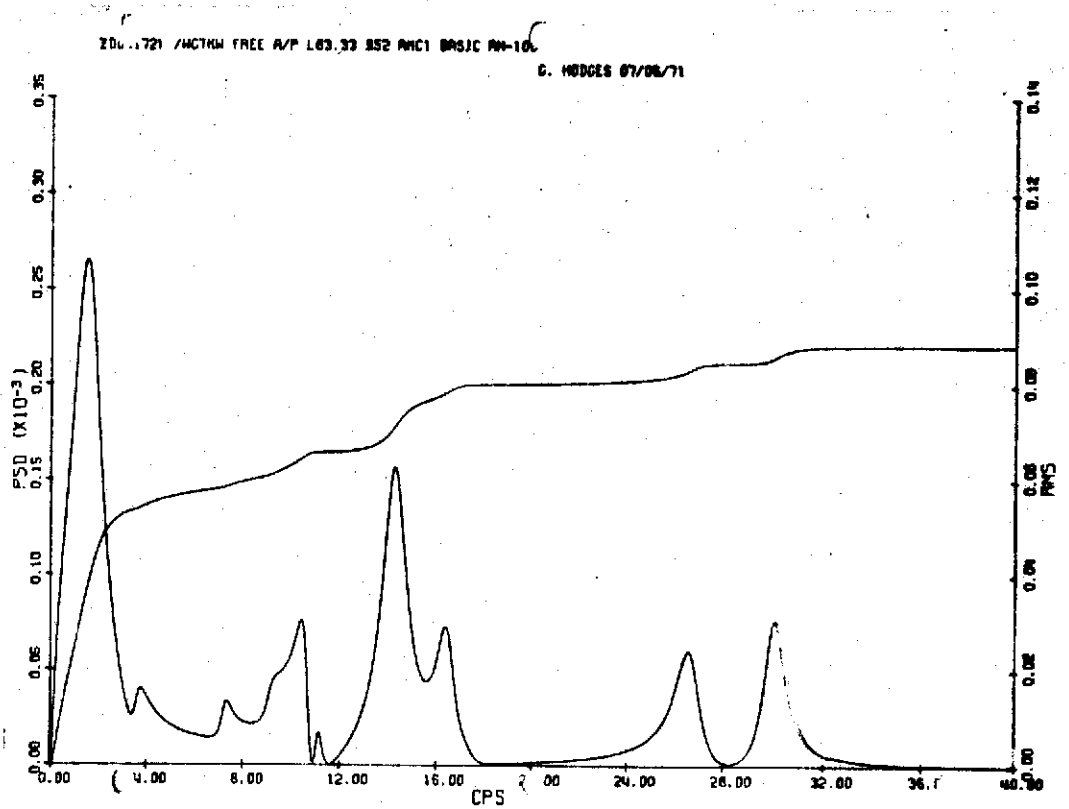


a) System Off

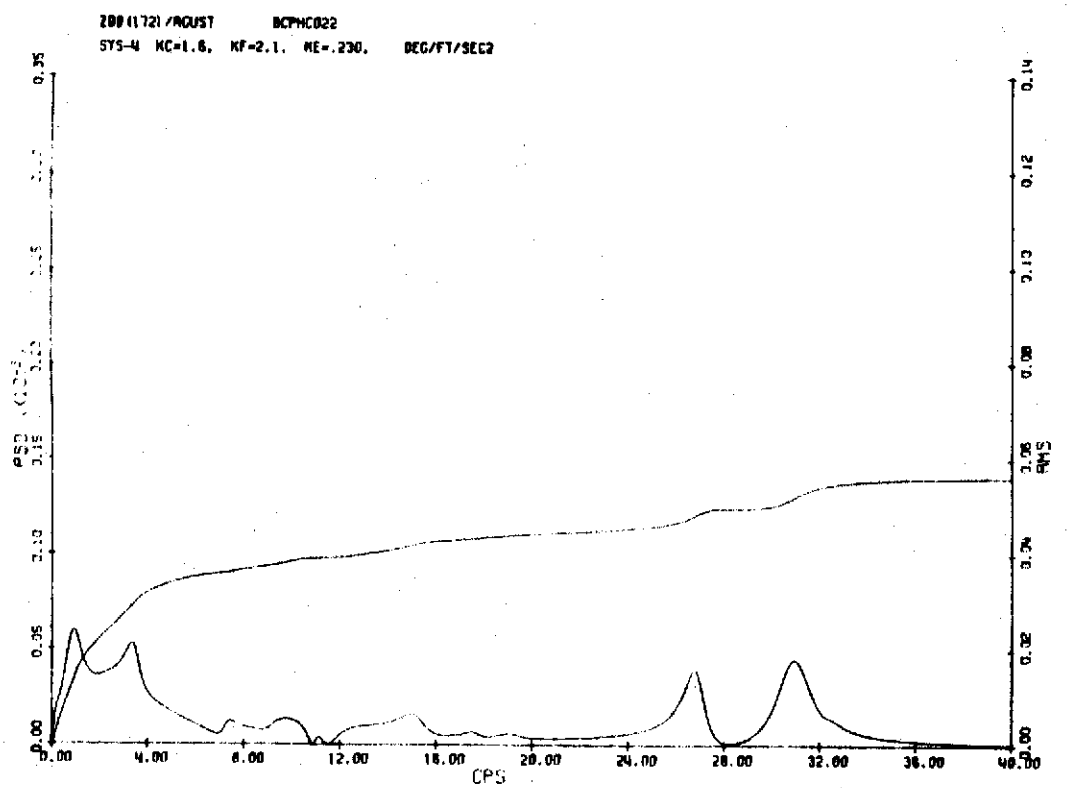


b) Canard-Flaperon-Elevator System On

BS 172 VERTICAL GUST RESPONSE

FIGURE 4.30

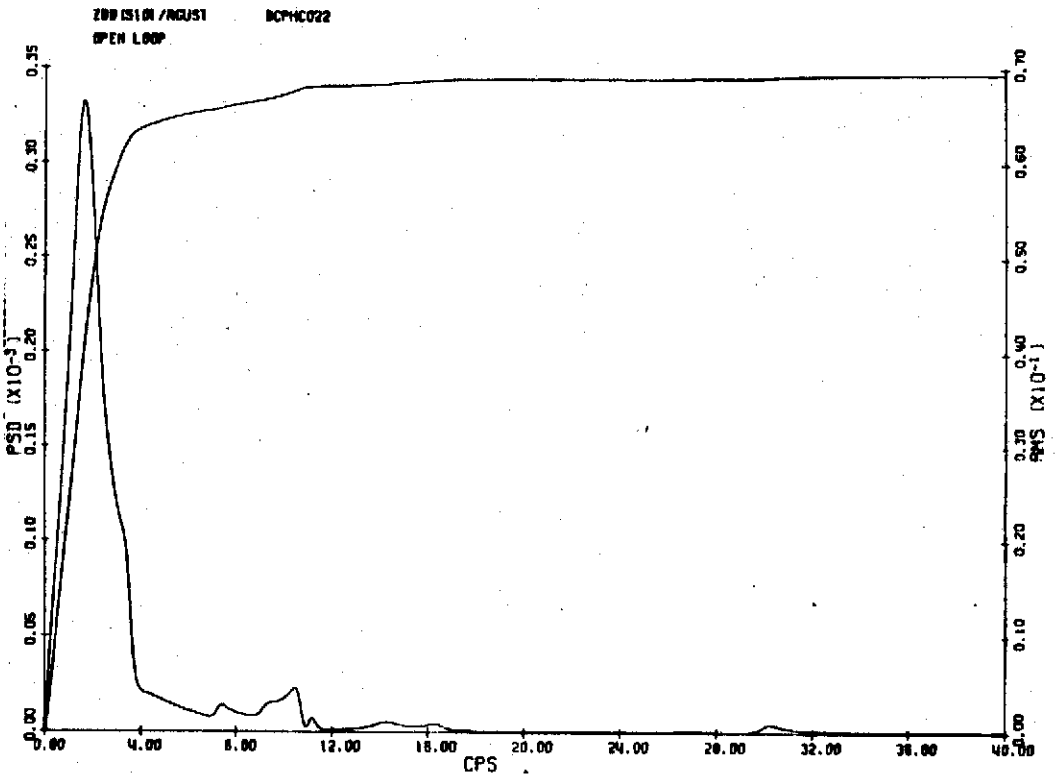


a) System Off

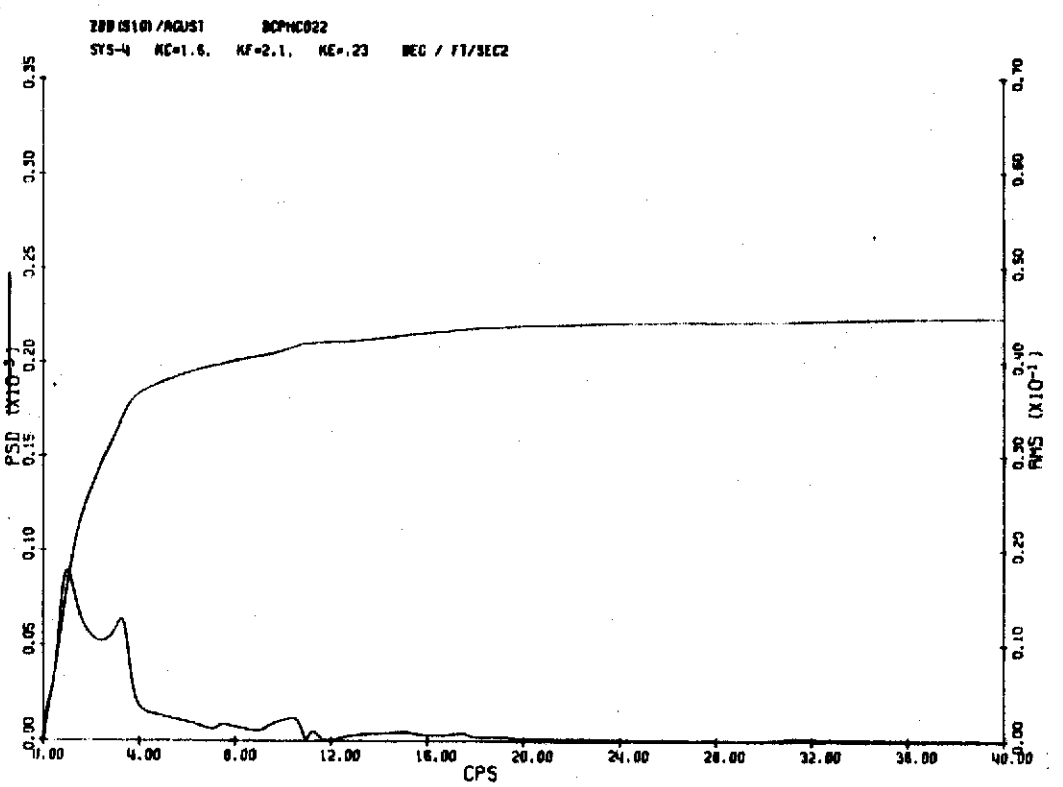


b) Canard-Flaperon-Elevator System On

BS 510 VERTICAL GUST RESPONSE

FIGURE 4.31

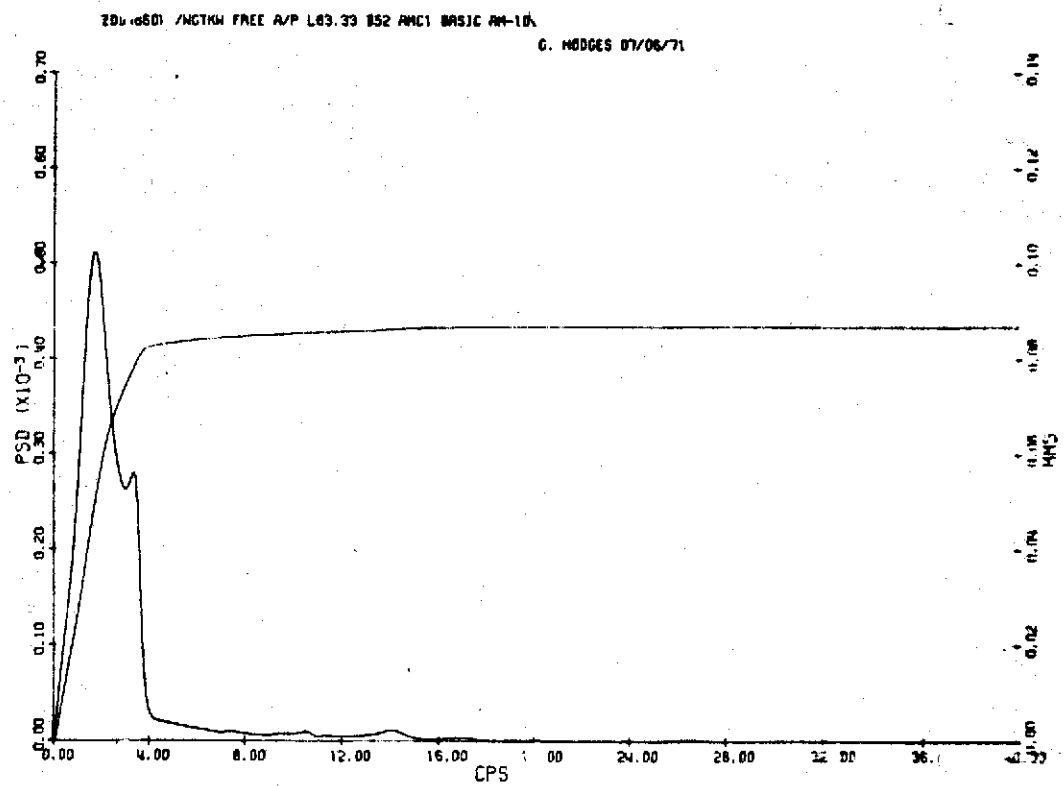


a) System Off

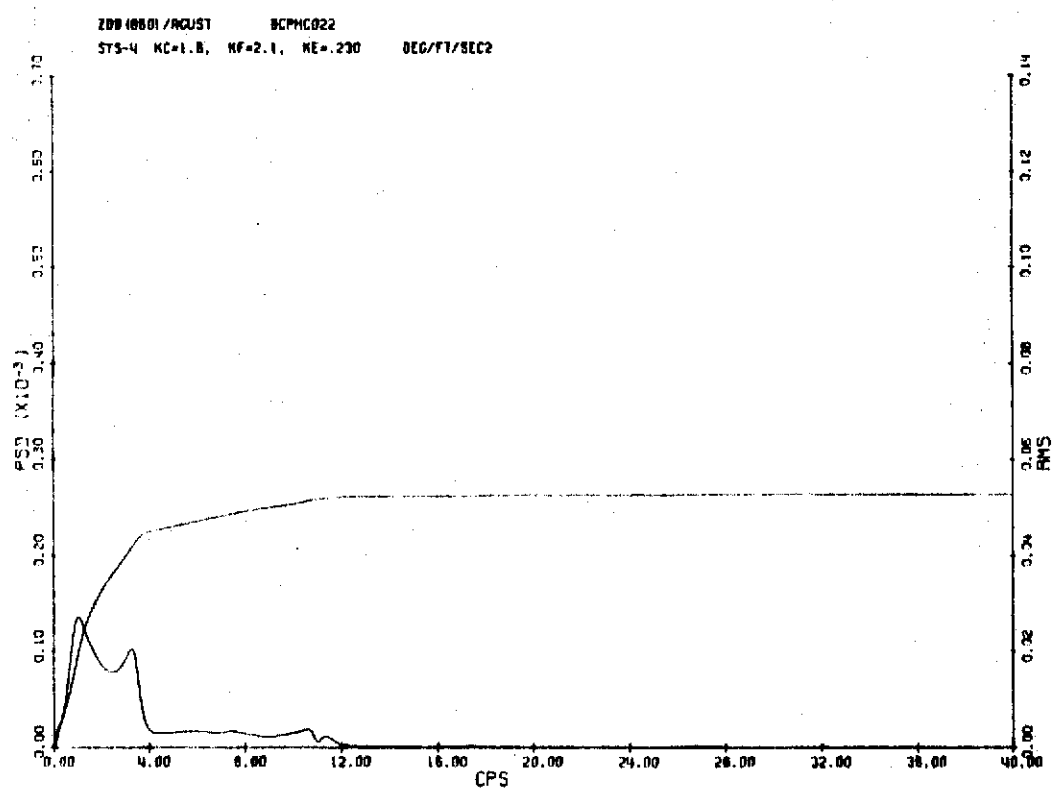


b) Canard-Flaperon-Elevator System On

BS 860 VERTICAL GUST RESPONSE

FIGURE 4.32

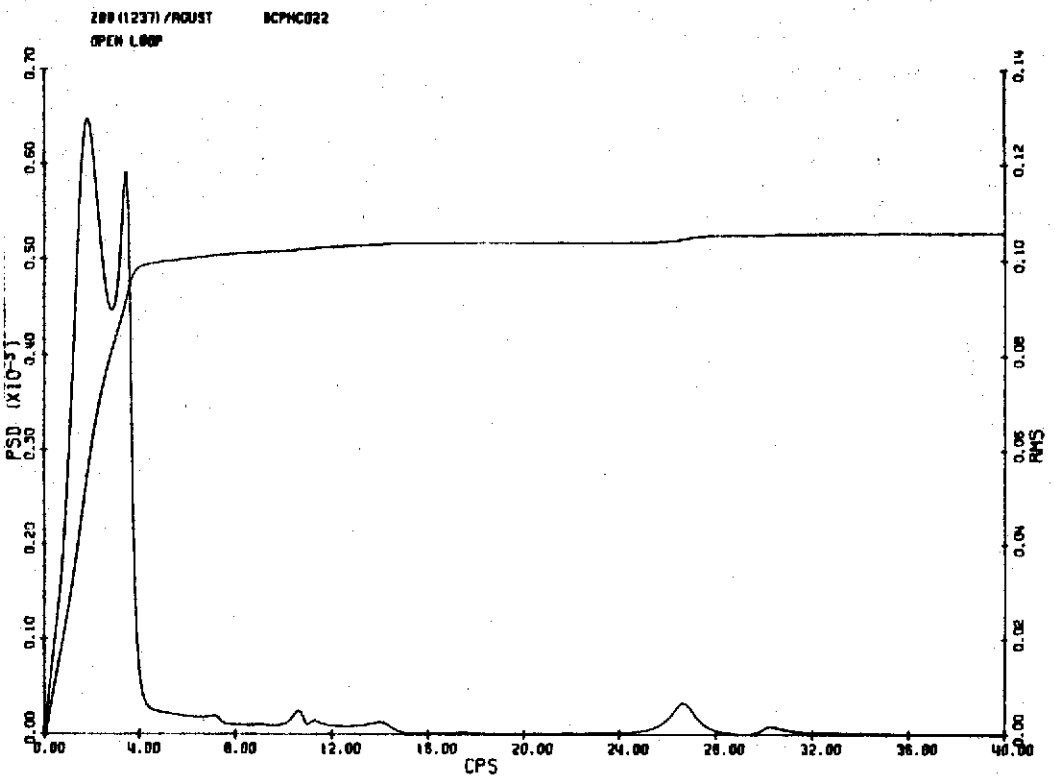


a) System Off

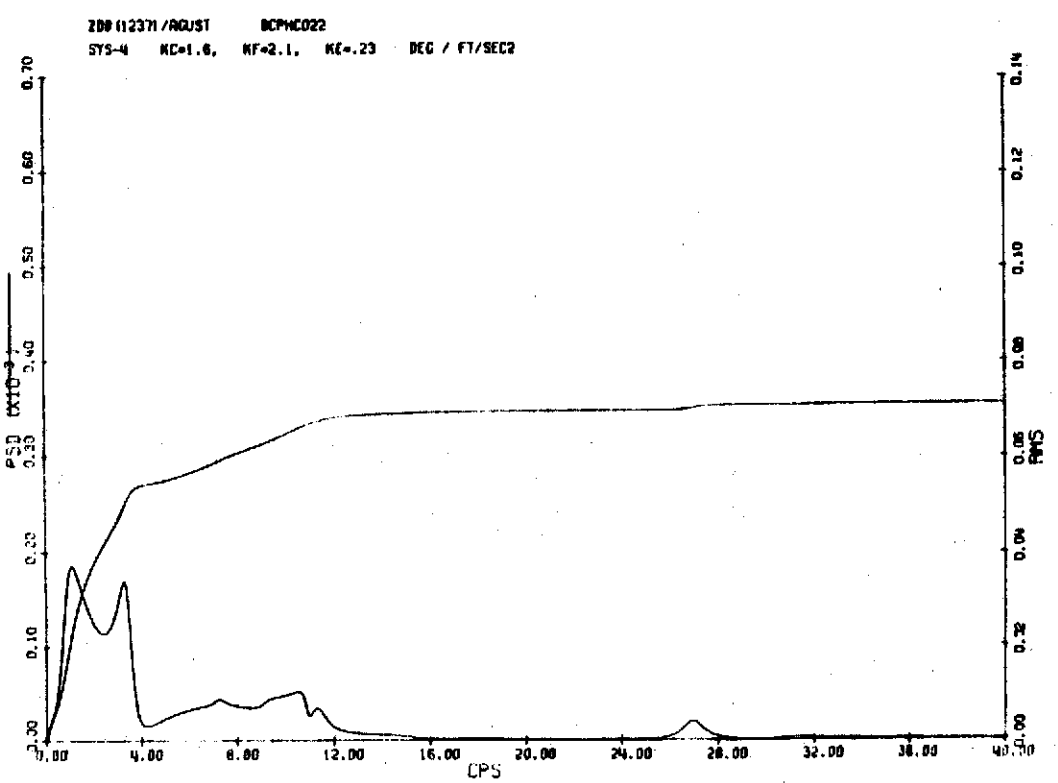


b) Canard-Flaperon-Elevator System On

BS 1237 VERTICAL GUST RESPONSE

FIGURE 4.33

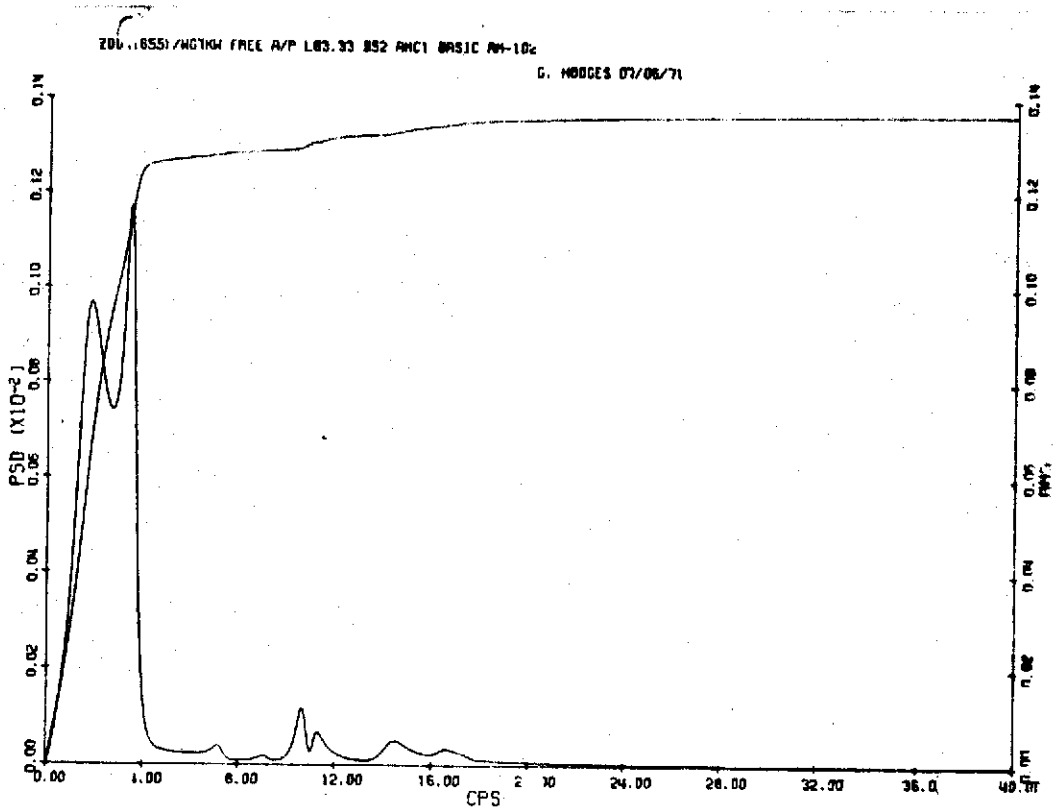


a) SYSTEM OFF

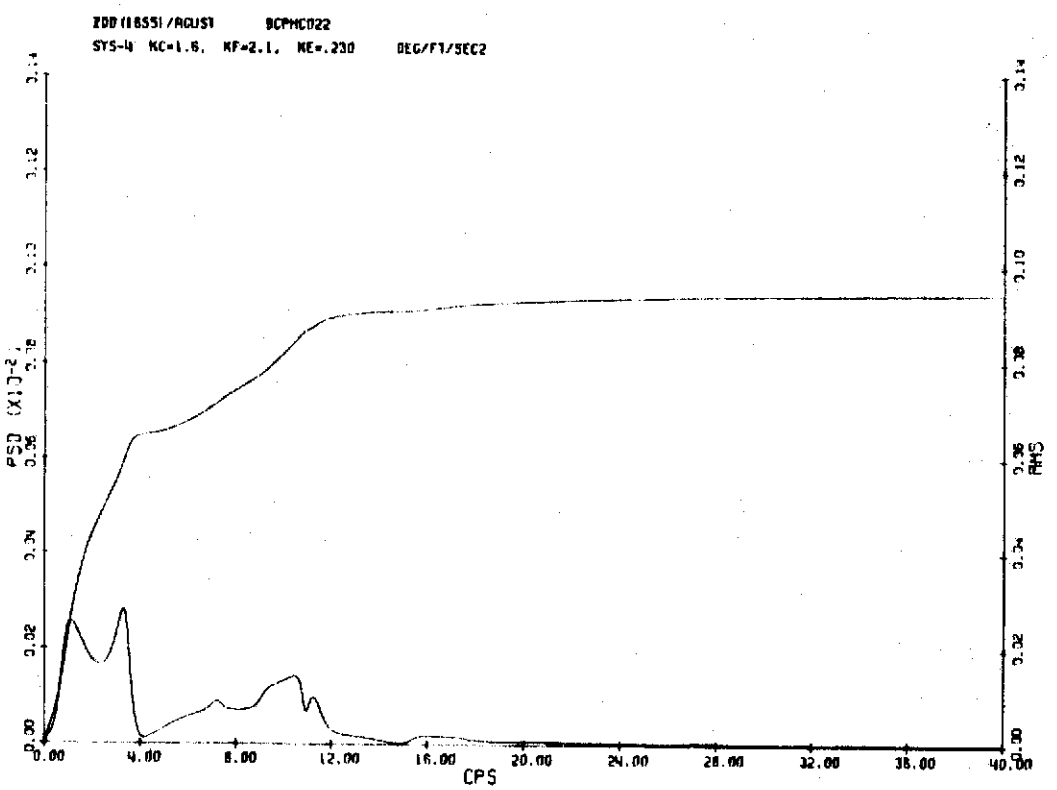


b) Canard-Flaperon-Elevator System on

BS 1655 VERTICAL GUST RESPONSE

FIGURE 4.34

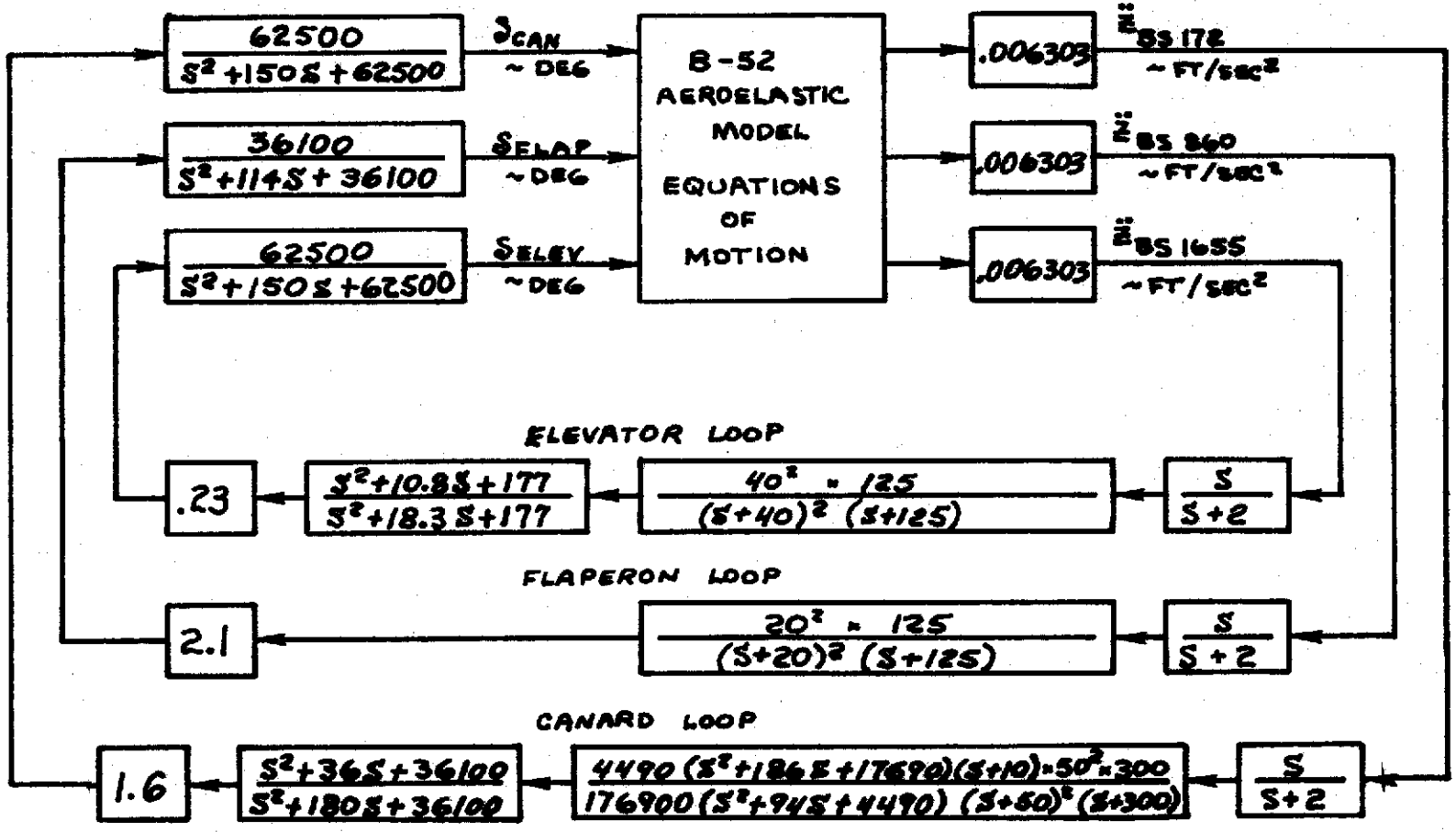


CANARD-FLAPERON-ELEVATOR RCS BLOCK DIAGRAM

FIGURE 4.35

Washout filters were included in each of the feedback systems to provide satisfactory handling qualities. Normal acceleration and pitch rate due to step elevator commands are presented in Figures 4.36 and 4.37 for the model with and without the suppression system. With the suppression system operating, the model response is slightly degraded but still considered acceptable.

The root locus of Figure 4.38 indicates the reason for the response degradation. The notch filter pole associated with the elevator loop moves closer to the origin than the short period mode, and thus becomes the dominant system root. The filter was introduced to provide lag at the short period frequency and lead at the 1st structural mode frequency (- and + 15 degrees respectively). Both the elevator and the flap loops are rolled off at relatively low frequencies. The canard loop, however, has a wide bandpass to make possible the vertical acceleration reduction for modes 2 through 10 shown in Figure 4.30. Additional compensation was introduced into the canard loop to provide the required gain margin of 6 db. The movement of the canard actuator root sets the upper limit for the canard loop gain. Nominal gains are those shown on the block diagram of Figure 4.35.

RMS control surface displacement and rate requirements per ft/sec gust are presented in Table IV. Equivalent airplane scale values can be obtained by dividing RMS displacement by the velocity scale factor, and RMS rate by the velocity and frequency scale factors. For example, in airplane scale, the canard rate would be $\frac{161.8}{(5.48)(5.48)} = 5.39 \frac{\text{deg/sec}}{\text{ft/sec}}$ .

TABLE IV

RMS CONTROL SURFACE REQUIREMENTS

| Surface | Displacement $\frac{\text{deg}}{\text{ft/sec}}$ | Rate $\frac{\text{deg/sec}}{\text{ft/sec}}$ |
|---|---|---|
| Canard | 3.77 | 161.8 |
| Flaperon | 2.16 | 28.2 |
| Elevator | 0.34 | 9.16 |

Figures 4.39 through 4.41 present the RMS-PSD plots from which Table IV was derived. Figures 4.42 through 4.47 present Bode magnitude plots of the control surface displacements and rates for 1 ft/sec simusoidal vertical gusts.

For reference, the RMS values corresponding to Figures 4.30 through 4.34 are tabulated as a function of frequency in Tables V. and VI. All percentage reductions quoted in this report have been based on the frequency range 0 to 40 cps.

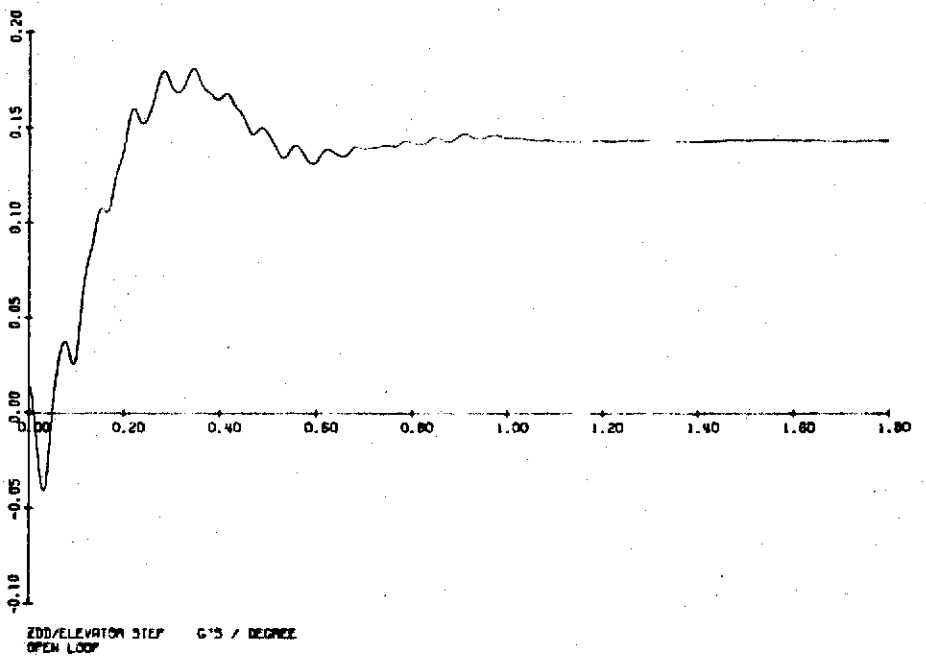


a) System Off

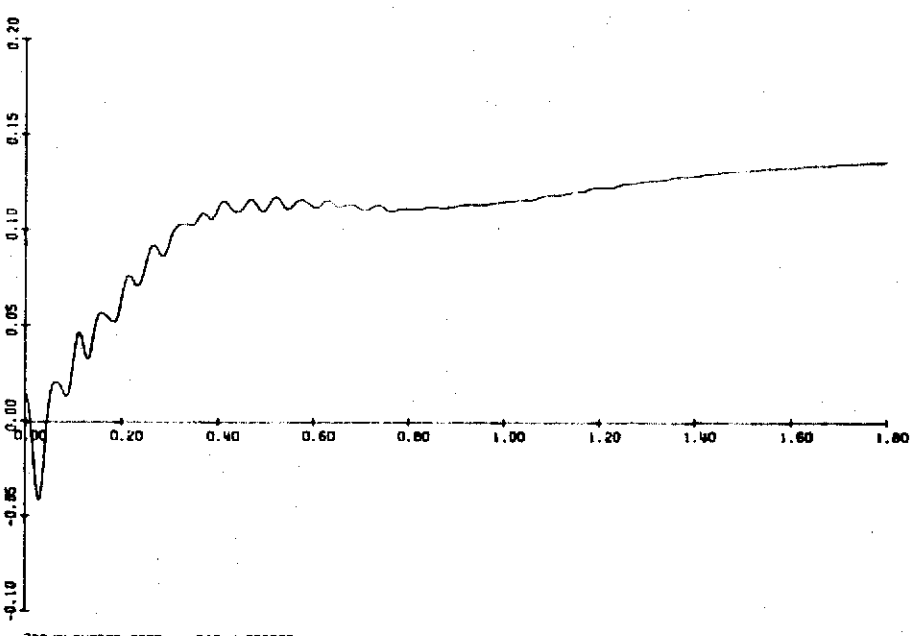


b) Canard-Flaperon-Elevator System On

NORMAL ACCELERATION/1 DEGREE STEP ELEVATOR

FIGURE 4.36

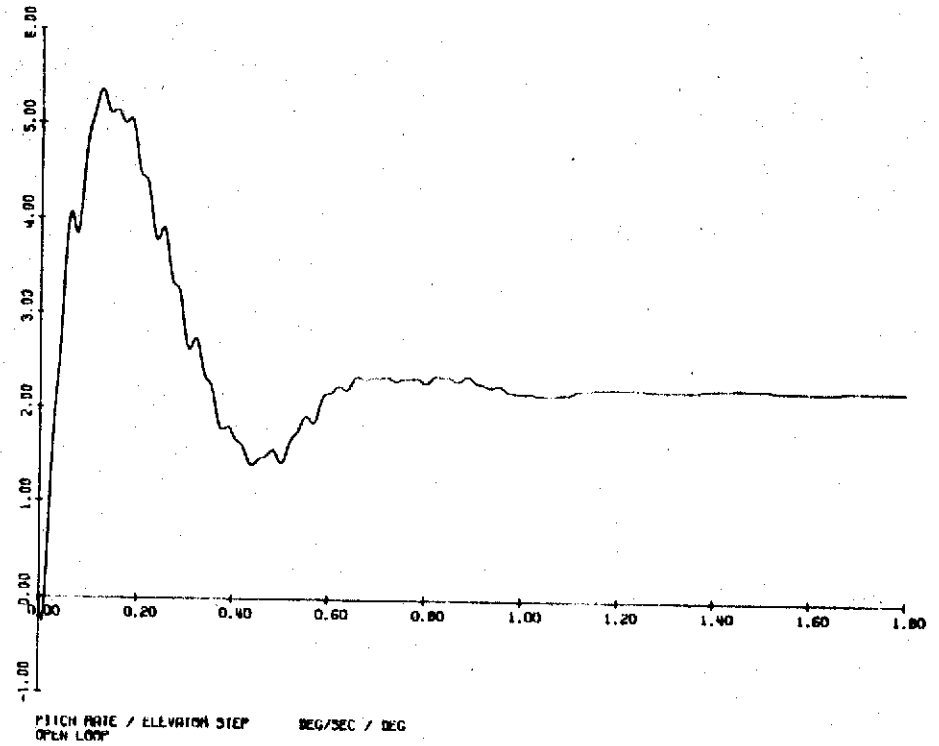


a) System Off

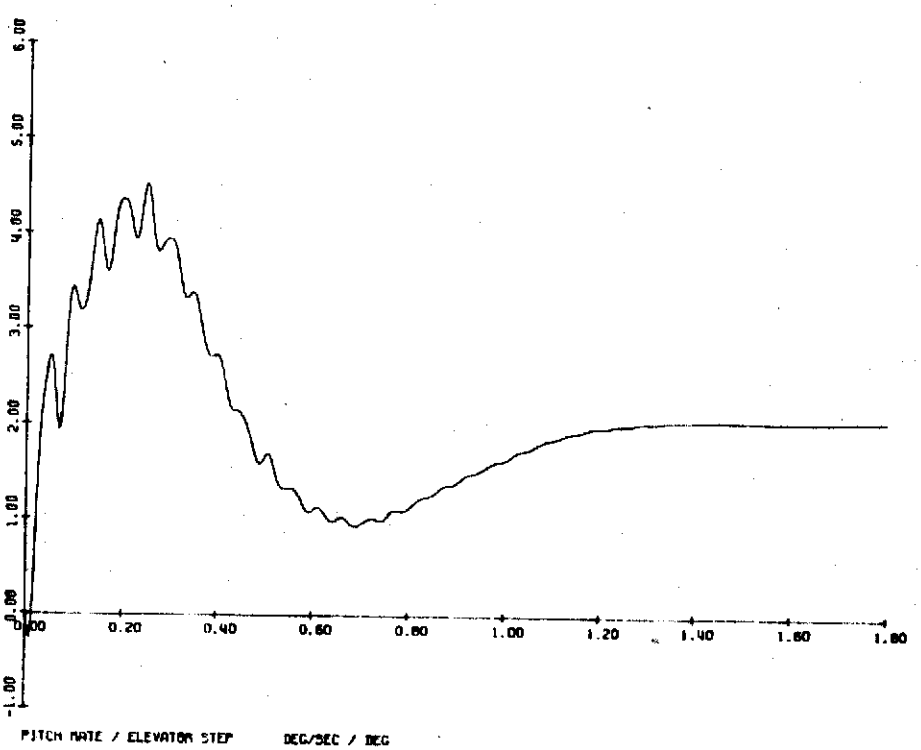


b) Canard-Flaperon-Elevator System On

PITCH RATE/1 DEGREE STEP ELEVATOR

FIGURE 4.37

B-52 AERODYNAMIC MODEL RIDE CONTROL SAS ROOT LOCUS

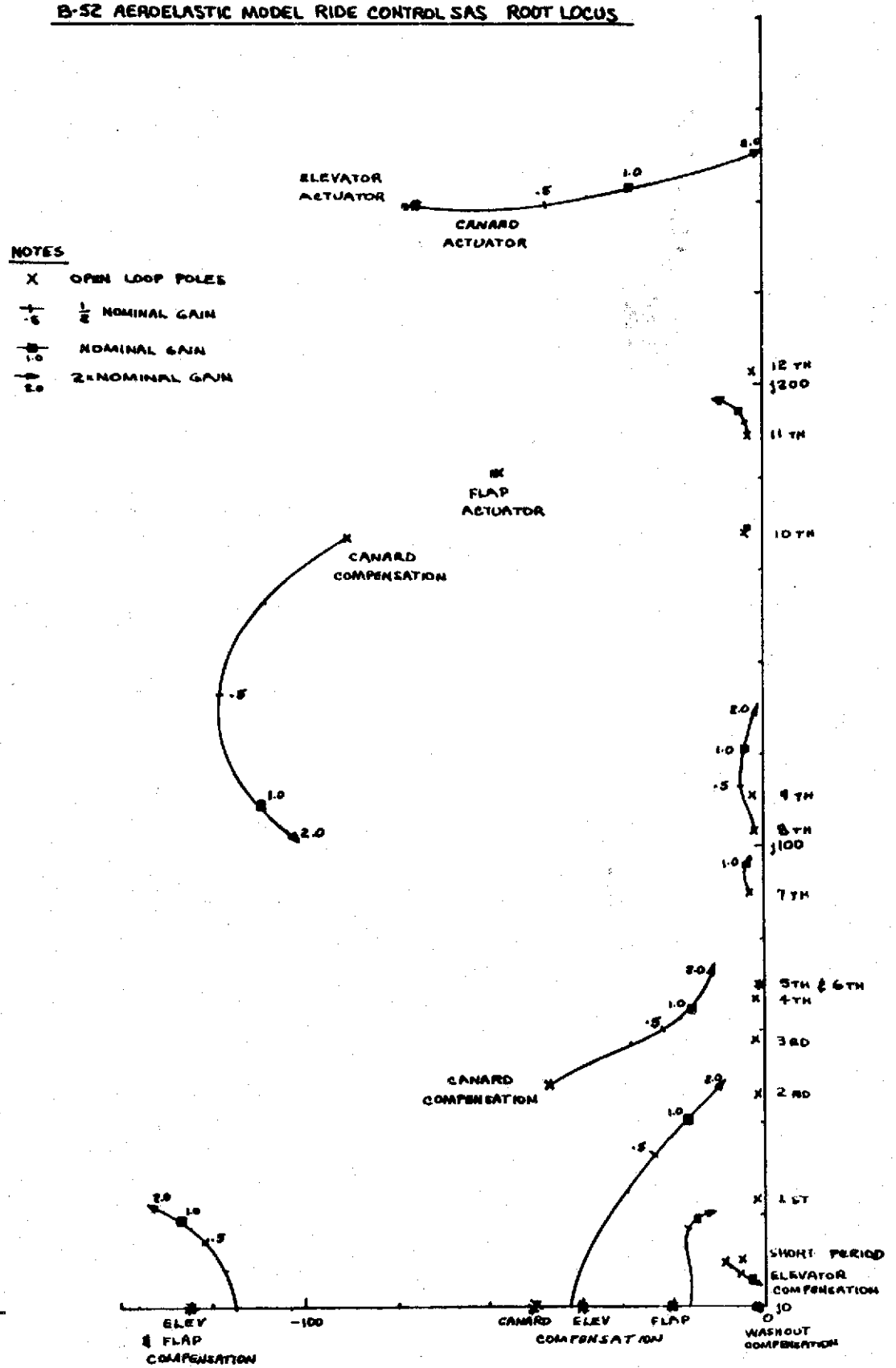


FIGURE 4.38

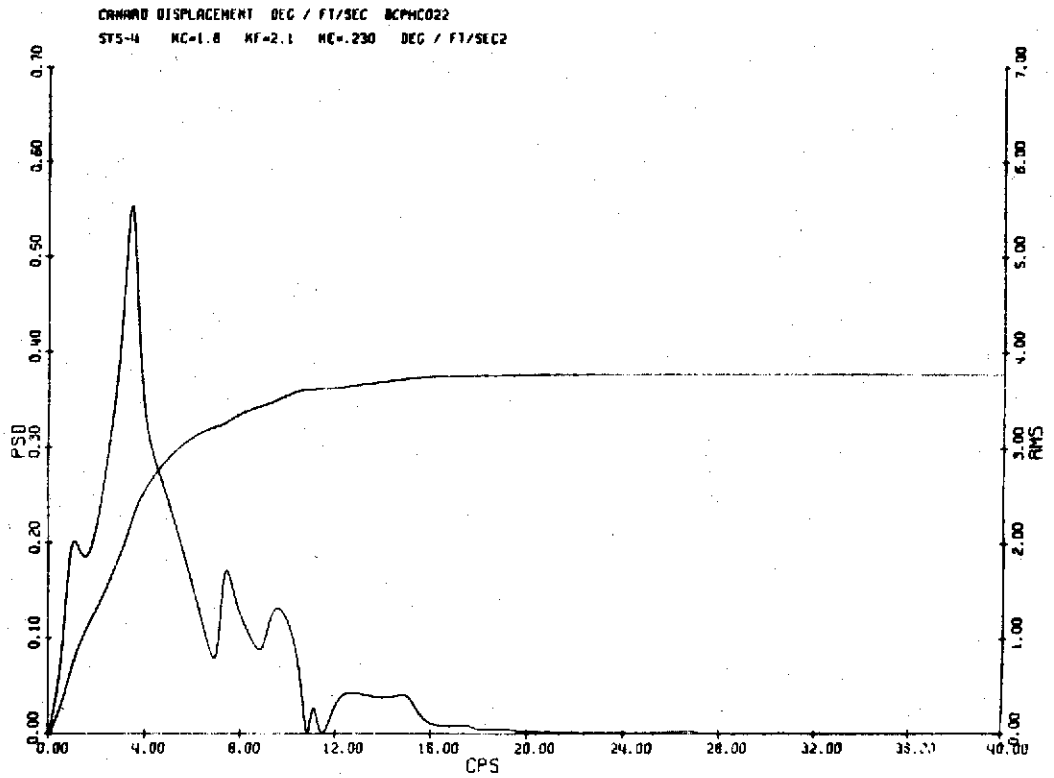


a) Canard Displacement

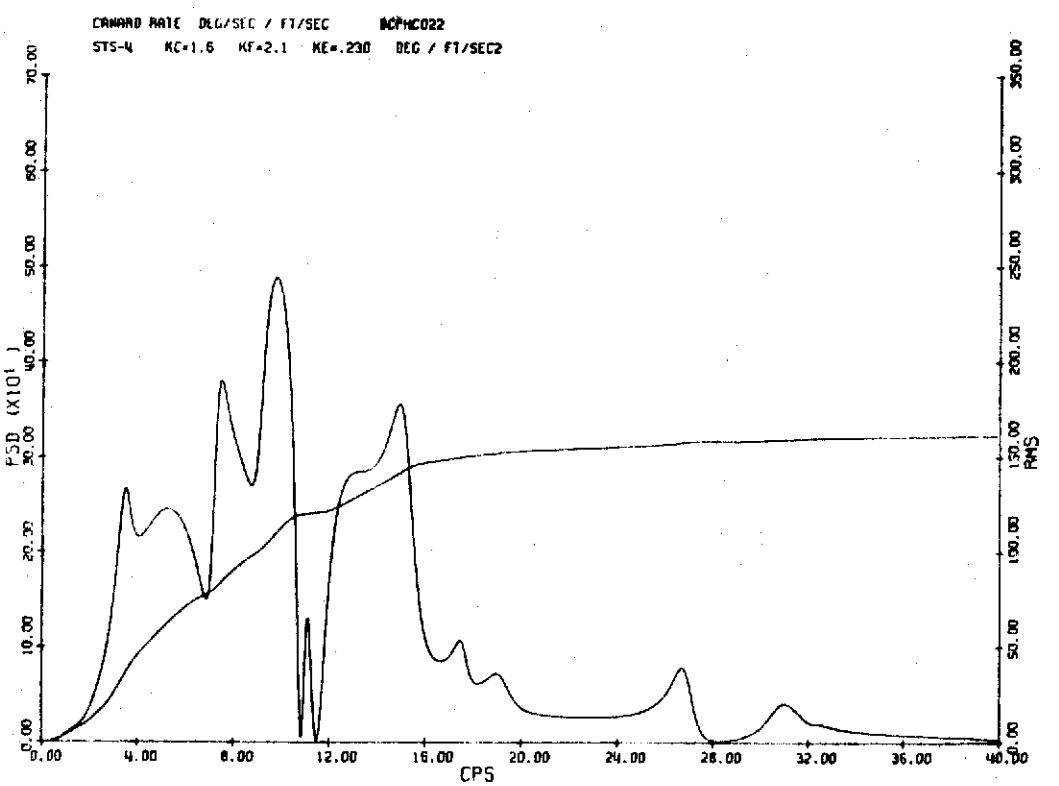


b) Canard Rate

CANARD EXCITATION/VERTICAL GUST

FIGURE 4.39

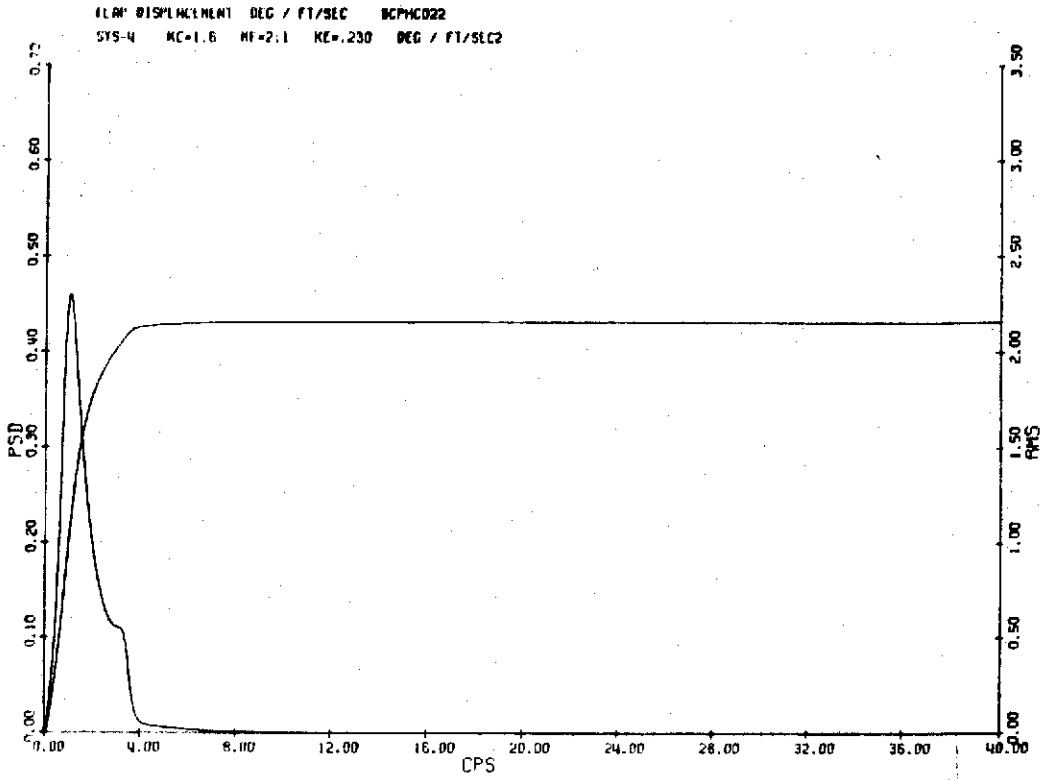


a) Flaperon Displacement

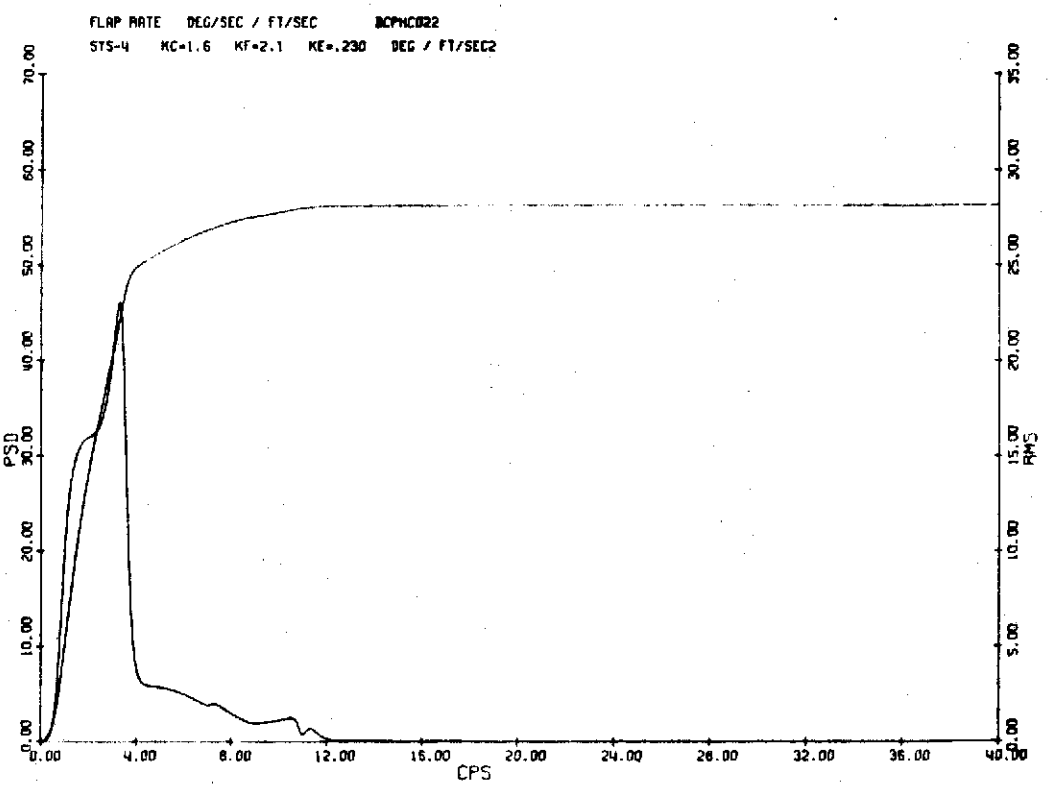


b) Flaperon Rate

FLAPERON EXCITATION/VERTICAL GUST

FIGURE 4.40

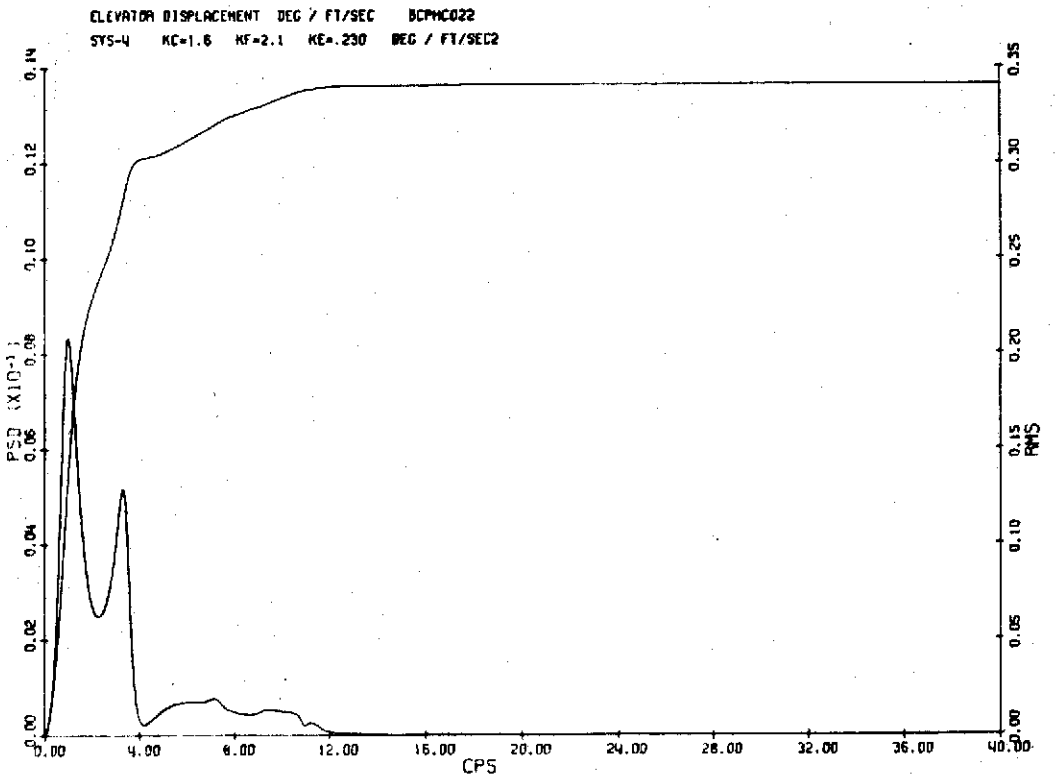


a) Elevator Displacement

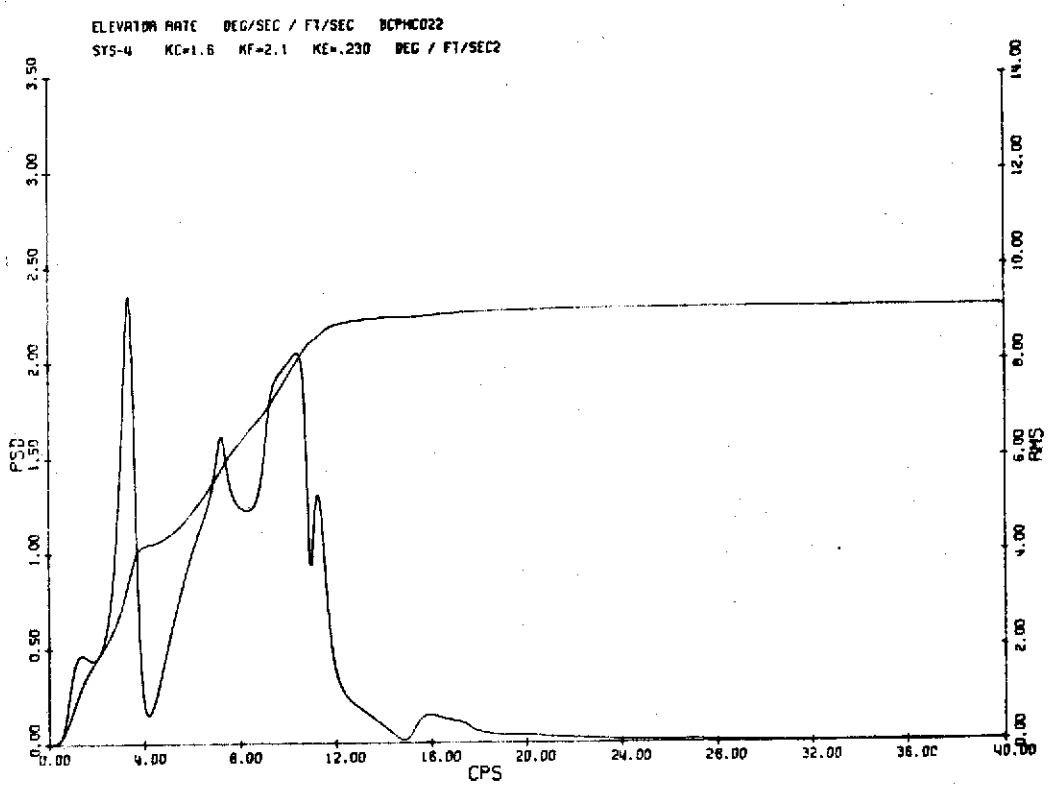


b) Elevator Rate

ELEVATOR EXCITATION/VERTICAL GUST

FIGURE 4.41

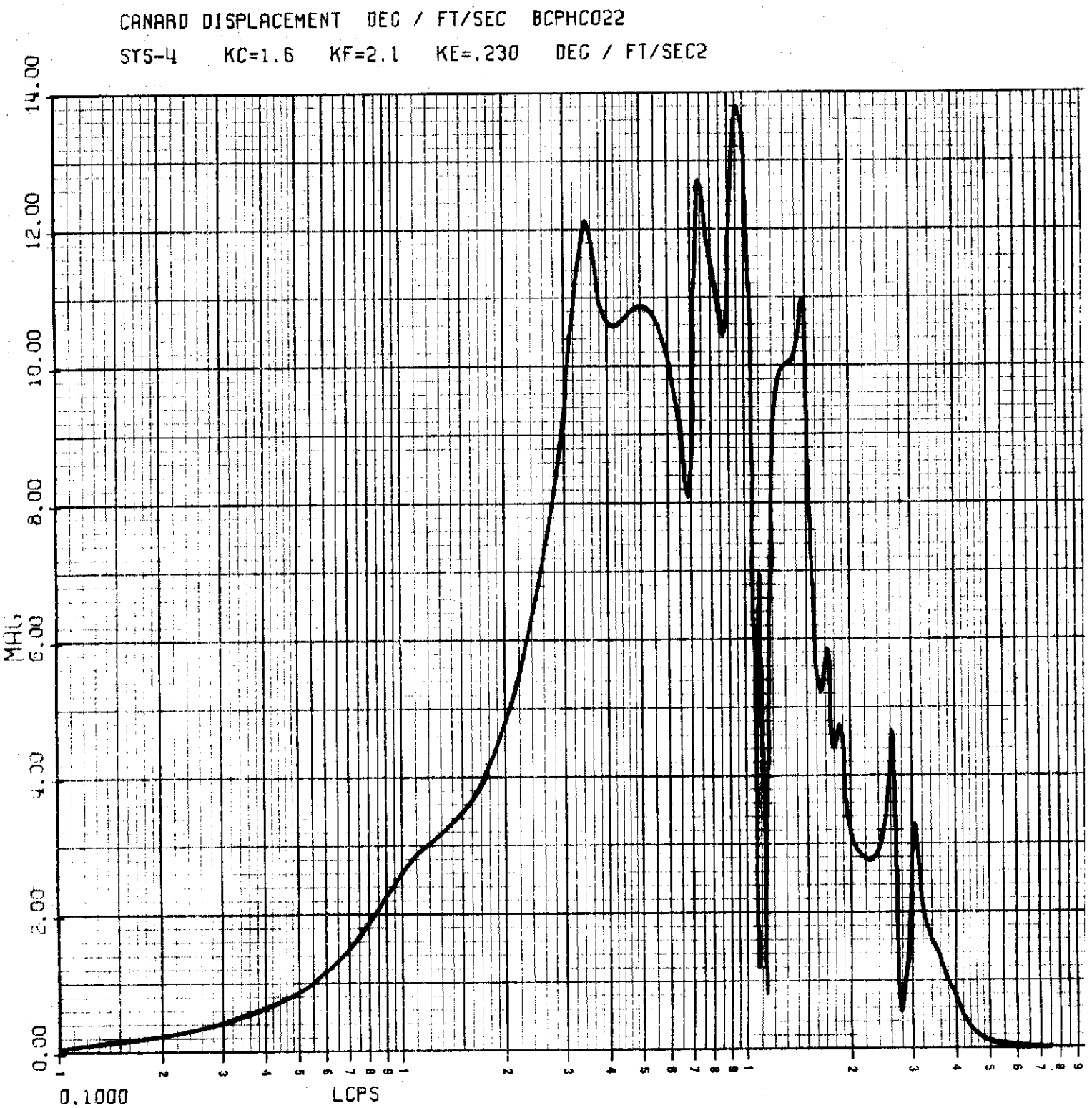


CANARD DISPLACEMENT/VERTICAL GUST
FREQUENCY RESPONSE

FIGURE 4.42

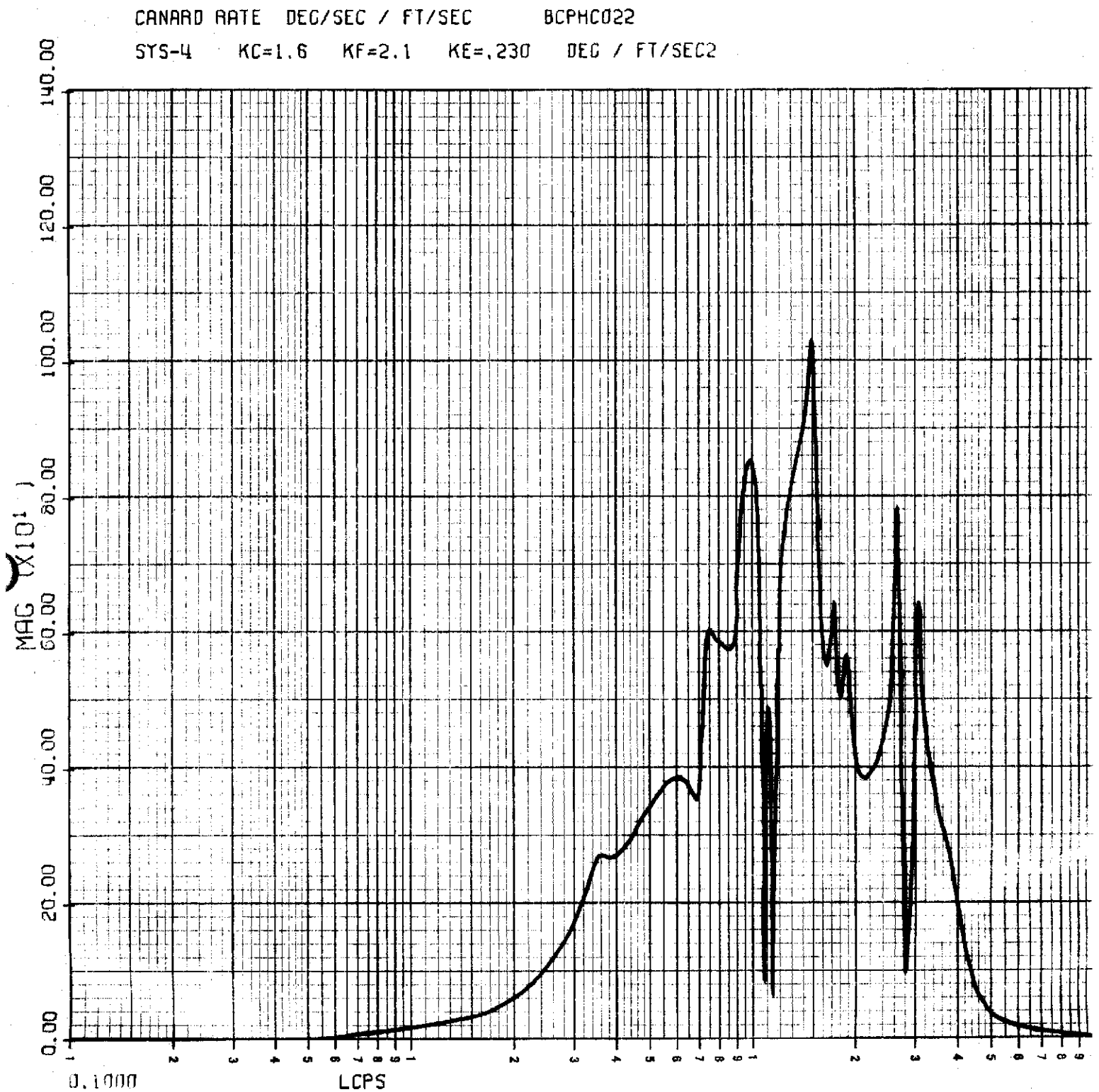


CANARD RATE/VERTICAL GUST
FREQUENCY RESPONSE

FIGURE 4.43

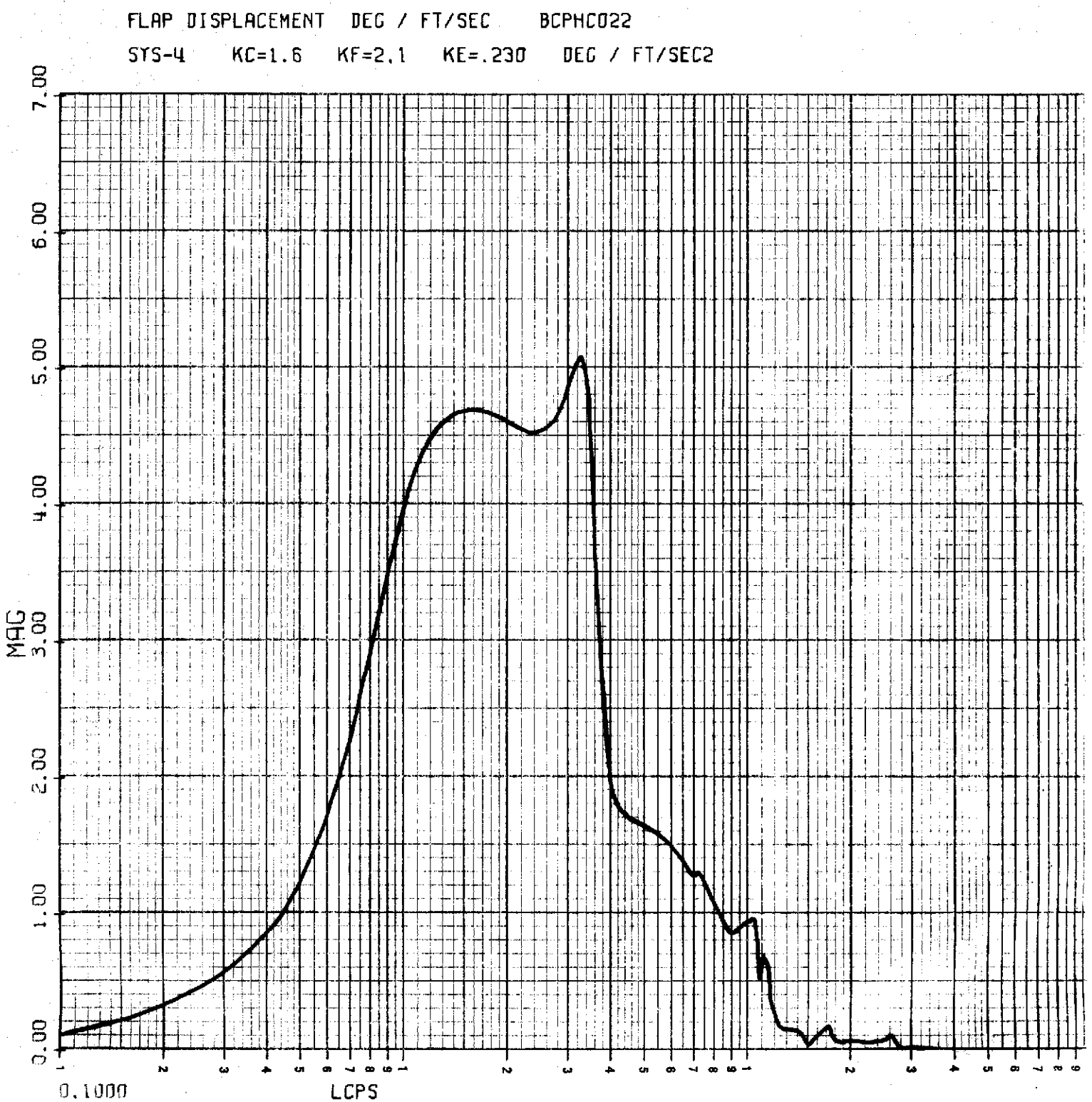


FLAPERON DISPLACEMENT/VERTICAL GUST
FREQUENCY RESPONSE

FIGURE 4.44

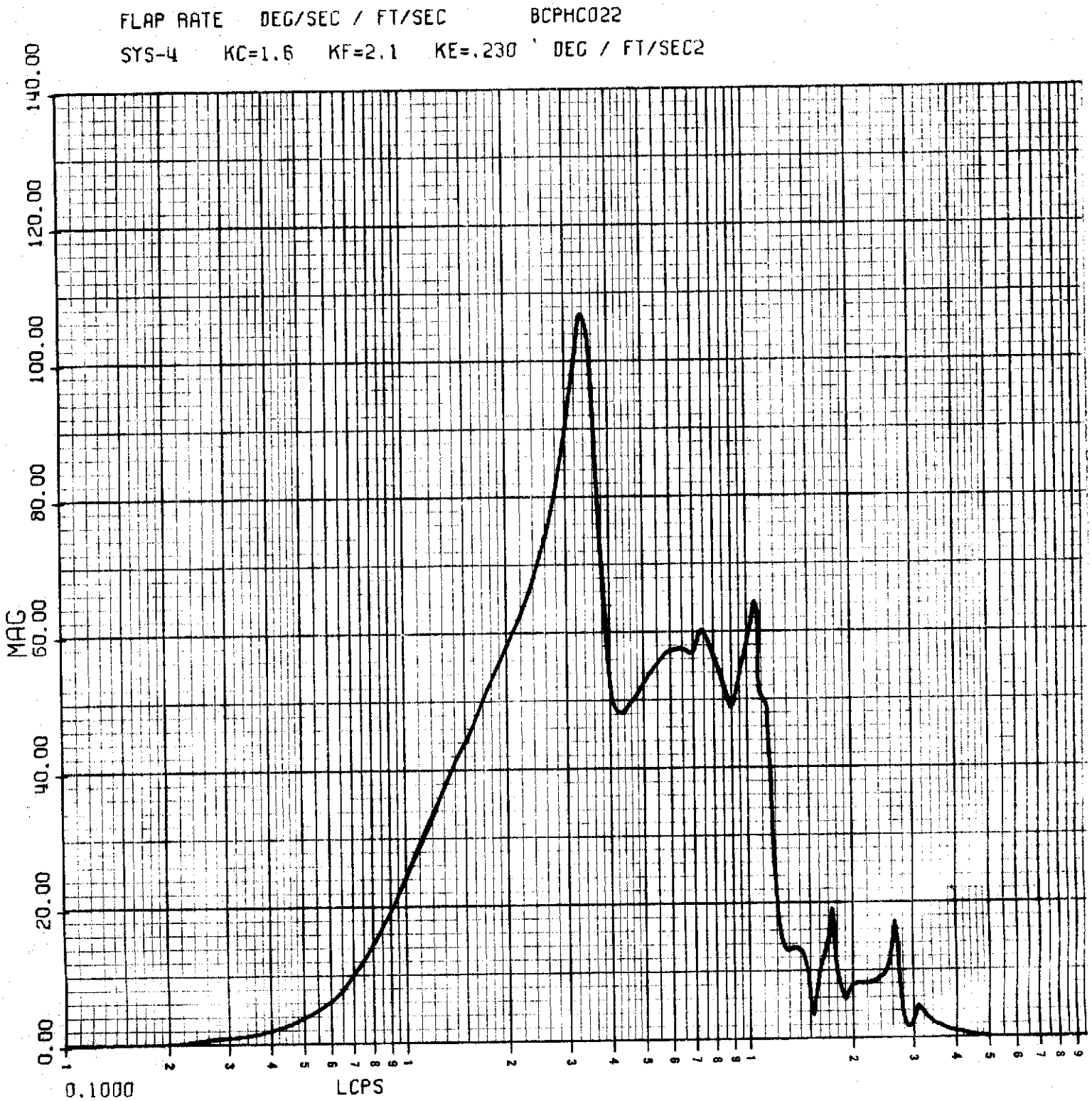


FLAPERON RATE/VERTICAL GUST
FREQUENCY RESPONSE

FIGURE 4.45

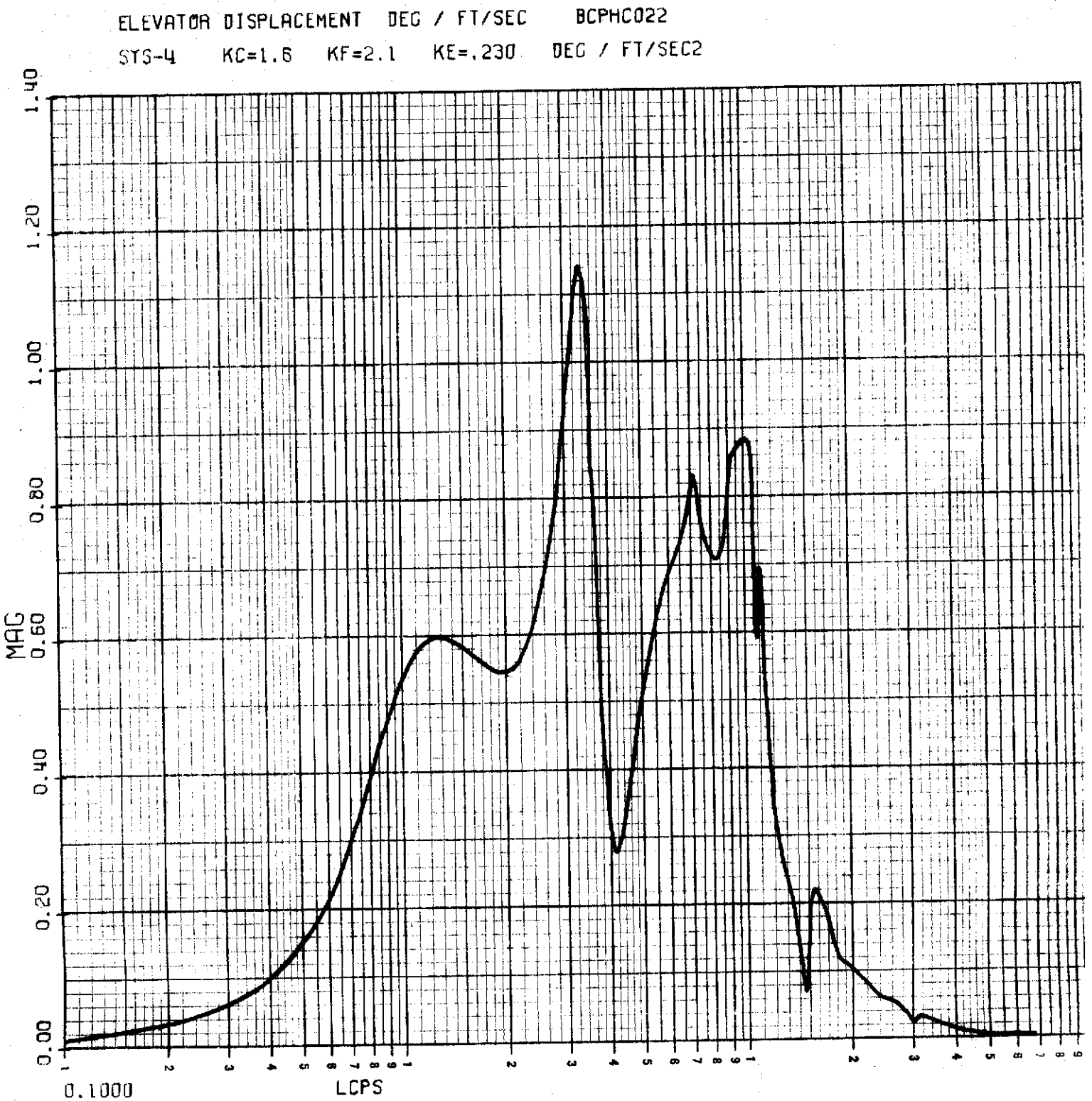


ELEVATOR DISPLACEMENT/VERTICAL GUST
FREQUENCY RESPONSE

FIGURE 4.4.6

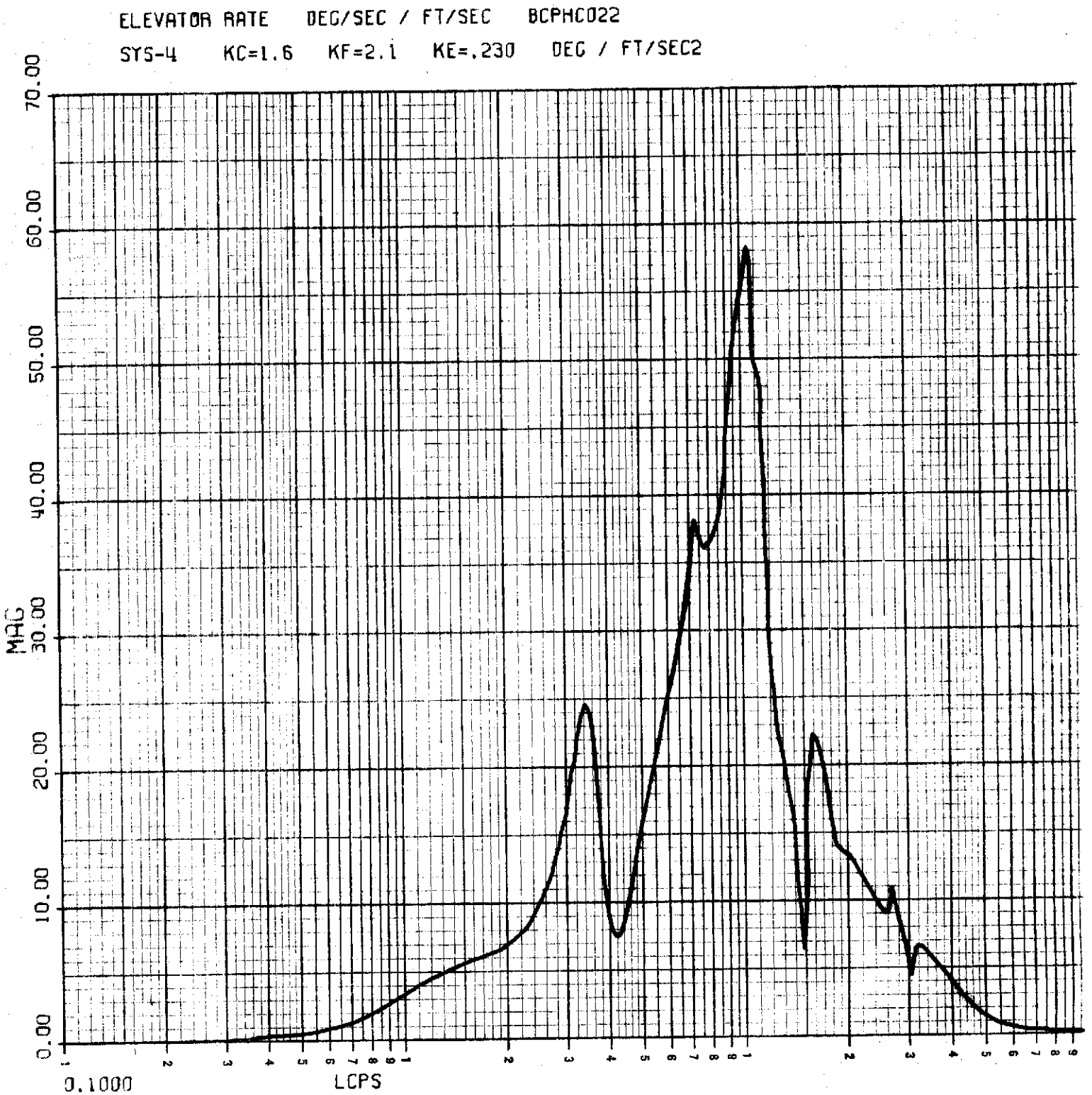


ELEVATOR RATE/VERTICAL GUST
FREQUENCY RESPONSE

FIGURE 4.47

TABLE V

CUMULATIVE RMS VERTICAL GUST RESPONSE - SAS OFF

| FREQUENCY CPS | BS 172 RMS | BS 510 RMS | BS 860 RMS | BS 1237 RMS | BS 1655 RMS | FREQUENCY CPS |
|---|---|---|---|---|---|---|
| 9.99999E-07 | 0.0 | 0.0 | 0.0 | 0.0 | 0.0 | 9.99999E-07 |
| 1.00000E 00 | 1.43876E-02 | 1.58850E-02 | 1.82065E-02 | 1.99817E-02 | 2.24803E-02 | 1.00000E 00 |
| 2.00000E 00 | 2.20579E-02 | 2.65798E-02 | 3.24208E-02 | 3.75888E-02 | 4.39076E-02 | 2.00000E 00 |
| 3.00000E 00 | 2.70809E-02 | 3.23320E-02 | 3.95666E-02 | 4.65898E-02 | 5.51690E-02 | 3.00000E 00 |
| 4.00000E 00 | 3.18255E-02 | 3.66891E-02 | 4.49437E-02 | 5.37680E-02 | 6.48425E-02 | 4.00000E 00 |
| 5.00000E 00 | 3.39194E-02 | 3.79461E-02 | 4.60189E-02 | 5.47953E-02 | 6.57696E-02 | 5.00000E 00 |
| 6.00000E 00 | 3.51965E-02 | 3.88809E-02 | 4.71093E-02 | 5.63599E-02 | 6.78909E-02 | 6.00000E 00 |
| 7.00000E 00 | 3.58834E-02 | 3.95402E-02 | 4.81641E-02 | 5.83042E-02 | 7.08885E-02 | 7.00000E 00 |
| 8.00000E 00 | 3.67556E-02 | 4.01433E-02 | 4.91887E-02 | 6.04500E-02 | 7.43722E-02 | 8.00000E 00 |
| 9.00000E 00 | 3.74684E-02 | 4.06264E-02 | 4.99725E-02 | 6.22585E-02 | 7.74631E-02 | 9.00000E 00 |
| 1.00000E 01 | 3.84502E-02 | 4.12466E-02 | 5.07562E-02 | 6.44253E-02 | 8.20667E-02 | 1.00000E 01 |
| 1.10000E 01 | 3.90829E-02 | 4.19528E-02 | 5.17402E-02 | 6.66976E-02 | 8.68428E-02 | 1.10000E 01 |
| 1.20000E 01 | 3.92464E-02 | 4.21196E-02 | 5.22192E-02 | 6.79591E-02 | 8.94279E-02 | 1.20000E 01 |
| 1.30000E 01 | 3.98899E-02 | 4.22453E-02 | 5.22991E-02 | 6.84237E-02 | 9.02074E-02 | 1.30000E 01 |
| 1.40000E 01 | 4.07216E-02 | 4.25081E-02 | 5.23474E-02 | 6.87244E-02 | 9.06696E-02 | 1.40000E 01 |
| 1.50000E 01 | 4.17729E-02 | 4.28251E-02 | 5.23872E-02 | 6.89632E-02 | 9.08335E-02 | 1.50000E 01 |
| 1.60000E 01 | 4.26337E-02 | 4.31066E-02 | 5.23985E-02 | 6.90779E-02 | 9.12273E-02 | 1.60000E 01 |
| 1.70000E 01 | 4.30145E-02 | 4.33276E-02 | 5.24399E-02 | 6.91291E-02 | 9.18219E-02 | 1.70000E 01 |
| 1.80000E 01 | 4.34603E-02 | 4.35783E-02 | 5.25188E-02 | 6.92065E-02 | 9.22766E-02 | 1.80000E 01 |
| 1.90000E 01 | 4.38254E-02 | 4.37198E-02 | 5.25390E-02 | 6.92852E-02 | 9.25385E-02 | 1.90000E 01 |
| 2.00000E 01 | 4.41830E-02 | 4.38435E-02 | 5.25503E-02 | 6.93176E-02 | 9.27703E-02 | 2.00000E 01 |
| 2.10000E 01 | 4.44228E-02 | 4.39283E-02 | 5.25681E-02 | 6.93290E-02 | 9.29962E-02 | 2.10000E 01 |
| 2.20000E 01 | 4.46729E-02 | 4.40010E-02 | 5.25859E-02 | 6.93355E-02 | 9.31897E-02 | 2.20000E 01 |
| 2.30000E 01 | 4.49643E-02 | 4.40649E-02 | 5.26038E-02 | 6.93390E-02 | 9.33540E-02 | 2.30000E 01 |
| 2.40000E 01 | 4.53290E-02 | 4.41206E-02 | 5.26222E-02 | 6.93439E-02 | 9.34942E-02 | 2.40000E 01 |
| 2.50000E 01 | 4.58392E-02 | 4.41685E-02 | 5.26433E-02 | 6.93614E-02 | 9.36142E-02 | 2.50000E 01 |
| 2.60000E 01 | 4.67247E-02 | 4.42083E-02 | 5.26735E-02 | 6.94420E-02 | 9.37192E-02 | 2.60000E 01 |
| 2.70000E 01 | 4.87781E-02 | 4.42312E-02 | 5.27389E-02 | 6.99432E-02 | 9.38380E-02 | 2.70000E 01 |
| 2.80000E 01 | 4.96259E-02 | 4.42352E-02 | 5.27722E-02 | 7.04635E-02 | 9.39626E-02 | 2.80000E 01 |
| 2.90000E 01 | 4.97220E-02 | 4.42403E-02 | 5.27754E-02 | 7.05602E-02 | 9.40411E-02 | 2.90000E 01 |
| 3.00000E 01 | 5.02597E-02 | 4.42413E-02 | 5.27768E-02 | 7.05743E-02 | 9.40931E-02 | 3.00000E 01 |
| 3.10000E 01 | 5.22726E-02 | 4.42752E-02 | 5.27818E-02 | 7.06189E-02 | 9.41206E-02 | 3.10000E 01 |
| 3.20000E 01 | 5.42659E-02 | 4.43695E-02 | 5.27912E-02 | 7.07409E-02 | 9.41648E-02 | 3.20000E 01 |
| 3.30000E 01 | 5.50863E-02 | 4.44437E-02 | 5.27976E-02 | 7.08287E-02 | 9.42186E-02 | 3.30000E 01 |
| 3.40000E 01 | 5.55158E-02 | 4.45016E-02 | 5.28026E-02 | 7.08933E-02 | 9.42714E-02 | 3.40000E 01 |
| 3.50000E 01 | 5.57612E-02 | 4.45468E-02 | 5.28070E-02 | 7.09393E-02 | 9.43198E-02 | 3.50000E 01 |
| 3.60000E 01 | 5.59227E-02 | 4.45838E-02 | 5.28110E-02 | 7.09743E-02 | 9.43640E-02 | 3.60000E 01 |
| 3.70000E 01 | 5.60373E-02 | 4.46151E-02 | 5.28147E-02 | 7.10021E-02 | 9.44046E-02 | 3.70000E 01 |
| 3.80000E 01 | 5.61202E-02 | 4.46420E-02 | 5.28181E-02 | 7.10245E-02 | 9.44420E-02 | 3.80000E 01 |
| 3.90000E 01 | 5.61791E-02 | 4.46655E-02 | 5.28212E-02 | 7.10425E-02 | 9.44763E-02 | 3.90000E 01 |
| 3.99500E 01 | 5.62177E-02 | 4.46853E-02 | 5.28237E-02 | 7.10562E-02 | 9.45063E-02 | 3.99500E 01 |

TABLE VI
CUMULATIVE RMS VERTICAL GUST RESPONSE
CANARD-FLAPERON-ELEVATOR SAS ON

| FREQUENCY CPS | BS 172 RMS | BS 510 RMS | BS 860 RMS | BS 1237 RMS | BS 1655 RMS | FREQUENCY CPS |
|---|---|---|---|---|---|---|
| 9.99999E-07 | 0.0 | 0.0 | 0.0 | 0.0 | 0.0 | 9.99999E-07 |
| 1.00000E 00 | 2.46172E-02 | 2.35760E-02 | 2.62943E-02 | 2.56255E-02 | 2.69042E-02 | 1.00000E 00 |
| 2.00000E 00 | 4.58178E-02 | 4.85250E-02 | 5.79975E-02 | 6.18999E-02 | 7.36891E-02 | 2.00000E 00 |
| 3.00000E 00 | 5.27165E-02 | 5.96512E-02 | 7.43340E-02 | 8.39053E-02 | 1.02618E-01 | 3.00000E 00 |
| 4.00000E 00 | 5.47659E-02 | 6.35628E-02 | 8.24389E-02 | 9.83389E-02 | 1.25093E-01 | 4.00000E 00 |
| 5.00000E 00 | 5.63619E-02 | 6.44841E-02 | 8.52720E-02 | 9.94127E-02 | 1.26553E-01 | 5.00000E 00 |
| 6.00000E 00 | 5.73815E-02 | 6.51362E-02 | 8.38962E-02 | 1.0007CE-01 | 1.27178E-01 | 6.00000E 00 |
| 7.00000E 00 | 5.82056E-02 | 6.55740E-02 | 8.42645E-02 | 1.00637E-01 | 1.27791E-01 | 7.00000E 00 |
| 8.00000E 00 | 5.96461E-02 | 6.61219E-02 | 8.46043E-02 | 1.01085E-01 | 1.28357E-01 | 8.00000E 00 |
| 9.00000E 00 | 6.08550E-02 | 6.65360E-02 | 8.48461E-02 | 1.01387E-01 | 1.28630E-01 | 9.00000E 00 |
| 1.00000E 01 | 6.31821E-02 | 6.72134E-02 | 8.51048E-02 | 1.01685E-01 | 1.28947E-01 | 1.00000E 01 |
| 1.10000E 01 | 6.56968E-02 | 6.79679E-02 | 8.53990E-02 | 1.02211E-01 | 1.30495E-01 | 1.10000E 01 |
| 1.20000E 01 | 6.59711E-02 | 6.81062E-02 | 8.55895E-02 | 1.02568E-01 | 1.31613E-01 | 1.20000E 01 |
| 1.30000E 01 | 6.66494E-02 | 6.81570E-02 | 8.57776E-02 | 1.02820E-01 | 1.32021E-01 | 1.30000E 01 |
| 1.40000E 01 | 6.96445E-02 | 6.82800E-02 | 8.60956E-02 | 1.03130E-01 | 1.32330E-01 | 1.40000E 01 |
| 1.50000E 01 | 7.52063E-02 | 6.84897E-02 | 8.63516E-02 | 1.03367E-01 | 1.33361E-01 | 1.50000E 01 |
| 1.60000E 01 | 7.73212E-02 | 6.86353E-02 | 8.64241E-02 | 1.03392E-01 | 1.34030E-01 | 1.60000E 01 |
| 1.70000E 01 | 7.96126E-02 | 6.87888E-02 | 8.65201E-02 | 1.03423E-01 | 1.34716E-01 | 1.70000E 01 |
| 1.80000E 01 | 7.99940E-02 | 6.88265E-02 | 8.66001E-02 | 1.03475E-01 | 1.35193E-01 | 1.80000E 01 |
| 1.90000E 01 | 8.00398E-02 | 6.88399E-02 | 8.66150E-02 | 1.03488E-01 | 1.35423E-01 | 1.90000E 01 |
| 2.00000E 01 | 8.00920E-02 | 6.88544E-02 | 8.66295E-02 | 1.03495E-01 | 1.35613E-01 | 2.00000E 01 |
| 2.10000E 01 | 8.01671E-02 | 6.88688E-02 | 8.66439E-02 | 1.03503E-01 | 1.35770E-01 | 2.10000E 01 |
| 2.20000E 01 | 8.02765E-02 | 6.88819E-02 | 8.66579E-02 | 1.03513E-01 | 1.35903E-01 | 2.20000E 01 |
| 2.30000E 01 | 8.04366E-02 | 6.88928E-02 | 8.66717E-02 | 1.03530E-01 | 1.36017E-01 | 2.30000E 01 |
| 2.40000E 01 | 8.06810E-02 | 6.89013E-02 | 8.66861E-02 | 1.03563E-01 | 1.36114E-01 | 2.40000E 01 |
| 2.50000E 01 | 8.10975E-02 | 6.89071E-02 | 8.67031E-02 | 1.03638E-01 | 1.36200E-01 | 2.50000E 01 |
| 2.60000E 01 | 8.20062E-02 | 6.89123E-02 | 8.67291E-02 | 1.03877E-01 | 1.36281E-01 | 2.60000E 01 |
| 2.70000E 01 | 8.39545E-02 | 6.89368E-02 | 8.67733E-02 | 1.04689E-01 | 1.36388E-01 | 2.70000E 01 |
| 2.80000E 01 | 8.44690E-02 | 6.89570E-02 | 8.67857E-02 | 1.05084E-01 | 1.36470E-01 | 2.80000E 01 |
| 2.90000E 01 | 8.45506E-02 | 6.89597E-02 | 8.67876E-02 | 1.05145E-01 | 1.36518E-01 | 2.90000E 01 |
| 3.00000E 01 | 8.55836E-02 | 6.89970E-02 | 8.67921E-02 | 1.05178E-01 | 1.36542E-01 | 3.00000E 01 |
| 3.10000E 01 | 8.75160E-02 | 6.91528E-02 | 8.68024E-02 | 1.05378E-01 | 1.36589E-01 | 3.10000E 01 |
| 3.20000E 01 | 8.79610E-02 | 6.92242E-02 | 8.68071E-02 | 1.05470E-01 | 1.36641E-01 | 3.20000E 01 |
| 3.30000E 01 | 8.81242E-02 | 6.92673E-02 | 8.68101E-02 | 1.05520E-01 | 1.36685E-01 | 3.30000E 01 |
| 3.40000E 01 | 8.82106E-02 | 6.92999E-02 | 8.68122E-02 | 1.05555E-01 | 1.36724E-01 | 3.40000E 01 |
| 3.50000E 01 | 8.82576E-02 | 6.93258E-02 | 8.68140E-02 | 1.05580E-01 | 1.36758E-01 | 3.50000E 01 |
| 3.60000E 01 | 8.82857E-02 | 6.93472E-02 | 8.68157E-02 | 1.05598E-01 | 1.36789E-01 | 3.60000E 01 |
| 3.70000E 01 | 8.83034E-02 | 6.93656E-02 | 8.68171E-02 | 1.05612E-01 | 1.36816E-01 | 3.70000E 01 |
| 3.80000E 01 | 8.83152E-02 | 6.93818E-02 | 8.68185E-02 | 1.05623E-01 | 1.36841E-01 | 3.80000E 01 |
| 3.90000E 01 | 8.83231E-02 | 6.93961E-02 | 8.68197E-02 | 1.05631E-01 | 1.36864E-01 | 3.90000E 01 |
| 3.99500E 01 | 8.83284E-02 | 6.94083E-02 | 8.68210E-02 | 1.05638E-01 | 1.36883E-01 | 3.99500E 01 |

Figure 4.48 shows the effect of reducing all feedback gains to .7 of the values given on the block diagram (Figure 4.35). Note that the slope of the curve for the aft body is considerably less than for the other two locations. It is estimated that operating at .7 of the normalized gains would reduce canard and flap displacement requirements by 22 percent and elevator displacements by 27 percent. Decreasing the gains to .7 increases the response of the short period and 1st structural mode as shown in Figure 4.49. At the same time, high frequency structural mode responses are increased on the forward body and decreased on the aft body. The dotted curve shows the effect of increasing the normalized elevator gain to 1. with the canard and flaperon gains remaining at .7. A summary of the percent RMS reductions associated with these gain variations is presented in Table VII.

TABLE VII

EFFECTS OF RCS FEEDBACK GAINS
ON RMS VERTICAL ACCELERATION

| Body Station | Percent Change in RMS Vertical Acceleration NORMALIZED FEEDBACK GAINS* | | |
|---|---|---|---|
| | $K_C = 1.$ $K_F = 1.$ $K_E = 1.$ | $K_C = .7$ $K_F = .7$ $K_E = .7$ | $K_C = .7$ $K_F = .7$ $K_E = 1.$ |
| 172 | -36.4 | -29.5 | -28.8 |
| 860 | -39.2 | -32.3 | -33.8 |
| 1655 | -31.0 | -28.0 | -31.8 |

## 4.3 Remaining Work

A ride control system has been synthesized to produce at least 30 percent reduction in vertical acceleration along the entire fuselage. This system was designed using model equations of motion that did not include the cable mount effects. The cable-mounted model equations of motion will be updated to account for the change in cable attach point, and will then be used to evaluate and refine the RCS before the wind tunnel tests.

A procedure must be established to bring the RCS on line on the model in the tunnel. Through analyses, the order of closing the RCS feedback loops and gain changes as necessary will be determined to ensure stability of the model during start up of the wind tunnel. Responses will be generated for comparison with model responses to monitor the model behavior during the test runs.

The wind tunnel tests will be accomplished with the sinusoidal gust vanes as the model disturbance. Theoretical frequency responses will be generated for direct correlation with the wind tunnel results.

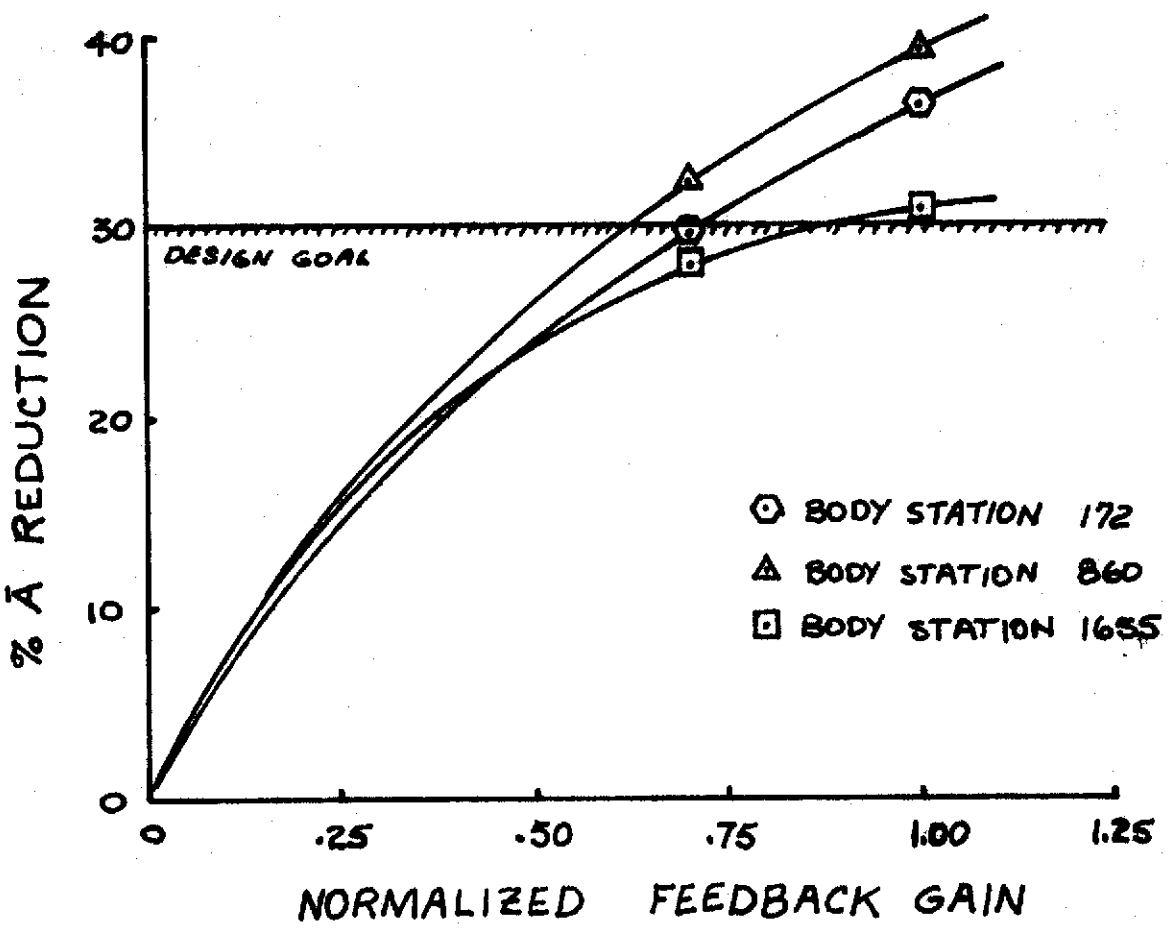


EFFECT OF RCS FEEDBACK GAINS ON
RMS VERTICAL ACCELERATION REDUCTION

FIGURE 4.48

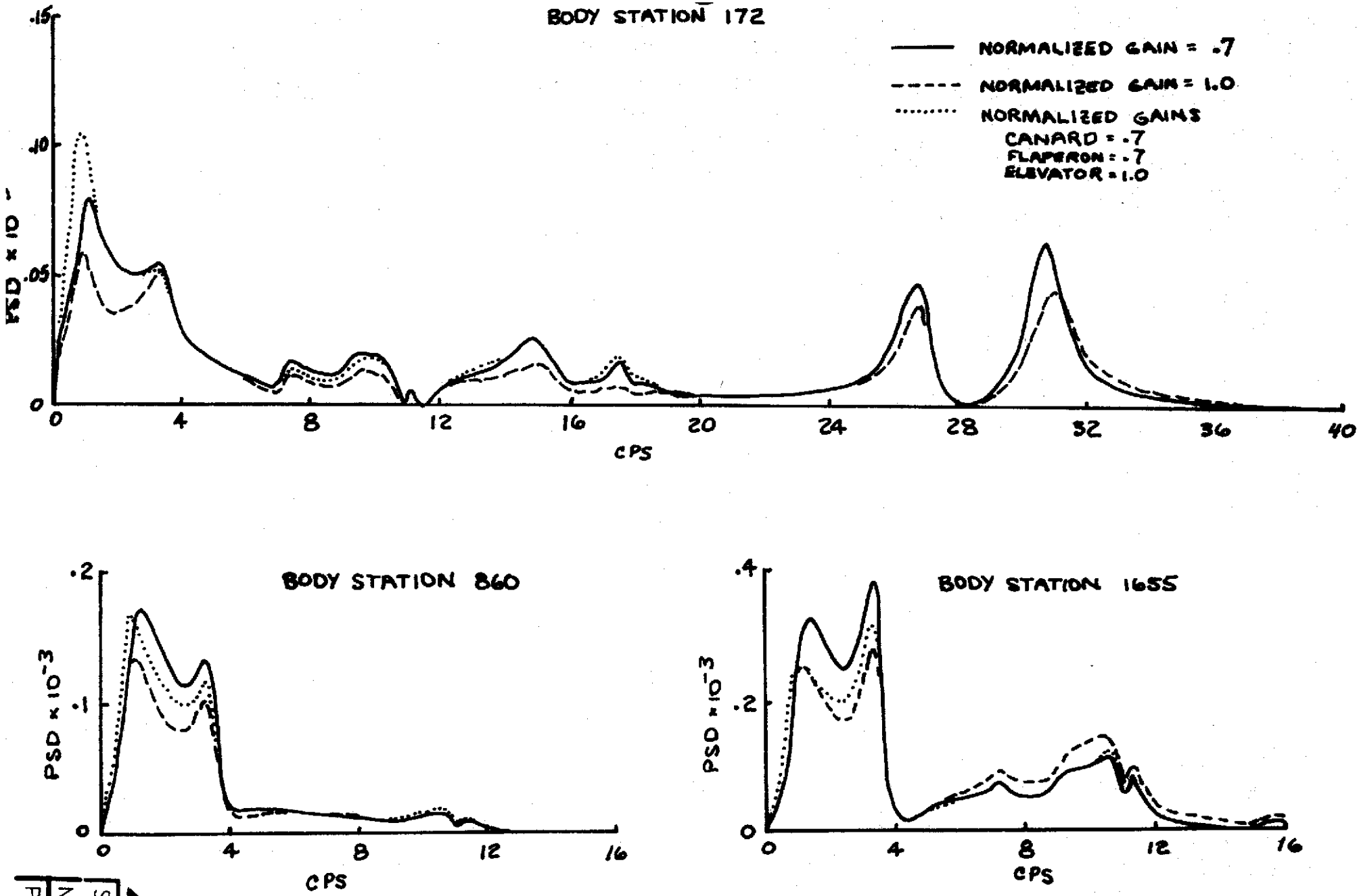


EFFECT OF RCS FEEDBACK GAINS ON VERTICAL ACCELERATION PSD'S

FIGURE 4.49

## 5.0 REFERENCES


1. Boeing Document D3-8390-1, "Analysis and Mechanization of NASA-Langley Flutter SAS Concepts," 21 September 1970.

2. Boeing Document D3-8390-4, "Analysis of Aeroelastic Model Stability Augmentation Systems - Final Report," 4 March 1971.

3. "Electrohydraulic Servomechanisms," Allen C. Morse, McGraw-Hill Book Company, 1963.

4. "Computing the Effects of Fluid Mass on Frequency Response," W. E. Schiesser, Control Engineering Magazine, February 1966.

5. Boeing Document D3-8390-2, "Design and Mechanization of Ride Control System for B-52 Aeroelastic Model - Work Statement."

6. Boeing Document D3-7348, "Wind Tunnel Measurement of B-52 Dynamic Response with a Stability Augmentation Flight Control System - Program Plan," 2 February 1967.